SEVEN-YEAR *WILKINSON MICROWAVE ANISOTROPY PROBE* (*WMAP*[*]) OBSERVATIONS: GALACTIC FOREGROUND EMISSION

B. GOLD[1], N. ODEGARD[2], J. L. WEILAND[2], R. S. HILL[2], A. KOGUT[3], C. L. BENNETT[1], G. HINSHAW[3], X. CHEN[4], J. DUNKLEY[5], M. HALPERN[6], N. JAROSIK[7], E. KOMATSU[8], D. LARSON[1], M. LIMON[9], S. S. MEYER[10], M. R. NOLTA[11], L. PAGE[7], K. M. SMITH[12], D. N. SPERGEL[7,12], G. S. TUCKER[13], E. WOLLACK[3], AND E. L. WRIGHT[14]

[1] Department of Physics & Astronomy, The Johns Hopkins University, 3400 N. Charles St., Baltimore, MD 21218-2686, USA; bgold@pha.jhu.edu
[2] Adnet Systems, Inc., 7515 Mission Dr., Suite A1C1 Lanham, MD 20706, USA
[3] Code 665, NASA/Goddard Space Flight Center, Greenbelt, MD 20771, USA
[4] Infrared Processing and Analysis Center, California Institute of Technology, 1200 E. California Blvd., Pasadena, CA 91125, USA
[5] Astrophysics, University of Oxford, Keble Road, Oxford OX1 3RH, UK
[6] Department of Physics and Astronomy, University of British Columbia, Vancouver, BC, Canada V6T 1Z1
[7] Department of Physics, Jadwin Hall, Princeton University, Princeton, NJ 08544-0708, USA
[8] Department of Astronomy, University of Texas, Austin, 2511 Speedway, RLM 15.306, Austin, TX 78712, USA
[9] Columbia Astrophysics Lab, Columbia University, Mail Code 5247, 550 W. 120th St., New York, NY 10027, USA
[10] Departments of Astrophysics and Physics, KICP and EFI, University of Chicago, Chicago, IL 60637, USA
[11] Canadian Institute for Theoretical Astrophysics, 60 St. George Street, University of Toronto, Toronto, ON, Canada M5S 3H8
[12] Department of Astrophysical Sciences, Peyton Hall, Princeton University, Princeton, NJ 08544-1001, USA
[13] Department of Physics, Brown University, 182 Hope St., Providence, RI 02912-1843, USA
[14] PAB 3-909, UCLA Physics & Astronomy, P.O. Box 951547, Los Angeles, CA 90095–1547, USA

ABSTRACT

We present updated estimates of Galactic foreground emission using seven years of *WMAP* data. Using the power spectrum of differences between multi-frequency template-cleaned maps, we find no evidence for foreground contamination outside of the updated (KQ85y7) foreground mask. We place a 15 μK upper bound on rms foreground contamination in the cleaned maps used for cosmological analysis. Further, the cleaning process requires only three power-law foregrounds outside of the mask. We find no evidence for polarized foregrounds beyond those from soft (steep-spectrum) synchrotron and thermal dust emission; in particular we find no indication in the polarization data of an extra "haze" of hard synchrotron emission from energetic electrons near the Galactic center. We provide an updated map of the cosmic microwave background (CMB) using the internal linear combination method, updated foreground masks, and updates to point source catalogs using two different techniques. With additional years of data, we now detect 471 point sources using a five-band technique and 417 sources using a three-band CMB-free technique. In total there are 62 newly detected point sources, a 12% increase over the five-year release. Also new are tests of the Markov chain Monte Carlo foreground fitting procedure against systematics in the time-stream data, and tests against the observed beam asymmetry. Within a few degrees of the Galactic plane, the behavior in total intensity of low-frequency foregrounds is complicated and not completely understood. *WMAP* data show a rapidly steepening spectrum from 20 to 40 GHz, which may be due to emission from spinning dust grains, steepening synchrotron, or other effects. Comparisons are made to a 1 deg 408 MHz map (Haslam et al.) and the 11 deg ARCADE 2 data (Singal et al.). We find that spinning dust or steepening synchrotron models fit the combination of *WMAP* and 408 MHz data equally well. ARCADE data appear inconsistent with the steepening synchrotron model and consistent with the spinning dust model, though some discrepancies remain regarding the relative strength of spinning dust emission. More high-resolution data in the 10–40 GHz range would shed much light on these issues.

Key words: cosmic background radiation – cosmology: observations – diffuse radiation – Galaxy: halo – Galaxy: structure – ISM: structure

1. INTRODUCTION

The *Wilkinson Microwave Anisotropy Probe* (*WMAP*) was launched in 2001 to observe the cosmic microwave background (CMB). In addition to measuring the CMB, *WMAP*, like any full-sky CMB experiment, also observes emission from our own Galaxy. With five frequency bands centered at 23, 33, 41, 61, and 94 GHz (respectively, denoted as K, Ka, Q, V, and W bands), full-sky coverage, polarization sensitivity, and control of systematics to the sub-percent level, *WMAP* is able to measure diffuse (1° and larger) emission with pre-cise temperature calibration. In this paper, we analyze seven years of *WMAP* data in order to better characterize Galactic foreground emission, the removal of which will be one of the largest challenges to future CMB experiments (Dunkley et al. 2009b).

This paper is part of a suite of papers describing the full details of the *WMAP* seven-year data release. An overall description of sky maps and basic results is in Jarosik et al. (2011), which also includes a description of the beam modeling used to produce maps smoothed to the common resolution of a 1° FWHM Gaussian. These maps serve as the starting point for foreground analysis in this work. Larson et al. (2011) describe the generation of power spectra from CMB maps, and Komatsu et al. (2011) discuss the cosmological implications of the spectra. Weiland et al. (2011) detail measurements of celestial calibrators, and

---

Bennett et al. (2011) investigate the status of some potential anomalies found in *WMAP* data.

The layout of this paper is as follows. Updates to masks and foreground fitting processes are described in Section 2. A comparison of *WMAP* data to that recently taken by the ARCADE instrument (Singal et al. 2009) is discussed in Section 3. Results of the fits and their implications for specific foreground emission processes are discussed in Section 4. A discussion of systematics follows in Section 5. Point sources and an update to the point source catalog are found in Section 6. Lastly, conclusions can be found in Section 7.

1.1. Science Overview

There are three primary mechanisms for diffuse Galactic radio emission. Relativistic electrons interact with the Galactic magnetic field to produce synchrotron emission, for which the standard template is 408 MHz data compiled by Haslam et al. (1981). Less energetic electrons scatter from each other and ionized nuclei to produce free–free radiation (also known as thermal Bremsstrahlung), which can be traced with Hα line emission (Finkbeiner 2003). Finally, dust grains emit a modified blackbody spectrum through excitation of their vibrational modes, for which the standard template is the fit of Finkbeiner et al. (1999) to data from the *Infrared Astronomical Satellite* (*IRAS*) and the *Cosmic Background Explorer* (*COBE*). Dust grains may also emit radiation through rotational modes or other excitations (Draine & Lazarian 1998a, 1998b, 1999).

WMAP was designed to measure the frequency range where the ratio of the CMB anisotropy to the rms fluctuations of all three foregrounds is at its maximum, to minimize foreground contamination. This also implies that two or more foreground components will be of comparable amplitude and that they will be relatively weak. Foreground templates, however, are best made by observing a foreground process at a frequency where it dominates the total emission. Hence, there will always be some extrapolation involved when attempting to account for foregrounds on top of CMB observations.

So how well does the extrapolation work? Simple power-law extrapolation of the 408 MHz synchrotron template from Haslam et al. (1981) does not explain very much of the observed emission at 20–40 GHz. Whether this is due to a new low-frequency emission process, errors in the extrapolation due to spatial variation in the spectral index, or both, is difficult to determine. Targeted observations of individual regions (Scaife et al. 2009; Tibbs et al. 2010) suggest a spinning dust-like component, but a model consistent across size scales and data sets remains elusive.

Free–free emission is extrapolated from a map of Hα, corrected for dust extinction using a reddening map based on 100 μm data (Schlegel et al. 1998; Bennett et al. 2003). Variations in electron temperature cause some uncertainty in this extrapolation, but the larger effect is likely uncertainty in the reddening correction. The overall ratio of radio to Hα brightness comes out lower than expected (Bennett et al. 2003); nevertheless, the template otherwise matches quite well with observations at 30–60 GHz, where free–free emission from the Galactic disk is particularly dominant.

The dust extrapolation has so far been tested least precisely by CMB experiments. While the model of Finkbeiner et al. (1999) incorporates *COBE* FIRAS data all the way down to 60 GHz, the uncertainty at those frequencies is large; most of the dust model comes from information at 100 and 240 μm. While the spectral index of dust at frequencies below 300 GHz has not yet been measured to enough accuracy to challenge the model, the morphology matches observations at lower frequencies, though some experiments suggest overall brightness levels different from the predictions (Veneziani et al. 2010; Culverhouse et al. 2010).

Analysis of data from previous *WMAP* releases has shown that CMB maps from different foreground removal techniques agree to within 11 μK (Gold et al. 2009) on average in the low Galactic emission regions used for CMB anisotropy measurements, though this does not provide an absolute limit to the amount of contamination. Even when templates are not directly used for foreground removal, they provide an important guide for the construction of masks and other foreground cleaning methods.

Several systems of units are in use throughout this work. Point sources are reported in flux units (Jansky), where the power-law index is denoted by α such that flux follows $S \sim \nu^\alpha$. Foreground modeling is most easily done in units of antenna temperature, defined by using the Rayleigh–Jeans limit of a blackbody spectrum (for which $S \sim \nu^2$) to convert flux per solid angle to a temperature. In these units the power-law index is denoted as $\beta = \alpha - 2$. *WMAP*'s frequency range is not quite in the Rayleigh–Jeans limit for a 2.7 K blackbody, so there is a frequency-dependent conversion factor $a(\nu) = (e^x - 1)^2/x^2 e^x$ (where $x = h\nu/k_B T_{\rm cmb}$) to convert antenna temperatures to thermodynamic temperatures convenient for CMB analysis.

2. SEVEN-YEAR FOREGROUND FITS

2.1. Masks

Foreground removal always has some uncertainty, so it is useful to mask part of the sky where foregrounds are too bright for CMB analysis. As in the five-year analysis, the starting points for the masks are K- and Q-band-average maps smoothed to 1 deg resolution. The maps are then converted to foreground-only maps by subtracting off an estimate of the CMB using the internal linear combination (ILC) method (see Hinshaw et al. 2007 and Section 2.2). A cumulative histogram in each band is formed to find the flux level above which a given percentage of sky can be cut, and the union of the pixels cut from each band at a given flux level is used to define a mask. We used two masks for most further analysis, based on cuts which leave 75% and 85% of the sky; these are denoted as KQ75 and KQ85, respectively.

For the seven-year analysis, the diffuse foreground masks have been extended based on a χ^2 analysis of residuals after foreground subtraction. Starting with foreground-reduced maps, differences are taken between bands (Q – V and V – W in thermodynamic units), eliminating any CMB signal. Ideally the only thing left in the resulting maps would be noise; in practice there are visible residuals near the Galactic plane. Given the noise per pixel of the maps, it is possible to compute a map of the χ^2 for each pixel.

After degradation to HEALPix $N_{\rm side} = 32$ (see Gorski et al. 2005 for a description of this pixelization scheme), regions of 4 or more contiguous pixels with χ^2 higher than four times that of the polar caps are identified and used to define two new masks, one from each difference map. These are then combined with the previous KQ75 and KQ85 masks (Gold et al. 2009) used for the five-year analysis. After promotion back to full resolution, edges of the mask are smoothed with a 3° FWHM Gaussian. The resulting changes to the final mask are primarily around the edge of the Galactic cut, particularly in the Gum and Ophiuchus
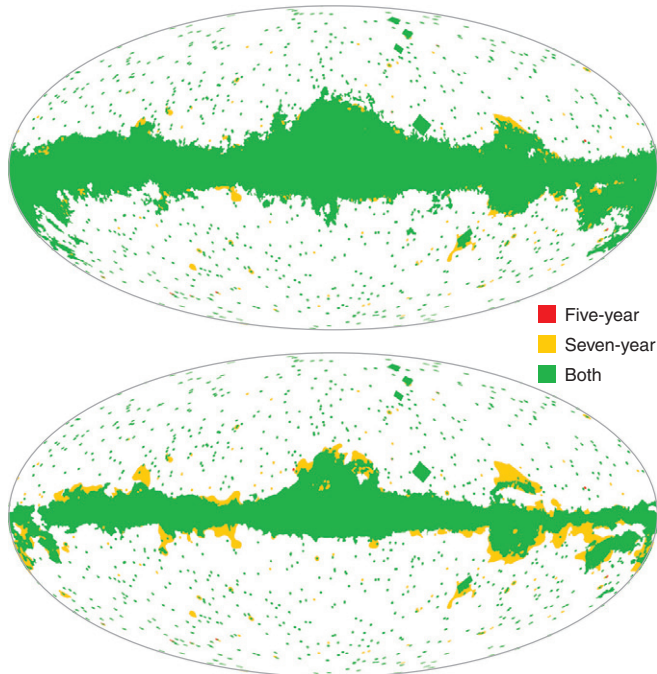
Figure 1. Comparison of seven-year masks to five-year masks. At the top KQ75 and KQ75y7 are compared, and at the bottom KQ85 and KQ85y7. Green regions are masked in both the seven-year and five-year masks, yellow regions are newly masked in the seven-year masks, and red regions are masked in the five-year masks but no longer in the seven-year masks.

Figure 2. Difference map between the seven-year ILC map and the five-year ILC map. Small-scale differences are consistent with pixel noise; large-scale differences are consistent with a change in dipole of 6.7 μK.

Table 1
ILC Coefficients Per Region[a]

Region	K band	Ka band	Q band	V band	W band
0	0.1495	−0.7184	−0.3188	2.3071	−0.4195
1	−0.0035	−0.2968	−0.1963	2.0533	−0.5567
2	0.0258	−0.3368	−0.3162	1.8368	−0.2096
3	−0.0945	0.1772	−0.6087	1.5541	−0.0281
4	−0.0771	0.0881	−0.4149	0.9559	0.4480
5	0.1928	−0.7451	−0.4538	2.4673	−0.4612
6	−0.0918	0.1946	−0.5586	1.0227	0.4332
7	0.1533	−0.7464	−0.2033	2.2798	−0.4834
8	0.2061	−0.2979	−1.5705	3.5678	−0.9056
9	−0.0889	−0.1241	−0.0816	1.2066	0.0880
10	0.1701	−0.8610	−0.1825	2.8264	−0.9530
11	0.2358	−0.8467	−0.6020	2.8336	−0.6206

Note. [a] The ILC temperature (in thermodynamic units) at pixel p of region n is $T_n(p) = \sum_{i=1}^{5} \zeta_{n,i} T^i(p)$, where ζ are the coefficients above and the sum is over *WMAP*'s frequency bands.

regions. The additional sky fraction cut from the KQ85 masked sky is 3.4%, and from the KQ75 masked sky is 1.0%.

These expanded masks are then combined with the point source mask as in previous releases, which has been updated with newly detected sources. Also, point sources brighter than 5 Jy have had the radius of their cut extended from 0°6 to 1°2, in order to minimize confusion at low frequencies where the instrument beam is large. The new masks, which we denote as KQ75y7 and KQ85y7, are shown in Figure 1 and are available on the LAMBDA Web site.[15] In total 70.6% (KQ75y7) and 78.3% (KQ85y7) of the sky now remains after the masking process.

2.2. Internal Linear Combination Method

The ILC method implemented by *WMAP* is a technique largely blind to assumptions about the frequency spectrum of foreground emission, which produces CMB maps with little visible foreground contamination. The ILC is a weighted combination formed from all five frequency bands, which are smoothed to a common 1° FWHM Gaussian beam using the symmetrized beam window functions produced by the beam analysis (Jarosik et al. 2011). The coefficients used to weight each individual frequency band are those that minimize the variance of the resulting map under the constraint that the sum of the coefficients is unity, which ensures that the CMB portion of the signal is passed through unaltered.

The details of the algorithm used to compute the *WMAP* seven-year ILC map are the same as that described in the three-year analysis (Hinshaw et al. 2007). In particular, we perform a bias correction step which uses simulations to estimate and correct for the tendency of the ILC method to produce
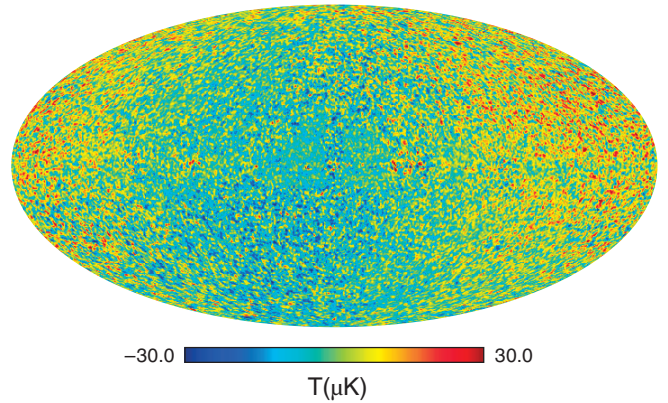
CMB maps anti-correlated with foreground fluctuations (for an overview of potential ILC pitfalls, see Vio & Andreani 2009). We have found this technique to be robust when applied to *WMAP* data: the variance between the ILC map and CMB maps made with other techniques is less than 116 μK^2 (Gold et al. 2009). Similar techniques by other authors have given CMB maps consistent with *WMAP*'s best-fit cosmological results (Kim et al. 2008).

Rather than use a single set of coefficients for the whole sky, to allow for variations in Galactic composition we subdivide the sky into 12 regions and find the ILC coefficients for each, shown in Table 1. All but region 0 lie along the Galactic plane. We retain the same number of regional subdivisions of the sky, and their spatial boundaries remain unchanged from the previous years (for details see Hinshaw et al. 2007). The frequency weights for each region are slightly different, however, reflecting the most recent updates to the calibration and beams. Figure 2 shows the difference between the seven-year and five-year ILC maps, which is dominated by a small change in the dipole. The seven-year ILC map is available on the LAMBDA Web site.

2.3. Maximum Entropy Method

The maximum entropy method (MEM) is a spatial and spectral fit that uses external templates, intended to distinguish between different emission sources. By design, the MEM output tends to revert to these templates in regions of low signal-to-

---
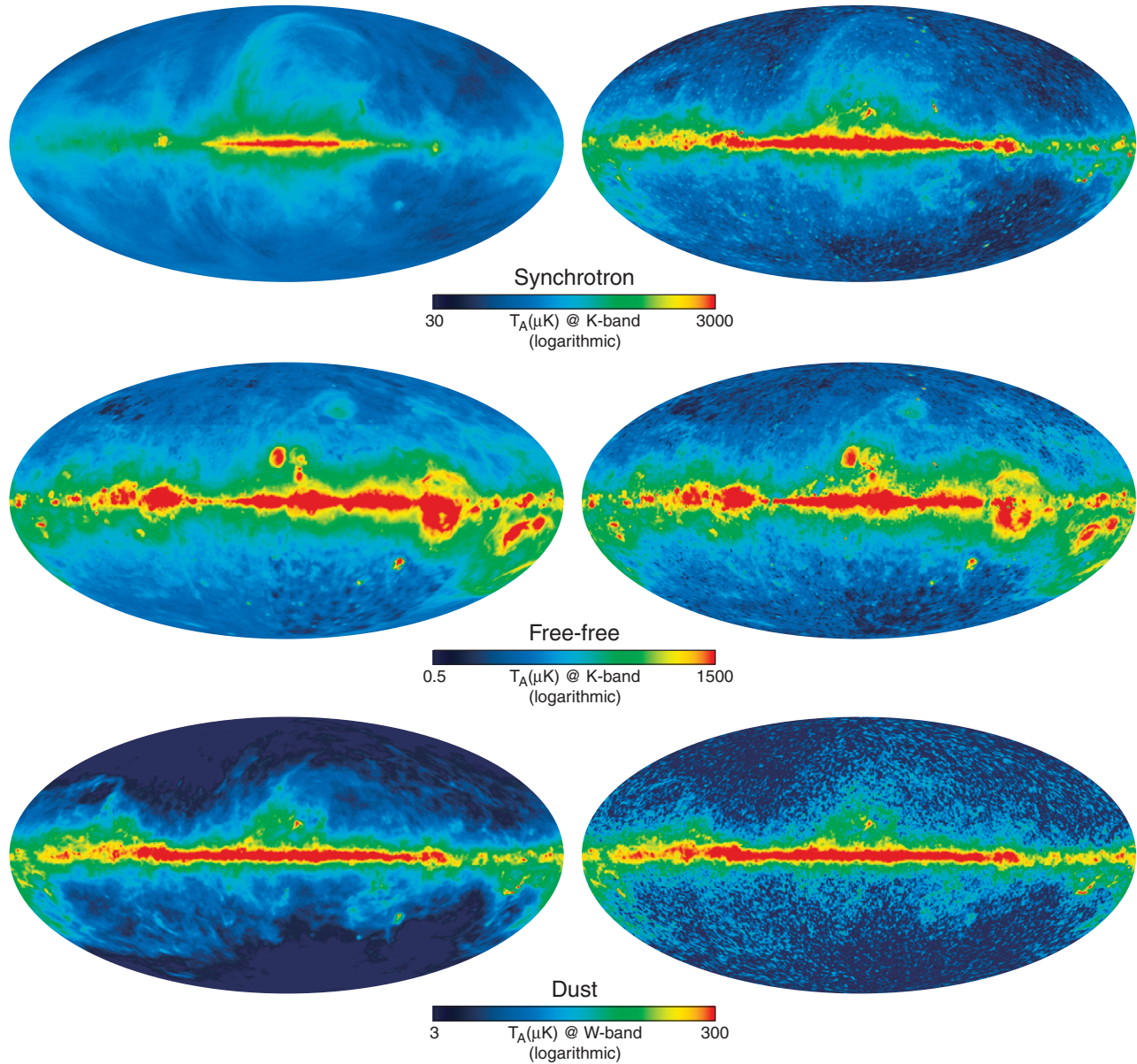
[15] http://lambda.gsfc.nasa.gov/

Figure 3. Galactic signal component maps as determined by the Maximum Entropy Method (MEM) analysis. On the left are the input prior maps, and on the right are the output MEM maps. From top to bottom are the synchrotron, free–free, and dust components. While the output maps show many features of the prior at higher latitudes, there are clear differences in regions of strong emission.

noise. Thus, the MEM results are most interesting in regions with higher signal.

The seven-year MEM analysis is largely unchanged from previous work (Hinshaw et al. 2007; Gold et al. 2009). As before, the analysis is done in all bands on the $1°$ smoothed sky maps, with the ILC map subtracted. The zero level of each map is set such that a csc $|b|$ fit, for HEALPix $N_{\mathrm{side}} = 512$ pixels at $b < -15°$ and outside of the KQ85y7 mask, yields a value of zero for the intercept. The maps are degraded to HEALPix $N_{\mathrm{side}} = 128$ pixelization, and a model is fit for each pixel p. Rather than simply minimize χ^2, the MEM minimizes a function

$$H = \chi^2 + \lambda \sum_c T_c(p) \ln \left[\frac{T_c(p)}{e P_c(p)} \right]. \qquad (1)$$

Here T_c and P_c are the model brightness and template prior for foreground component c (e is the base of natural logarithms). The second term is what enforces the prior when the signal-to-

noise becomes low, and the parameter λ sets the threshold for the transition from signal-dominated to noise-dominated behavior. The spectra of the free–free and dust components are fixed power laws, with $\beta = -2.14$ for free–free and $\beta = +2.0$ for dust. An iterative procedure uses residuals from the fit at each iteration to adjust the spectrum of the synchrotron component for each pixel. Hence, any anomalous component such as electric dipole emission from spinning dust is included in the synchrotron component. The adopted priors are unchanged from previous analyses and are based on the 408 MHz map of Haslam et al. (1981) with an extragalactic brightness of 5.9 K subtracted (Lawson et al. 1987) for synchrotron, an extinction-corrected Hα map (Finkbeiner 2003; Bennett et al. 2003) for free–free, and model 8 of Finkbeiner et al. (1999) for dust.

The prior map and output map are shown in Figure 3 for each foreground component. The zero level of the output synchrotron map is slightly lower (~ 50 μK) than that of the synchrotron prior. This reflects the difference between the zero level of
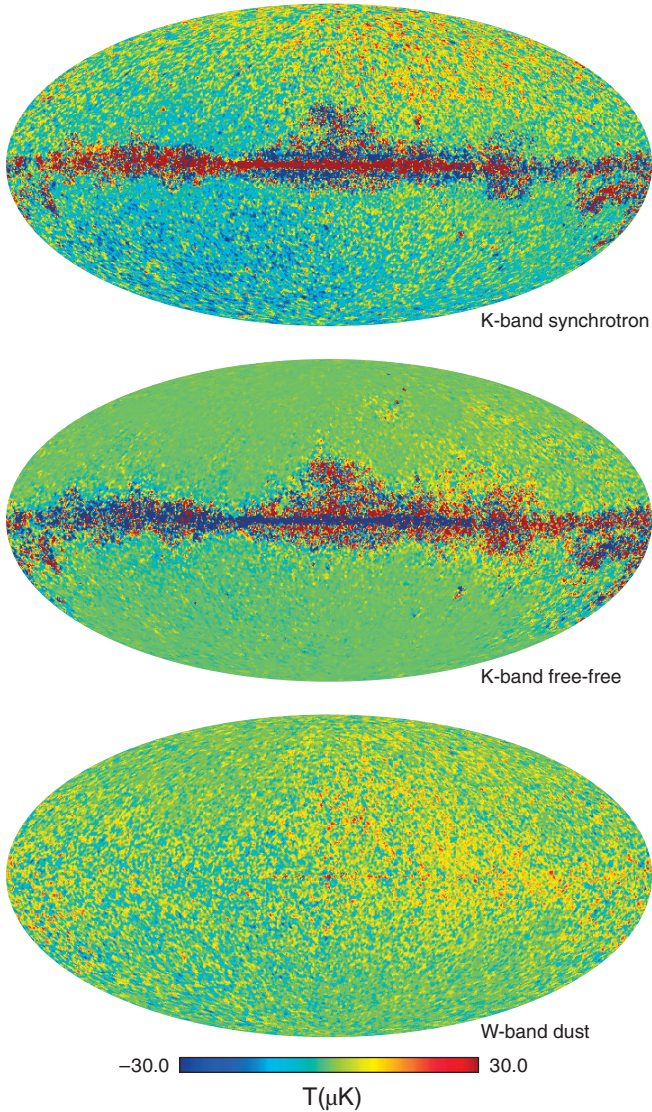
Figure 4. Difference maps between the seven-year MEM foreground maps and the five-year MEM foreground maps. Apart from a small dipole shift and noise fluctuations, the only visible feature is a small shift of 0.17% of K-band flux from free–free to synchrotron.

Table 2
Template Cleaning Temperature Coefficients

DA[a]	b_1	b_2 (μK R^{-1})	b_3	β_s[b]	h_{ff}[c] (μK R^{-1})
Q1	0.234	1.206	0.203	−3.26	7.12
Q2	0.232	1.240	0.201	−3.30	7.13
V1	0.048	0.791	0.466	−3.63	7.20
V2	0.045	0.772	0.483	−3.64	7.21
W1	0.000	0.436	1.277	. . .	7.24
W2	0.000	0.430	1.291	. . .	7.24
W3	0.000	0.438	1.257	. . .	7.24
W4	0.000	0.432	1.285	. . .	7.24

Notes.
[a] *WMAP* has two differencing assemblies (DAs) for the Q and V bands and four for the W band; the high signal-to-noise in total intensity allows each DA to be fitted independently.
[b] Power-law slope relative to the K band, as derived from b_1; W-band values are less than −4.
[c] Free–free to Hα ratio at the K band, as derived from b_1 and b_2. The expected value for an electron temperature of 8000 K is 11.4 μK R^{-1} (Bennett et al. 2003).

latitudes because this is where zero level normalization of the sky maps is determined by csc |b| fitting. The MEM maps are available on the LAMBDA Web site.

2.4. Template Cleaning

WMAP continues to use a template cleaning method to produce the foreground-reduced maps used for power spectrum analysis (Hinshaw et al. 2007; Page et al. 2007). For temperature maps, the templates are a K−Ka difference map, an extinction-corrected Hα map, and a dust map (Finkbeiner et al. 1999). For polarization, the templates are the K-band map for synchrotron, and a dust model described in detail below.

The temperature cleaning is applied to seven-year Q-, V-, and W-band maps (K and Ka are used for a template). The model has the form

$$M(\nu, p) = b_1(\nu)[T_K(p) - T_{Ka}(p)]$$
$$+ b_2(\nu)I_{H\alpha}(p) + b_3(\nu)M_{dust}(p), \quad (2)$$

where p indicates the pixel, the frequency dependence is entirely contained in the coefficients b_i, and the spatial templates are the *WMAP* K−Ka temperature difference map ($T_K - T_{Ka}$), the Finkbeiner (2003) composite Hα map with an extinction correction applied ($I_{H\alpha}$), and the Finkbeiner et al. (1999) dust model evaluated at 94 GHz (M_{dust}). Because the first template has contributions from both synchrotron and free–free emission, foreground parameters are a mixture of $b_1(\nu)$ and $b_2(\nu)$. For free–free emission, the ratio of K-band radio temperature to Hα intensity is

$$h_{ff} = \frac{b_2(\nu)}{S_{ff}(\nu) - 0.552\, b_1(\nu)}, \quad (3)$$

where $S_{ff}(\nu)$ is the free–free emission spectrum converted to thermodynamic temperature units, normalized to unity at the K band and is assumed to be a power law in antenna temperature with $\beta = -2.14$. The synchrotron spectral index (relative to the K band) is found via

$$\beta_s = \frac{\log [0.67\, b_1(\nu)a(\nu)]}{\log(\nu/\nu_K)}, \quad (4)$$

where $a(\nu)$ is the conversion factor from antenna temperature to thermodynamic units.

the K-band csc |b| normalized map and that of the prior. For comparison, the 1σ uncertainty in the prior zero level, based on the quoted uncertainty in the 408 MHz map zero level, is 27 μK. Also, there is a dependence on the adopted extragalactic brightness at 408 MHz. If the ARCADE 2 value (Fixsen et al. 2009) were used, the zero level of the prior would be ∼37 μK below that of the csc |b| normalized map. Figure 3 can be compared with Figure 5 of Hinshaw et al. (2007) to see the improvement in signal-to-noise ratio (S/N) of the output maps between the three-year and seven-year analyses.

Differences between seven-year MEM maps and five-year MEM maps are shown in Figure 4. The seven-year MEM foreground component maps tend to be slightly brighter than the five-year versions at mid to high northern Galactic latitudes. This is due to small dipole differences between the seven-year and five-year sky maps, which are caused by a combination of a change in the calibration dipole and small (less than 0.2%) changes in radiometer calibrations between the seven-year and five-year analyses. The seven-year and five-year foreground component maps are in better agreement at southern Galactic

Table 3
Template Cleaning Polarization Coefficients

Band	a_1[a]	$\beta_s(\nu_K, \nu)$[b]	a_2[a]	$\beta_d(\nu, \nu_W)$[b]
Ka	0.3202	−3.13	0.0144	1.43
Q	0.1683	−3.13	0.0177	1.54
V	0.0613	−2.93	0.0355	1.50
W	0.0412	−2.41	0.0770	...

Notes.
[a] The a_i coefficients are dimensionless and produce model maps from templates.
[b] The spectral indices refer to antenna temperature.

The coefficients of the model fit to the seven-year data are presented in Table 2. Small changes in the seven-year coefficients compared to previous values reflect small changes in the absolute calibration and beam profiles.

For polarization cleaning the maps are degraded to low resolution ($N_{side} = 16$). The model has the form

$$[Q(\nu, p), U(\nu, p)]_{model} = a_1(\nu)[Q(p), U(p)]_K$$
$$+ a_2(\nu)[Q(p), U(p)]_{dust}. \quad (5)$$

The templates used are the *WMAP* K-band polarization for synchrotron ($[Q, U]_K$), and a low-resolution version of the dust template used above with polarization direction derived from starlight measurements ($[Q, U]_{dust}$) and a geometric suppression factor to account for the magnetic field geometry (Page et al. 2007). The coefficients of the model fit to the seven-year data are in Table 3. For polarization, the template maps are assumed to have a one-to-one correspondence with foreground emission, so the spectral indices for synchrotron and dust are simply the power-law slopes of the coefficients $a_1(\nu)$ and $a_2(\nu)$. If the dust model is correct then the ratio a_2/b_3 gives the polarization fraction; for the W band this is ∼6%.

The full-resolution ($N_{side} = 512$) foreground-reduced Stokes Q and U maps were produced using the same cleaning coefficients as derived for the low-resolution maps, but with full-resolution templates. The K band and dust intensity templates can be produced at full resolution from available data, and the starlight polarization map used to determine polarization direction was upgraded to full resolution using nearest-neighbor sampling. The templates subtracted from *WMAP* data are smoothed to 1° FWHM, potentially leaving artifacts in the foreground-reduced maps due to small-scale power or beam asymmetries. In practice, we find no sign of these effects, as discussed in Section 4.1 and Section 5. All data sets used for templates are available on the LAMBDA Web site.

2.5. Markov Chain Monte Carlo Fitting

We again perform a pixel-based Markov chain Monte Carlo (MCMC) fitting technique to the five bands of *WMAP* data. Our method is similar to that of Eriksen et al. (2007), but we focus more on Galactic foregrounds rather than CMB. The fit results of the five-year release have been reproduced, with the "base" model, which uses three power-law foregrounds, producing virtually the same reduced χ^2 per pixel. The MCMC fitting has benefited from further understanding of the zero point of the maps. We have used the 408 MHz map of Haslam et al. (1981) with a zero point determined using the same csc $|b|$ method as for the *WMAP* data and investigated the effect on the fit of error in this zero point.

The MCMC fit is performed on 1 deg smoothed maps downgraded to HEALPix $N_{side} = 64$. An MCMC chain is run

for each pixel, where the basic model is

$$T(\nu) = T_s \left(\frac{\nu}{\nu_K}\right)^{\beta_s(\nu)} + T_f \left(\frac{\nu}{\nu_K}\right)^{\beta_f} + a(\nu)T_{cmb} + T_d \left(\frac{\nu}{\nu_W}\right)^{\beta_d} \quad (6)$$

for the antenna temperature. The subscripts s, f, d stand for synchrotron, free–free, and dust emission, ν_K and ν_W are the effective frequencies for the K and W bands (22.5 and 93.5 GHz), and $a(\nu)$ accounts for the slight frequency dependence of a 2.725 K blackbody using the thermodynamic to antenna temperature conversion factors found in Bennett et al. (2003). The fit always includes polarization data as well, where the model is

$$Q(\nu) = Q_s \left(\frac{\nu}{\nu_K}\right)^{\beta_s(\nu)} + Q_d \left(\frac{\nu}{\nu_W}\right)^{\beta_d} + a(\nu)Q_{cmb} \quad (7)$$

$$U(\nu) = U_s \left(\frac{\nu}{\nu_K}\right)^{\beta_s(\nu)} + U_d \left(\frac{\nu}{\nu_W}\right)^{\beta_d} + a(\nu)U_{cmb} \quad (8)$$

for Stokes Q and U parameters. Thus, there are a total of 15 pieces of data for each pixel (T, Q, and U for five bands).

As for the five-year release, the noise for each pixel at $N_{side} = 64$ is computed from maps of N_{obs} at $N_{side} = 512$. To account for the smoothing process, the noise is then rescaled by a factor calculated from simulated noise maps for each frequency band. The MCMC fit treats pixels as independent and does not use pixel–pixel covariance, which leads to small correlations in χ^2 between neighboring pixels. This has negligible effect on results as long as goodness of fit is averaged over large enough regions.

We fit three categories of models. All use the K band as a template for the polarization angle of synchrotron and dust emission, so U_s and U_d are not independent parameters, identical to the previous analysis. All models also fix the free–free spectral index to $\beta_f = -2.16$, a slight change from $\beta_f = -2.14$ used in the previous analysis. This change was motivated as an attempt to better match the effective spectral index at Q and V bands, due to their use in cosmological analysis, but was not found to make a difference to the fits.

The "base" model uses three power-law foregrounds, where the synchrotron spectral index $\beta_s(\nu)$ is taken to be independent of frequency but may vary spatially, and the dust spectral index β_d is allowed to vary spatially. We assume the same spectral indices for polarized synchrotron and dust emission as for total intensity emission. This model has a total of 10 free parameters per pixel: $T_s, T_f, T_d, T_{cmb}, \beta_s, \beta_d, Q_s, Q_d, Q_{cmb}$, and U_{cmb}.

A steepening synchrotron model uses the same three foregrounds but allows for a steepening of the synchrotron spectral index by adding a new parameter c_s, defined by

$$\beta_s(\nu) = \begin{cases} \beta_s & \nu < \nu_K \\ \beta_s + c_s \ln\left(\frac{\nu}{\nu_K}\right) & \nu > \nu_K \end{cases}. \quad (9)$$

For the steepening model the dust spectral index is fixed[16] to $\beta_d = +2.0$. Therefore, this model also has 10 free parameters per pixel.

---

[16] The precise choice of dust index here and for the spinning dust model does not make much difference; when allowed to vary it is poorly constrained by the MCMC fits and uncorrelated with the synchrotron or free–free components (Gold et al. 2009).

For models with a spinning dust component, another term is added to Equation (6):

$$T_{sd}(\nu) = A_{sd} \frac{(\nu/\nu_{sd})^{\beta_d+1}}{\exp(\nu/\nu_{sd}) - 1}. \qquad (10)$$

The spinning dust component is assumed to have negligible polarization, as theoretical expectations for the polarization fraction are low compared to synchrotron radiation (Lazarian & Draine 2000), and the polarization data thus far show no evidence that such a component is necessary (see Section 4.5). The spinning dust amplitude A_{sd} was allowed to vary spatially as a new parameter. Both β_s and β_d were fixed to -3.0 and $+2.0$, respectively, to avoid degeneracies from having too many parameters in the fit. Allowing ν_{sd} to spatially vary was not found to result in any improvement of the fit, but fits were performed with different global values of ν_{sd} to find the best overall value. Thus, with fixing of the spectral indices, this model has nine free parameters per pixel.

MCMC fits for the seven-year release were performed with the addition of the 408 MHz data compiled by Haslam et al. (1981). The error on the zero point for this data was estimated in that work to be ± 3 K, with an overall calibration error of 10%. Lawson et al. (1987) use a comparison with 404 MHz data to find a uniform (presumably extragalactic) component with a brightness of 5.9 K. As the MCMC method treats all input maps equally, for consistency we estimate and subtract off a nominal zero-point offset of 7.4 K, as determined by the same csc $|b|$ method we use for the *WMAP* sky maps. However, the 408 MHz data resemble a csc $|b|$ behavior much less than the *WMAP* data, due to the increased relative prominence of large-scale features such as the Northern Polar Spur. Therefore, we attempted the csc $|b|$ fitting procedure on different hemispheres and with different cuts, and estimate the uncertainty in procedure to be ± 4 K. MCMC fits were run for each model with zero points of 3.4 K and 11.4 K in addition to the nominal value, and the effect of these on foregrounds is discussed in Section 4.4. A full set of maps and MCMC variance estimates for the three models is available on the LAMBDA Web site.

3. COMPARISON WITH ARCADE 2

The ARCADE collaboration has made available absolute temperature measurements of Galactic emission for part of the sky (Kogut et al. 2009). ARCADE observations do not cover the full sky and the instrument's beam is significantly larger than *WMAP*'s. Therefore, we limit our comparison to two regions where ARCADE's scan crosses the Galactic plane and observes the brightest emission, the first at Galactic longitude of 34° and the second at 93°.

Figure 5 shows the Galactic spectrum for these two regions. *WMAP* data have been smoothed to 11°.6, to match the ARCADE resolution. The ARCADE maps have had the CMB monopole removed, and the *WMAP* maps have had CMB anisotropies removed using the ILC map (though this has little effect). The ARCADE data have not had any extragalactic component (as found by Fixsen et al. 2009) removed. Instead, all maps have been treated as equally as possible, removing a zero point by fitting a csc $|b|$ model to the available data and subtracting the constant term.

The uncertainty in this zero-point subtraction is largest for ARCADE due to the limited sky coverage of the experiment. We tested the zero-point subtraction by fitting to several partial-sky subsets of the full-sky *WMAP* maps and find that the variations
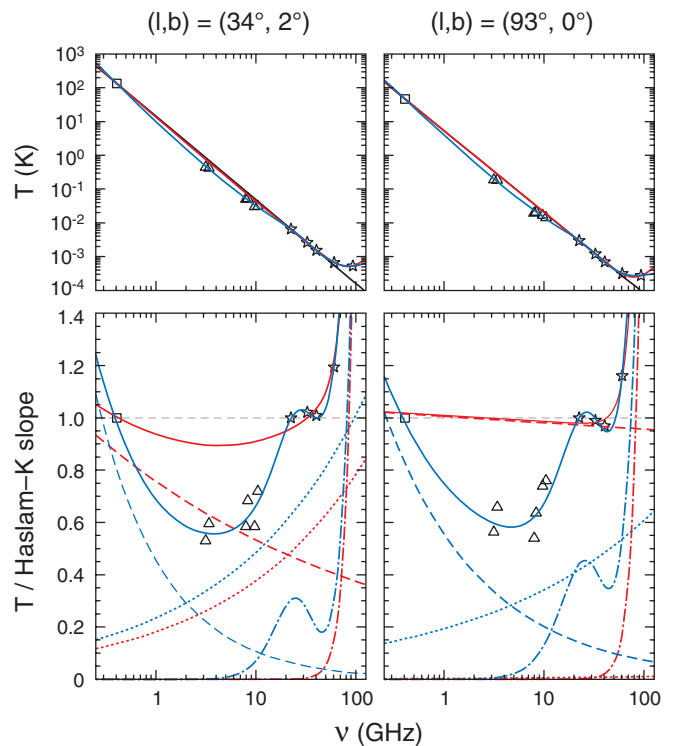
Figure 5. Galactic emission from two regions in the Galactic plane. ARCADE (triangles), *WMAP* (stars), and 408 MHz data (square) are all shown, smoothed to a common resolution. Upper panels show antenna temperature (absent a monopole component). The black line is a power law connecting 408 MHz to 22 GHz ($\beta = -2.48$ for the left panel, $\beta = -2.41$ for the right panel), which is divided out in the bottom panels to better show deviations from power-law behavior. Red lines show the result of a fit to the data using three power-law components for foregrounds (representing synchrotron, free–free, and dust). Blue lines show the fit resulting when an extra component representing spinning dust is added. Solid lines show the total flux, with individual components shown by dashed lines (synchrotron), dotted lines (free–free), and dot-dashed lines (dust plus spinning dust). Errors in the data are dominated by systematics and highly correlated between data points, but are estimated to be 5%–15%, depending on experiment.

imply an uncertainty in the ARCADE points of up to 15% of the CMB-subtracted flux. Also included is the 408 MHz map as a reference point at low frequency. As discussed in the previous section, the csc $|b|$ model performs most poorly for this map, with uncertainties of ± 4 K. However, in these two regions the emission is bright enough that this is still less than 10% of the total emission.

Two fits were applied to the data in each region. The first used three power-law foregrounds: synchrotron, free–free, and dust, where the spectral indices for synchrotron and dust were left free for the fit. The second fit added a spinning dust component using the functional form of Equation (10), with the amplitude and ν_{sd} as free parameters. Because the maps are highly smoothed, errors are dominated by systematic issues and difficult to characterize. We chose to use 2% fractional error for *WMAP* and 5% fractional error for other observations when performing the fit. Using larger errors does not remove the sharp difference in χ^2 between the two models unless the errors are taken to be larger than 50%. For the fit without spinning dust, the ARCADE data were not used in the fit as they were found to be incompatible with such a model.

The resulting fits are shown in Figure 5, with the spinning dust fit in blue and the power-law-only fit in red. The top panels show the data and fits in absolute temperature units after monopole
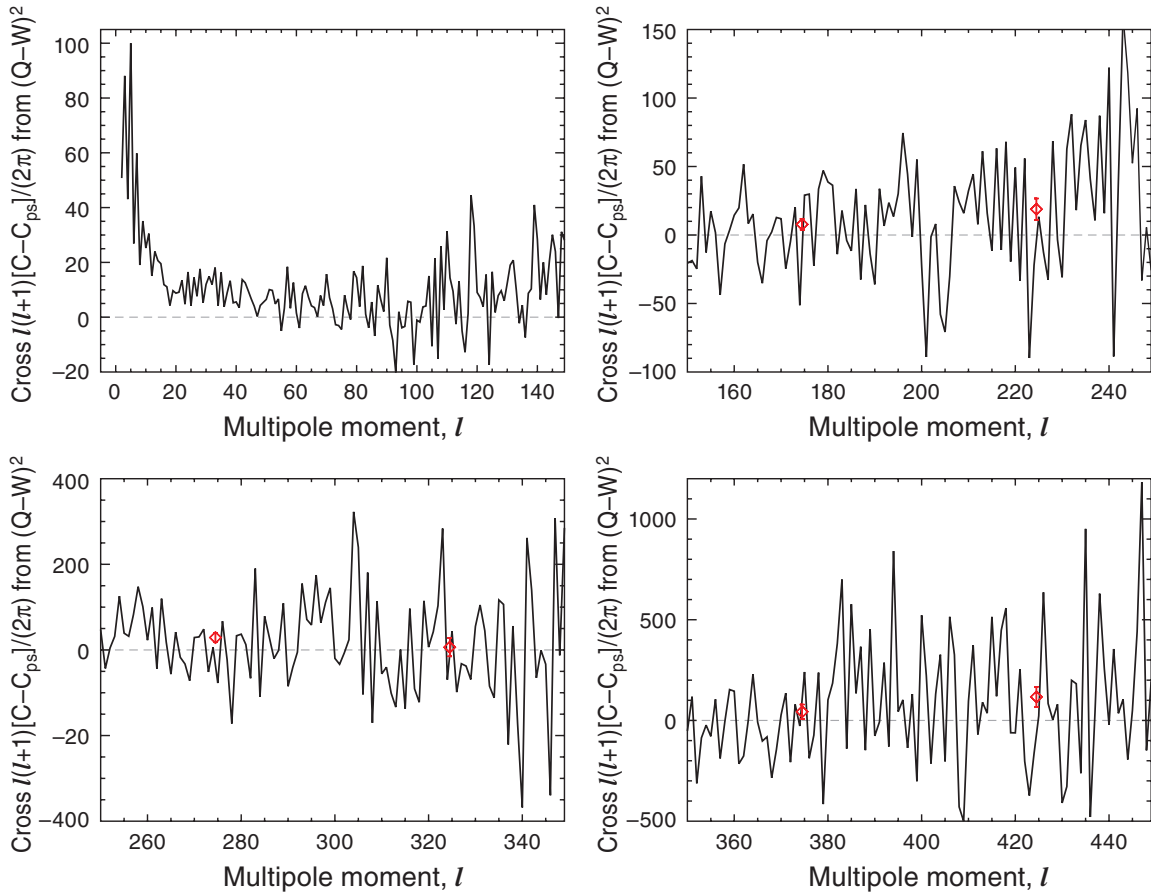
Figure 6. Power spectrum of the difference between foreground-reduced maps. Q band minus W band is shown here, with a point source contribution subtracted off. Note the changing scale between panels. Red points with error bars are averages over bins with $\Delta \ell = 50$. Deviations from zero are below $100\,\mu K^2$ outside the KQ85y7 mask, and the upper bound to foreground contamination in the foreground-reduced maps is $15\,\mu K$.

subtraction. The bottom panels show the same data and fits, but where all temperatures have had the 0.408–22 GHz slope divided out, to facilitate comparison with Figure 9 of Kogut et al. (2009). The ARCADE data show a clear deficit over the 3–10 GHz range, which cannot be explained with power-law foregrounds alone; a fit including a spinning dust component is much more consistent. Dotted, dashed, and dash-dotted lines in the figure show the contribution of each individual component to the total, with thermal dust and spinning dust shown together. In the spinning dust model, synchrotron emission is weak in the *WMAP* bands, where free–free is the dominant emission process. At 93° longitude the spinning dust emission is approximately as bright as the free–free emission at 23 GHz, and at 34° longitude it is several times fainter at all frequencies.

4. FOREGROUND RESULTS

4.1. Residuals in Template-cleaned Maps

As a test of the template-based foreground subtraction process, power spectra of difference maps were made. Figure 6 shows the power spectrum of the difference between the foreground-reduced Q-band and W-band maps, with the point source contribution to the power spectrum subtracted off. Averaging over bins of $\Delta \ell = 50$, no bin with more than $120\,\mu K^2$ of power is seen, with an upper limit of $\sim 220\,\mu K^2$ in power ($15\,\mu K$ in amplitude), and the results are consistent with zero within the expected error. For comparison, CMB power in the range $30 < \ell < 500$ is $1000\,\mu K^2$ or more (Larson et al.

2011). Differences between foreground-reduced V band and W band were also computed, and the power in that case was even smaller.

4.2. Polarization Power Spectra of Synchrotron and Dust

While Galactic foregrounds are not fully described by a two-point function (i.e., an angular power spectrum), due to the importance of the CMB it is often useful to examine the power spectrum of foregrounds. Specifically, the relevant quantity to calculate is the contribution of foreground emission to the angular power spectrum in a particular patch of sky of interest for CMB analysis.

A general trend of $\ell(\ell + 1)C_\ell \sim \ell^{-0.6}$ was found from examination of raw polarization data outside the P06 mask (Page et al. 2007), as the result of a combined fit to *WMAP* data in both multipole and frequency space. With the MCMC fitting procedure it is possible to separate polarized synchrotron from dust and examine the two components individually. The results, shown in Figure 7, show behavior largely consistent with the previous analysis.

In detail, MCMC maps from the "base" model including Haslam data were used. Power spectra from the spinning dust model MCMC maps were also inspected and found to be nearly identical at large scales. A union of the polarization analysis mask and the mask of pixels flagged by the MCMC was applied, and the C_ℓ^{EE} and C_ℓ^{BB} spectra were computed for both synchrotron and dust. As the MCMC process uses 1 deg smoothed maps, an appropriate correction for the beam window
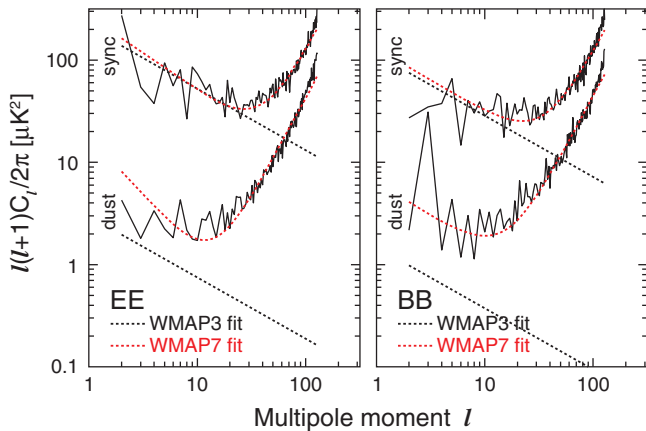
Figure 7. Power spectra of polarized foreground components as determined by the MCMC model. On the left are C_ℓ^{EE} and on the right are C_ℓ^{BB}; for foregrounds these should be of comparable magnitude. The black dotted lines are the foreground fit to raw three-year WMAP data from Page et al. (2007), and the red dotted lines are the combined foreground and noise fit to MCMC maps from this work, with coefficients given in Table 4. Synchrotron results are in good agreement with the previous analysis. The seven-year dust results spectra appear to have a higher amplitude, but the signal-to-noise for $\ell \geqslant 10$ is 2.8 or less for dust.

Table 4
Foreground Power Spectrum Parameters

Component	$\mathcal{B}_c$ (μK^2)[a]	m[a]	N (μK)[a]
Synchrotron EE	271 ± 31	-0.73 ± 0.04	0.109 ± 0.001
Synchrotron BB	130 ± 8.6	-0.61 ± 0.02	0.107 ± 0.001
Dust EE	17.7 ± 2.5	-1.13 ± 0.06	0.065 ± 0.001
Dust BB	6.41 ± 1.1	-0.65 ± 0.06	0.066 ± 0.001

Note. [a] Quoted errors are only statistical uncertainty from the fitting process.

function was applied. Each power spectrum was then fit with a model consisting of a power law plus a pixel noise term

$$\ell(\ell+1)C_\ell^{XX}/2\pi = \mathcal{B}_c\ell^m + \ell(\ell+1)N^2, \qquad (11)$$

where $\mathcal{B}_c$ is the amplitude for foreground component c, m is the power-law index, and N is the noise amplitude.

Values for the fit parameters and an estimate of their errors can be found in Table 4. Because the power spectra are taken from highly processed maps, detailed error propagation is difficult. We used the diagonal portion of the published C_ℓ Fisher errors plus cosmic variance to perform the fit; covariance between multipoles will cause the true errors to be somewhat larger. If all foreground power spectra are assumed to have the same power-law behavior, then the weighted mean $m = -0.67 \pm 0.24$.

4.3. Free–Free Emission

That the ratio of radio brightness to Hα intensity from the MEM fits is consistently lower than the expected value has long been of concern. The MCMC fits offer some insight, though unfortunately do not resolve the difference. The most important difference between the MEM and the MCMC fits in this case is that the MEM uses the Hα template as a prior in low signal-to-noise regions, while the MCMC fit does not. The result is that in regions of low signal, the degeneracy between synchrotron and free–free causes the MCMC uncertainty in free–free brightness to be large enough to accommodate a large range of possible radio to Hα ratios. Therefore, it becomes necessary to exclude low signal-to-noise regions when calculating the ratio from the MCMC maps.

Due to the uncertainty in the reddening correction to the Hα map itself, it is also customary to exclude regions where the Hα optical depth due to reddening is greater than some value. This unfortunately excludes regions that would otherwise have *high* signal-to-noise. These two cuts together exclude much of the MCMC maps as unsuitable for analysis. The remaining portion of sky contains bright, mostly discontiguous free–free regions which are also low on dust (and therefore Hα extinction). The largest of these is a region around Gum nebula.

Starting with the free–free maps made from the MCMC process, we define a S/N map as the free–free amplitude divided by the square root of the MCMC variance. We then keep only pixels with S/N > 10, $\tau < 1$, and no MCMC error flags. The pixels that remain are largely concentrated in three regions, the Gum nebula, the Ophiuchus complex, and the Orion/Eridanus bubble. The Gum region contains nearly half of the pixels surviving the cut, so for simplicity we restrict our attention to this region, defining it to be any pixel within $30°$ of $(260°, 0°)$ in Galactic coordinates. Summing all free–free emission in this region and dividing by the total Hα intensity in this region, we estimate that the ratio of radio brightness to Hα intensity h_{ff} is 9.3 ± 3.2 μK R^{-1} at the K band for the spinning dust fit, with similar values for the other MCMC models. The uncertainty comes from the variance of the ratio from pixel to pixel; increasing the signal-to-noise threshold decreases the uncertainty somewhat but does not significantly affect the central value. While the central value is consistent with the prediction of 11.4 μK R^{-1} within this uncertainty, it is also compatible with a reduced electron temperature of 5500 K, an overestimation of the reddening correction by $\Delta\tau = 0.3$, or some combination of the two.

4.4. Spinning Dust Emission

We find that in order to best fit the 408 MHz data, the spinning dust fit from the five-year MCMC process needs to have its peak frequency adjusted downward by 14% from $\nu_{sd} = 4.9$ GHz to $\nu_{sd} = 4.2$ GHz, nearly independent of the offset used for the map. For this value, the frequency at which the *flux* from the spinning dust component alone peaks is 21 GHz. We have not found any improvement in the fit from including "warm" spinning dust with a peak near 40 GHz, as found by Dobler & Finkbeiner (2008b). The 408 MHz data also introduce some tension, such that the spinning dust model no longer is such a large improvement inside the Galactic plane; in this region $\chi^2_\nu = 1.80$ for the spinning dust model, compared to $\chi^2_\nu = 2.61$ for the "base" fit, for 8.7 effective number of degrees of freedom (see Kunz et al. 2006; Gold et al. 2009 for detailed description of effective dof). These values are for the fitted offset of 7.4 K for the 408 MHz map; using a larger offset value of 11.4 K provides slightly better fits ($\Delta\chi^2_\nu = 0.008$) for the spinning dust models, while a smaller offset value of 3.4 K provides slightly better fits ($\Delta\chi^2_\nu = 0.074$) for models without spinning dust.

The steepening synchrotron model fits the combination of *WMAP* and 408 MHz data nearly equally as well as the spinning dust model, with $\chi^2_\nu = 1.81$ in the Galactic plane. The amplitude of c_s is large in the Galactic plane, implying a change of spectral index greater than one per e-fold increase in frequency. This is a sharper change than models of synchrotron steepening predict from aging effects, and so the physical motivation for the model is unclear.

The ARCADE data are not directly comparable to the MCMC fits, due to their greatly different beam and sky coverage. The
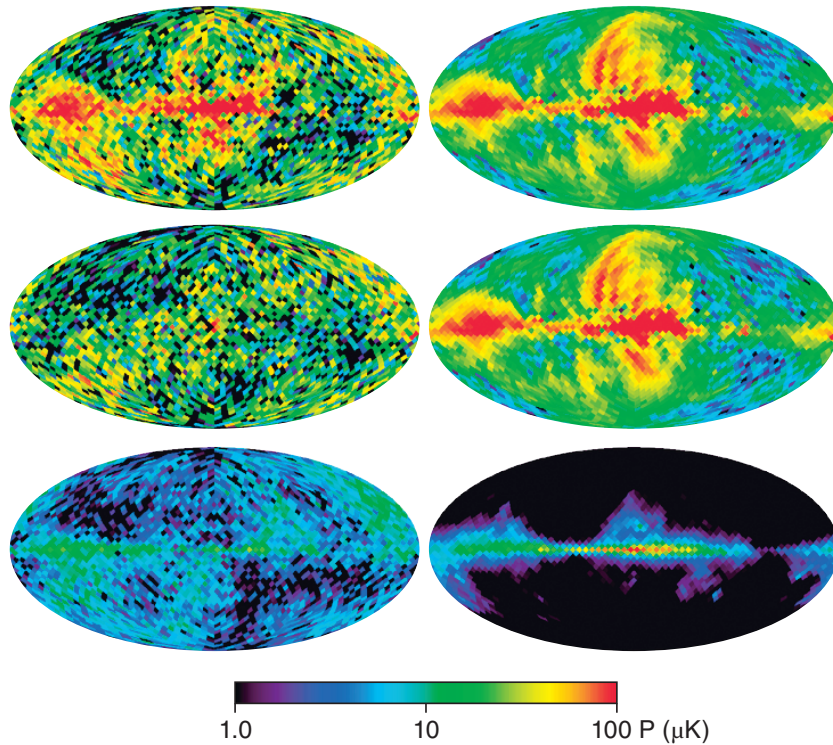
Figure 8. Comparison of the templates used for polarization cleaning to a low-resolution ($N_{side} = 16$) MCMC fit to polarization data using a three-component model with fixed spectral indexes to search for any hard synchrotron component. The left column shows the results of the MCMC fit to polarization data using three components: soft synchrotron ($\beta = -3.1$) at top, hard synchrotron ($\beta = -2.39$) at middle, and dust ($\beta = +2.0$) at bottom. For comparison, the right column shows the templates used for polarization cleaning: synchrotron at top and middle, and dust at bottom. All plots are of polarization intensity $P = \sqrt{Q^2 + U^2}$, with a logarithmic scale from 1 to 100 μK. Synchrotron intensity is measured at a reference frequency of 23 GHz, and dust intensity at 94 GHz. The MCMC maps are noisy and have been corrected for a noise bias in P caused by noise in Q and U. Excess noise in the plane of the ecliptic due to the scan pattern is also clearly visible in the MCMC fits. Given the noise level, hard synchrotron emission does not appear to be significant.

spinning dust component of the fits for the two regions in the Galactic plane, however, does peak in flux at 22 GHz, consistent with the location of the MCMC peak. The relative amplitude is more difficult to ascertain. For ARCADE, spinning dust is 29% (at $l = 33.8$) or 43% (at $l = 93$) of the total flux at 22 GHz, but with the large beam it is impossible to say whether the spinning dust component is relatively diffused or localized on the Galactic plane. For the MCMC fits to *WMAP* data, the mean spinning dust fraction is considerably lower, at 18% inside the KQ85y7 mask, which suggests that spinning dust may be patchy. Outside of the KQ85y7 mask, the MCMC fits show a mean level of spinning dust consistent with zero within the uncertainty of the fit.

4.5. The Haze

In its low-frequency bands, *WMAP* observes an excess of emission above what was predicted by scaling the 408 MHz to higher frequencies using the expected spectral index for synchrotron emission. Determining the exact nature of this emission has proven difficult; *WMAP* has generally treated it as a hard (flatter spectrum) synchrotron component without attempting to explain the origin of such a component. Other suggestions have involved combinations of different types of spinning dust (Finkbeiner 2004; Dobler & Finkbeiner 2008b), though there is typically still a residual "haze" even after those components are fit out (Dobler & Finkbeiner 2008a).

It has been argued that this remainder low-frequency emission has an ellipsoidal shape and is consistent with hard synchrotron emission, possibly from dark matter annihilation in the core
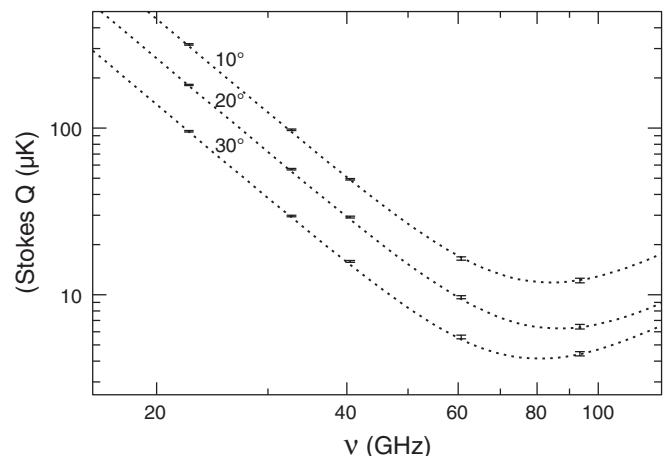
Figure 9. Frequency spectrum of polarized emission around the Galactic center. Average antenna temperature of Stokes Q is shown for three oval regions defined by $\sqrt{l^2 + (2b)^2} < 10°, 20°, 30°$, where l and b are Galactic longitude and latitude. Stokes U is negligible at all frequencies except the W band. Error bars indicate statistical uncertainty from the diagonal part of the pixel–pixel noise matrix. Dotted lines show the sum of a synchrotron component with $\beta = -3.2$ and a dust component with $\beta = +2.0$; in all cases this two-component model is sufficient to explain the observations.

of the Galaxy (Hooper et al. 2007). There has been tentative detection of a haze in gamma rays using preliminary data from the *Fermi* telescope (Dobler et al. 2010).

Interpretation of polarization information toward the center of the Galaxy is difficult, as depolarization through line-of-
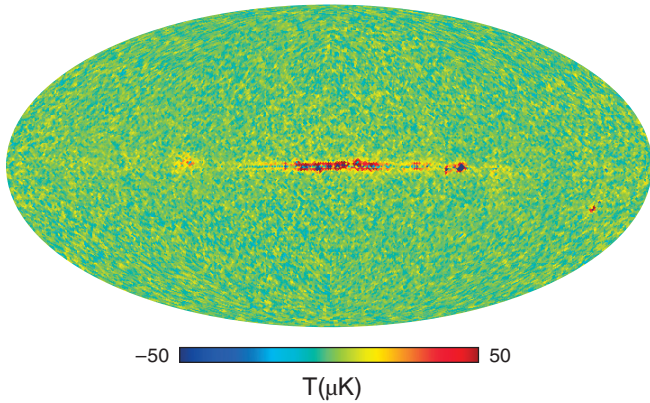
Figure 10. Comparison between a simulated input sky and the resulting maps after scanning and map making. The K band is shown; differences in other bands are at least four times smaller. The only visible structure, along the Galactic plane, is entirely consistent with residuals from gain reconstruction within the quoted uncertainties (0.2%).

sight changes in the orientation of the magnetic field can affect the signal significantly. Nonetheless, we search for a hard component in the polarization data using a simplified version of the low-resolution MCMC fit of Dunkley et al. (2009a), shown in Figure 8. We do not detect any significant change of synchrotron spectral index as a function of Galactocentric distance.

This special fit was done at HEALPix $N_{side} = 16$ using only *WMAP* polarization data, so as to be insensitive to any uncertainties regarding the presence or absence of spinning dust. The fit attempts to model the sky as a sum of three power-law foregrounds: a soft synchrotron component with $\beta = -3.1$, a hard synchrotron component with $\beta = -2.39$, and a dust component with $\beta = +2.0$. These power-law indices were those suggested by the work of Dobler & Finkbeiner (2008a).

The results of the fit are shown in Figure 8. Residuals after the fit are small compared to the noise, and over all bands the mean reduced χ^2 per pixel is 1.1. For comparison, the synchrotron and dust templates used for polarization cleaning are shown in

the right column of the figure. The MCMC result for the soft synchrotron template appears to be essentially a noisy version of the synchrotron template, indicating that the K band is indeed a good proxy for polarized synchrotron emission. For dust, the MCMC and template results differ somewhat. The MCMC hard synchrotron results show no spatial structure beyond *WMAP*'s noise pattern and are consistent with the level of noise bias expected in a map of $P = \sqrt{Q^2 + U^2}$.

Figure 9 shows the frequency spectrum of polarized emission for elliptical regions around the Galactic center. In these regions the polarization direction is nearly vertical, and so the Stokes U parameter is negligible for bands K through V and small for W band. The spectra for three different regions are shown, sized $10° \times 5°$, $20° \times 10°$, and $30° \times 15°$. We find no evidence for emission other than soft synchrotron ($\beta = -3.2$) and dust ($\beta = +2.0$), in particular, no "haze" component appears to be necessary for polarization.

5. FOREGROUND SYSTEMATICS AND TESTS

5.1. Pipeline Simulation

A full simulation of the *WMAP* instrument was used to test the MCMC and template cleaning methods, in order to investigate the interaction of systematics in both time-domain data and sky maps. Starting with a set of synthetic sky inputs for the CMB and foregrounds (described below), the scanning of the instrument was applied to the inputs to produce a time stream of data, which was then put through the same entire calibration and map-making pipeline as used for real data.

A random CMB realization was created, starting from the publicly available best-fit cosmological parameters of a ΛCDM model to the combination of five-year *WMAP* data with supernovae and baryon acoustic oscillations. The CAMB software package (Lewis et al. 2000) was used to generate a model power spectrum and then SYNFAST (Gorski et al. 2005) was used to generate the random sky realization.

Several foregrounds were then added, using high-resolution templates. A synchrotron intensity template was constructed
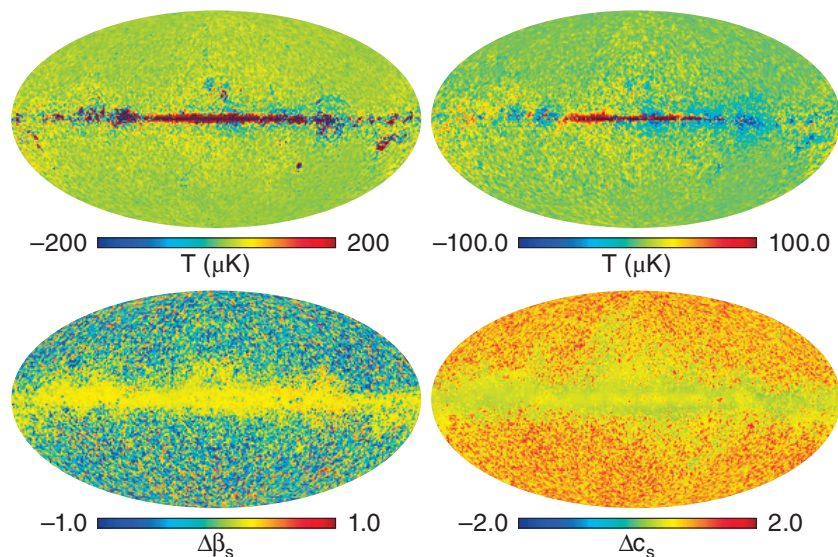
Figure 11. Comparison between the input foreground spatial and spectral behavior and that recovered by the MCMC fit. Upper left: difference between MCMC result and input $T_s + T_f$. Upper right: difference between MCMC result and input T_d. Lower left: difference between MCMC result and input β_s. Lower right: difference between MCMC result and input c_s. The main feature is that the simulated synchrotron model contained more steepening in the synchrotron spectrum than the model allowed for, which then biases the recovered β_s by 0.2 in high signal-to-noise regions. The apparent bias off the Galactic plane only occurs where the signal-to-noise is low and the parameter error is larger than the bias.

from the 408 MHz data of Haslam et al. (1981), and scaled
to higher frequencies with a spectral index with both spatial
variations and steepening, in order to test the effects of fitting
a simpler model to complicated synchrotron spectral features.
A free–free template was made from an extinction-corrected
version of the Hα map of Finkbeiner (2003), with a few bright
high-latitude sources removed and assuming a spectral index
of $\beta = -2.15$. The dust template is the 94 GHz prediction
of model 8 of Finkbeiner et al. (1999), scaled to other *WMAP*
frequencies with a spectral index of $\beta = 2.0$.

Once the simulation inputs were generated, they were passed
through a simulation of *WMAP*'s scan strategy, including such
effects as thermal gains and baselines in the time-ordered data,
loss imbalance and bandpass mismatches, and detector noise
with a $1/f$ component. This simulated time-ordered data was
then processed and analyzed in exactly the same way as real
observations.

Figure 10 shows a comparison between the "true" simulated
input sky maps and the output maps after the map-making
process. These are used to test the template cleaning method, as
the simulated input foregrounds are generated with structure on
scales smaller than the templates used for cleaning. However, no
effects due to residual foreground contamination are seen; the
cosmological parameters used as input are recovered. Figure 11
then compares the results of the MCMC foreground fit to the
input foreground behavior. The largest difference found between
the input and output maps from the simulation is in the Galactic
plane. This difference is a fraction of a percent of the total
intensity, and is entirely consistent with the expected uncertainty
in the gain reconstruction.

The MCMC reconstructs the foregrounds to within the
MCMC error, which includes large covariance between syn-
chrotron and free–free brightness. The most important system-
atic deviation was in the reconstructed synchrotron spectral
shape, parameterized with β_s and c_s. This is largely because
the simulated model spectrum was more complicated than a
power law with constant steepening. This resulted in a bias in
the recovered β_s bias of approximately +0.2 in the Galactic
plane. This bias was still within the MCMC errors.

5.2. Testing Beam Systematics with Six-month Maps

Over the course of a full year, the *WMAP* satellite's scan
pattern is such that most points on the sky are observed with a
nearly uniform distribution of orientations. The distribution is
most symmetric at the ecliptic poles, and least symmetric on
the ecliptic plane. Fortuitously, the Galactic center lies near the
plane of the ecliptic, with a large angle between the planes of
the Galaxy and the ecliptic. The result is that the year can be
divided into halves, where *WMAP*'s scanning direction when
observing the inner Galactic plane is rotated 180° between the
two halves.

This means that maps made from such six-month segments
of data are sensitive to beam asymmetries, particularly those
where the beam is not equal to itself rotated 180°. This effect is
largest in the K band. Figure 12 shows the measured difference
of the beam between the six-month intervals, a simple beam
model which recreates the effect, and sky maps of the residuals
between six-month sky maps and a full year of observation.

We used this effect to investigate the sensitivity of foreground
fitting to beam systematics. For the first five years of data, each
year was divided into six months of one scan direction relative
to the Galactic center, and six months where the scan direction
was reversed. These were then stacked to produce two sets of
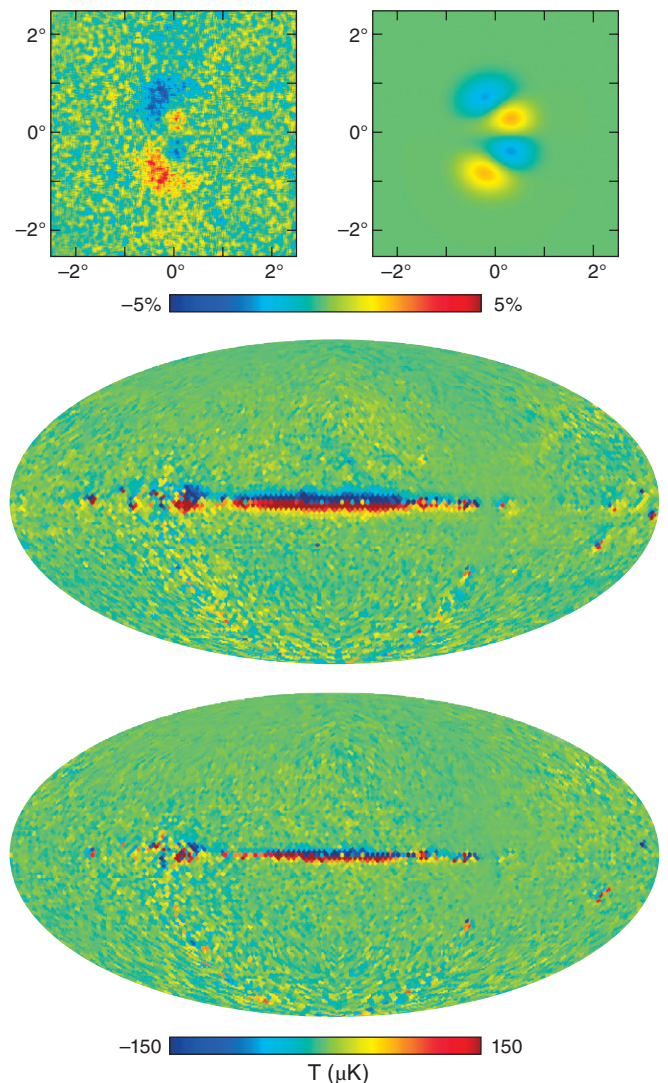
Figure 12. Flight data and a simple model for differences between maps made
with six months of data and those made with a full year. Top left: difference
between observed K1 beam and 180° rotated K1 beam (scale is ±5%). Top right:
difference between a model beam consisting of a sum of Gaussians and its 180°
rotation. Middle: observed difference map between six months and a full year
for the K band. Bottom: simulated difference map created using the beam of the
upper right panel. While this simple beam model does not completely resemble
the observed beam, it qualitatively reproduces the effects observed in the maps.

five-year maps, where the scan directions along the ecliptic have
the greatest relative asymmetry. The MCMC foreground fitting
was then run for both sets of maps.

The result is shown in Figure 13. Since the largest beam
difference is in the K band, low-frequency foregrounds are most
strongly affected. The spectral index inferred for synchrotron
shows a small gradient across the Galactic plane, with amplitude
$\sim \pm 0.1$ for $|b| < 5°$. The effect on the CMB is limited; variance
outside the KQ85y7 mask is less than $480\,\mu K^2$ (an order of
magnitude smaller than intrinsic variance of the CMB), and
most of this is from MCMC variations in the dust model. We also
emphasize that the six-month intervals were chosen to maximize
this asymmetry, which is not seen when full years of data are
used to make maps.
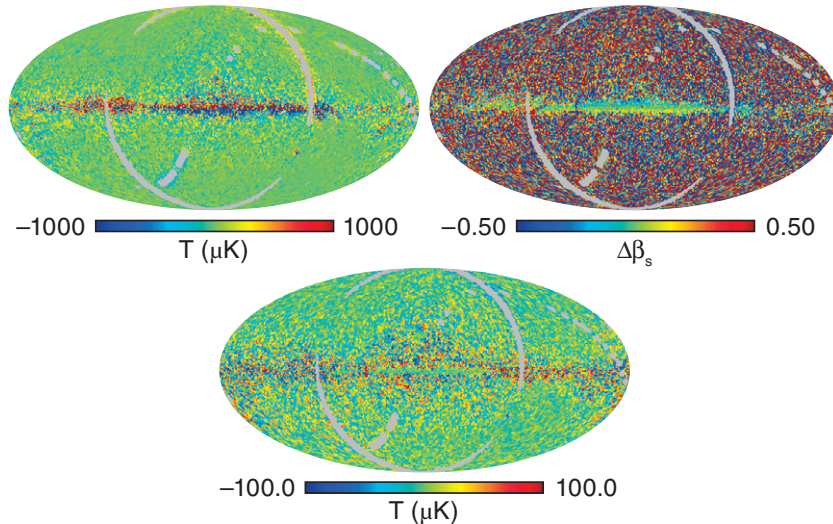
Figure 13. Effect of beam anisotropy on the MCMC foreground fits, using stacks of six-month maps. Pixels near the boundary of the six-month scans are masked (gray) due to poor coverage. Top left: difference in MCMC synchrotron temperature. As the combination of synchrotron and free–free is largely constrained to match the K band, the free–free difference is nearly the opposite of this map. Top right: difference in MCMC synchrotron spectral index. Away from the Galactic plane this map is mostly noise, but a slight gradient with $\Delta\beta_s = \pm 0.1$ is visible near the plane. Bottom: difference in MCMC CMB temperature. Most of the variation is noise in the MCMC dust model, rather than due differences between the six-month maps.

6. POINT SOURCE CATALOGS

As for the five-year analysis, two separate methods have been used for identification of point sources from sky map data and two separate point source tables have been produced. The first method has been used in all *WMAP* data releases and is largely unchanged from the five-year analysis (Wright et al. 2009). The seven-year S/N map in each wavelength band is filtered in harmonic space by $b_l/(b_l^2 C_l^{cmb} + C_l^{noise})$ (Tegmark & de Oliveira-Costa 1998; Refregier et al. 2000), where b_l is the transfer function of the *WMAP* beam response (Jarosik et al. 2011), C_l^{cmb} is the CMB angular power spectrum, and C_l^{noise} is the noise power. The filtering suppresses CMB and Galactic foreground fluctuations relative to point sources. For peaks in the filtered maps that are $>5\sigma$ in any band, the unfiltered temperature maps are fit with the sum of a Gaussian profile and a planar base level. The Gaussian amplitude is converted to a source flux density using the conversion factors given in Table 2 of Jarosik et al. (2011), and flux density uncertainty is calculated from the 1σ uncertainty in the fit amplitude. The source is entered into the catalog if the fit source width is within a factor of two of the beam width. Flux density values are entered for bands where they exceed 2σ. A point source catalog mask is used to exclude sources in Galactic plane and Magellanic cloud regions. This mask has changed from the five-year analysis. A map pixel is outside of the new mask if it is either outside of the diffuse component of the seven-year KQ85y7 temperature analysis mask or outside of the five-year point source catalog mask. This mask admits 82% of the sky, compared to 78% for the five-year version. We identify possible 5 GHz counterparts to the *WMAP* sources by cross-correlating with the GB6 (Gregory et al. 1996), PMN (Griffith et al. 1994, 1995; Wright et al. 1994, 1996), Kühr et al. (1981), and Healey et al. (2009) catalogs. A 5 GHz source is identified as a counterpart if it lies within 11′ of the *WMAP* source position (the mean *WMAP* source position uncertainty is 4′ and can be twice as large for faint sources near the detection threshold). When two or more 5 GHz sources are within 11′, the brightest is assumed to be

the counterpart and a multiple identification flag is entered in the catalog.

The second method of point source identification is the CMB-free method originally applied to one-year and three-year V- and W-band maps by Chen & Wright (2008) and to five-year V- and W-band maps by Wright et al. (2009). The method used here is that applied to five-year Q, V, and W maps by Chen & Wright (2009). The V- and W-band maps are smoothed to Q-band resolution. A special ILC map is then formed from the three maps using weights such that CMB fluctuations are removed, flat-spectrum point sources are retained with fluxes normalized to Q band, and the variance of the ILC map is minimized. The ILC map is filtered to reduce the noise and suppress large angular scale structure. Peaks in the filtered map that are $>5\sigma$ and outside of the seven-year point source catalog mask are identified as point sources, and source positions are obtained by fitting the beam profile plus a baseline to the filtered map for each source. Source fluxes are estimated by integrating the Q, V, and W temperature maps within 1°.25 of each source position, with a weighting function to enhance the contrast of the point source relative to background fluctuations, and applying a correction for Eddington bias due to noise. Detected sources were identified with sources in the five-year *WMAP* five-band catalog (Wright et al. 2009) and the five-year QVW catalog (Chen & Wright 2009) if the positions agreed within 15′. They were also correlated against the 5 GHz GB6, PMN, and Kühr et al. (1981) catalogs to identify possible 5 GHz counterparts within 15′. Optical identifications were made by searching the NASA Extragalactic Database.

The seven-year five-band point source catalog is presented in Table 5 and the seven-year QVW point source catalog is presented in Table 6. The five-band catalog contains 471 sources, the QVW catalog contains 417 sources, and the two catalogs have 346 sources in common. For comparison, the five-year five-band catalog contained 390 sources, the five-year QVW catalog contained 381 sources, and they had 287 sources in common. Differences in the source populations detected by the two search methods do not appear to be mainly due to

13

Table 5
WMAP Five-band Point Source Catalog

R.A. (hms)	Decl. (dm)	ID	K (Jy)	Ka (Jy)	Q (Jy)	V (Jy)	W (Jy)	α	5 GHz ID
00 03 30	−47 50		0.7 ± 0.06	0.7 ± 0.05	0.7 ± 0.07	. . .	. . .	0.1 ± 0.5	. . .
00 06 07	−06 23	060	2.3 ± 0.06	2.1 ± 0.1	2.1 ± 0.1	1.9 ± 0.2	. . .	−0.2 ± 0.2	PMN J0006-0623
00 10 37	11 01		0.9 ± 0.07	1.0 ± 0.09	1.0 ± 0.1	1.2 ± 0.2	1.2 ± 0.3	0.2 ± 0.3	GB6 J0010+1058
00 12 47	−39 52	202	1.3 ± 0.04	1.2 ± 0.07	0.9 ± 0.07	0.8 ± 0.1	0.7 ± 0.2	−0.4 ± 0.2	PMN J0013-3954
00 19 12	26 01		0.7 ± 0.06	0.5 ± 0.09	0.7 ± 0.1	0.5 ± 0.1	. . .	−0.3 ± 0.5	GB6 J0019+2602
00 19 40	20 20		1.0 ± 0.05	1.1 ± 0.07	0.9 ± 0.08	1.1 ± 0.2	. . .	0.0 ± 0.3	GB6 J0019+2021
00 25 22	−26 03		0.9 ± 0.05	0.7 ± 0.07	0.5 ± 0.08	. . .	. . .	−0.8 ± 0.5	PMN J0025-2602[a]
00 26 06	−35 10		1.1 ± 0.06	1.2 ± 0.08	1.4 ± 0.1	1.1 ± 0.1	0.5 ± 0.2	0.0 ± 0.3	PMN J0026-3512
00 29 33	05 54		1.1 ± 0.05	1.2 ± 0.08	1.1 ± 0.09	0.6 ± 0.1	1.0 ± 0.2	−0.2 ± 0.2	GB6 J0029+0554B[a]
00 38 14	−24 59		0.9 ± 0.05	0.9 ± 0.09	0.8 ± 0.1	1.1 ± 0.2	. . .	0.1 ± 0.4	PMN J0038-2459
00 43 07	52 08		1.0 ± 0.03	0.6 ± 0.06	0.5 ± 0.07	0.4 ± 0.1	. . .	−1.2 ± 0.4	GB6 J0043+5203
00 47 20	−25 13	062	1.2 ± 0.05	0.9 ± 0.09	1.1 ± 0.09	1.0 ± 0.1	0.9 ± 0.2	−0.2 ± 0.2	PMN J0047-2517
00 47 57	−73 13		. . .	. . .	1.7 ± 0.06	1.3 ± 0.1	1.1 ± 0.2	−0.6 ± 0.3	PMN J0047-7308
00 49 19	−42 21		1.3 ± 0.03	1.0 ± 0.05	0.5 ± 0.07	. . .	. . .	−0.8 ± 0.3	. . .
00 49 48	−57 39	179	1.6 ± 0.05	1.5 ± 0.06	1.3 ± 0.06	1.3 ± 0.1	0.7 ± 0.2	−0.3 ± 0.2	PMN J0050-5738
00 50 47	−06 49		1.2 ± 0.05	1.3 ± 0.08	1.0 ± 0.1	1.3 ± 0.2	. . .	−0.0 ± 0.3	PMN J0051-0650
00 50 48	−42 23		1.2 ± 0.03	1.3 ± 0.05	1.1 ± 0.06	0.6 ± 0.1	0.8 ± 0.3	−0.2 ± 0.2	PMN J0051-4226
00 50 57	−09 26	077	1.1 ± 0.05	1.2 ± 0.09	0.9 ± 0.08	1.2 ± 0.3	. . .	−0.0 ± 0.3	PMN J0050-0928
00 57 25	55 02		. . .	. . .	0.7 ± 0.07	0.4 ± 0.1	. . .	−1.6 ± 2	. . .
00 57 54	30 21		0.8 ± 0.08	1.1 ± 0.2	0.9 ± 0.2	0.9 ± 0.3	. . .	0.2 ± 0.6	GB6 J0057+3021
00 59 39	−56 56		0.7 ± 0.05	0.9 ± 0.07	0.9 ± 0.06	0.6 ± 0.1	. . .	0.2 ± 0.3	PMN J0058-5659
01 00 15	−72 12		3.2 ± 0.04	2.4 ± 0.06	1.7 ± 0.06	1.1 ± 0.1	0.8 ± 0.3	−1.0 ± 0.1	PMN J0059-7210
01 06 07	48 23		0.6 ± 0.05	0.9 ± 0.08	0.7 ± 0.08	0.4 ± 0.2	. . .	0.3 ± 0.5	GB6 J0105+4819
01 06 44	−40 35	171	2.7 ± 0.04	2.7 ± 0.06	2.5 ± 0.08	2.1 ± 0.1	1.3 ± 0.3	−0.2 ± 0.09	PMN J0106-4034
01 08 29	13 19	079	1.5 ± 0.05	1.1 ± 0.09	0.8 ± 0.1	. . .	. . .	−1.0 ± 0.5	GB6 J0108+1319
01 08 43	01 35	081	1.8 ± 0.05	1.7 ± 0.07	1.5 ± 0.09	1.5 ± 0.2	. . .	−0.2 ± 0.2	GB6 J0108+0135[a]
01 15 21	−01 29		1.0 ± 0.05	1.3 ± 0.07	1.0 ± 0.08	1.1 ± 0.1	. . .	0.2 ± 0.2	PMN J0115-0127
01 15 50	−73 20		0.6 ± 0.08	0.7 ± 0.06	0.5 ± 0.08	0.7 ± 0.1	. . .	0.0 ± 0.5	PMN J0114-7318[a]
01 16 20	−11 37		1.2 ± 0.06	0.9 ± 0.09	1.0 ± 0.1	1.3 ± 0.2	. . .	−0.1 ± 0.3	PMN J0116-1136
01 21 46	11 50		1.4 ± 0.05	1.3 ± 0.1	1.3 ± 0.1	0.9 ± 0.2	0.9 ± 0.2	−0.3 ± 0.3	GB6 J0121+1149
01 25 18	−00 10	086	1.1 ± 0.06	1.2 ± 0.09	1.1 ± 0.08	0.9 ± 0.2	. . .	−0.0 ± 0.3	PMN J0125-0005[a]
01 26 10	−52 39		0.4 ± 0.04	0.2 ± 0.05	0.4 ± 0.07	0.5 ± 0.1	1.2 ± 0.2	0.8 ± 0.4	PMN J0126-5228
01 32 38	−16 53	097	1.8 ± 0.05	1.7 ± 0.07	1.6 ± 0.09	1.4 ± 0.1	1.6 ± 0.2	−0.1 ± 0.1	PMN J0132-1654
01 33 09	−52 00	168	0.9 ± 0.05	1.1 ± 0.07	0.7 ± 0.06	. . .	. . .	−0.2 ± 0.3	PMN J0133-5159
01 33 27	−36 26		0.7 ± 0.05	0.6 ± 0.09	0.4 ± 0.1	. . .	. . .	−0.7 ± 0.7	PMN J0134-3629[a]
01 37 01	47 53	080	3.8 ± 0.05	3.8 ± 0.07	3.5 ± 0.08	3.2 ± 0.2	1.7 ± 0.3	−0.2 ± 0.08	GB6 J0136+4751
01 37 31	33 15		0.9 ± 0.06	0.6 ± 0.1	0.4 ± 0.1	. . .	. . .	−1.4 ± 1	GB6 J0137+3309
01 37 37	−24 28		1.3 ± 0.05	1.3 ± 0.08	1.6 ± 0.1	1.3 ± 0.2	. . .	0.1 ± 0.2	PMN J0137-2430
01 49 13	05 54		1.0 ± 0.06	0.7 ± 0.08	0.8 ± 0.1	. . .	2.2 ± 1	−0.2 ± 0.4	GB6 J0149+0555
01 52 26	22 09		1.0 ± 0.09	1.3 ± 0.1	1.2 ± 0.1	1.3 ± 0.2	. . .	0.2 ± 0.3	GB6 J0152+2206
02 04 49	15 13	092	1.3 ± 0.05	1.3 ± 0.1	1.2 ± 0.1	1.2 ± 0.2	. . .	−0.1 ± 0.3	GB6 J0204+1514
02 05 02	32 12	085	2.0 ± 0.06	1.8 ± 0.09	1.5 ± 0.1	1.1 ± 0.2	. . .	−0.4 ± 0.2	GB6 J0205+3212
02 05 10	−17 03		0.8 ± 0.08	. . .	0.9 ± 0.1	0.7 ± 0.2	. . .	0.0 ± 0.5	PMN J0204-1701
02 10 51	−51 00	158	2.8 ± 0.04	2.7 ± 0.07	2.8 ± 0.08	2.6 ± 0.1	1.8 ± 0.2	−0.1 ± 0.09	PMN J0210-5101
02 18 18	01 39	096	1.5 ± 0.04	1.4 ± 0.07	0.9 ± 0.09	1.1 ± 0.3	. . .	−0.5 ± 0.3	GB6 J0217+0144
02 20 49	35 58		1.3 ± 0.05	1.3 ± 0.07	1.0 ± 0.08	0.9 ± 0.1	1.0 ± 0.3	−0.3 ± 0.2	GB6 J0221+3556
02 22 48	−34 39	137	1.0 ± 0.03	1.0 ± 0.04	0.8 ± 0.05	0.5 ± 0.1	. . .	−0.3 ± 0.2	PMN J0222-3441
02 23 10	43 03	084	1.9 ± 0.05	1.5 ± 0.08	1.4 ± 0.1	0.9 ± 0.1	. . .	−0.6 ± 0.2	GB6 J0223+4259[a]
02 31 38	−47 42		0.7 ± 0.04	0.9 ± 0.07	0.8 ± 0.06	1.1 ± 0.1	1.2 ± 0.2	0.4 ± 0.2	PMN J0231-4746
02 31 38	13 20		1.4 ± 0.06	1.2 ± 0.08	1.2 ± 0.08	1.0 ± 0.2	. . .	−0.2 ± 0.3	GB6 J0231+1323
02 37 59	28 48	093	3.7 ± 0.06	3.3 ± 0.09	3.1 ± 0.1	2.9 ± 0.2	2.6 ± 0.4	−0.3 ± 0.1	GB6 J0237+2848
02 38 49	16 36		1.4 ± 0.07	1.5 ± 0.1	1.6 ± 0.1	1.6 ± 0.2	1.4 ± 0.4	0.1 ± 0.2	GB6 J0238+1637
02 41 16	−08 21		1.0 ± 0.05	0.8 ± 0.07	0.6 ± 0.08	. . .	. . .	−0.8 ± 0.5	PMN J0241-0815
02 45 19	−44 55		0.5 ± 0.04	0.6 ± 0.08	0.6 ± 0.07	0.6 ± 0.2	0.6 ± 0.2	0.2 ± 0.4	PMN J0245-4459
02 53 33	−54 41	155	2.4 ± 0.04	2.5 ± 0.06	2.4 ± 0.06	2.0 ± 0.1	1.5 ± 0.3	−0.1 ± 0.09	PMN J0253-5441
02 59 31	−00 16		1.2 ± 0.06	1.4 ± 0.08	1.1 ± 0.07	0.9 ± 0.1	. . .	−0.2 ± 0.2	PMN J0259-0020
03 03 36	−62 12	162	1.5 ± 0.05	1.5 ± 0.09	1.5 ± 0.07	1.5 ± 0.1	1.0 ± 0.2	−0.1 ± 0.1	PMN J0303-6211
03 03 43	47 17		0.8 ± 0.06	1.0 ± 0.09	0.8 ± 0.09	0.7 ± 0.1	. . .	0.0 ± 0.4	GB6 J0303+4716
03 08 30	04 05	102	1.4 ± 0.06	1.3 ± 0.1	1.2 ± 0.09	1.0 ± 0.2	0.9 ± 0.3	−0.3 ± 0.3	GB6 J0308+0406
03 09 19	10 27		1.0 ± 0.07	1.3 ± 0.1	1.2 ± 0.09	1.4 ± 0.3	1.2 ± 0.4	0.3 ± 0.3	GB6 J0309+1029
03 09 50	−61 03	160	1.0 ± 0.04	1.2 ± 0.06	0.9 ± 0.05	0.9 ± 0.1	. . .	−0.0 ± 0.2	PMN J0309-6058
03 12 10	−76 46	174	1.1 ± 0.04	1.2 ± 0.07	1.1 ± 0.07	0.9 ± 0.1	1.0 ± 0.3	−0.0 ± 0.2	PMN J0311-7651
03 12 54	01 32		0.8 ± 0.05	0.7 ± 0.1	0.8 ± 0.1	0.7 ± 0.1	0.6 ± 0.3	−0.1 ± 0.4	GB6 J0312+0132
03 19 46	41 31	094	12.2 ± 0.05	9.6 ± 0.08	8.0 ± 0.1	6.2 ± 0.2	4.2 ± 0.4	−0.7 ± 0.03	GB6 J0319+4130
03 20 26	−38 38		. . .	. . .	0.4 ± 0.05	0.2 ± 0.1	. . .	−1.8 ± 3	PMN J0320-3837
03 22 25	−37 11	138	18.6 ± 0.04	12.5 ± 0.05	10.7 ± 0.06	8.6 ± 0.1	. . .	−0.8 ± 0.2	1Jy 0320-37[b]
03 29 48	−23 54	123	1.3 ± 0.04	1.3 ± 0.06	1.2 ± 0.08	1.0 ± 0.1	. . .	−0.1 ± 0.2	PMN J0329-2357

Table 5
(Continued)

R.A. (hms)	Decl. (dm)	ID	K (Jy)	Ka (Jy)	Q (Jy)	V (Jy)	W (Jy)	α	5 GHz ID
03 34 17	−40 07	146	1.3 ± 0.04	1.3 ± 0.06	1.5 ± 0.07	1.3 ± 0.1	. . .	0.1 ± 0.2	PMN J0334-4008
03 37 07	−36 12		0.6 ± 0.06	0.7 ± 0.06	0.6 ± 0.08	0.7 ± 0.2	. . .	0.1 ± 0.5	PMN J0336-3615
03 39 24	−01 43	106	2.5 ± 0.06	2.4 ± 0.1	2.1 ± 0.09	1.9 ± 0.1	2.0 ± 0.3	−0.3 ± 0.1	PMN J0339-0146
03 40 28	−21 20		1.1 ± 0.04	1.1 ± 0.07	1.1 ± 0.08	1.2 ± 0.1	1.0 ± 0.2	0.0 ± 0.2	PMN J0340-2119
03 48 33	−16 08		0.6 ± 0.06	. . .	0.7 ± 0.1	1.2 ± 0.3	. . .	0.5 ± 0.5	PMN J0348-1610
03 48 53	−27 47	129	1.3 ± 0.03	1.1 ± 0.05	1.0 ± 0.06	1.4 ± 0.1	0.7 ± 0.2	−0.3 ± 0.2	PMN J0348-2749
03 58 45	10 27		1.1 ± 0.08	1.1 ± 0.2	. . .	1.0 ± 0.3	. . .	−0.1 ± 0.6	GB6 J0358+1026
04 03 58	−36 04	136	2.9 ± 0.04	3.2 ± 0.07	3.0 ± 0.07	2.7 ± 0.1	2.6 ± 0.2	0.0 ± 0.08	PMN J0403-3605
04 05 37	−13 04	114	2.1 ± 0.05	1.8 ± 0.08	1.7 ± 0.09	1.5 ± 0.2	. . .	−0.4 ± 0.2	PMN J0405-1308
04 07 07	−38 25	141	1.2 ± 0.05	1.1 ± 0.09	1.0 ± 0.07	0.8 ± 0.1	0.8 ± 0.3	−0.4 ± 0.2	PMN J0406-3826
04 08 36	−75 06		0.9 ± 0.04	0.6 ± 0.05	0.3 ± 0.06	. . .	. . .	−1.4 ± 0.5	PMN J0408-7507
04 11 19	76 55	082	1.1 ± 0.05	0.9 ± 0.09	0.7 ± 0.09	0.8 ± 0.2	0.7 ± 0.2	−0.4 ± 0.3	1Jy 0403+76
04 16 35	−20 52		1.1 ± 0.04	1.0 ± 0.06	1.0 ± 0.07	0.7 ± 0.2	. . .	−0.2 ± 0.3	PMN J0416-2056
04 23 17	−01 20	110	7.6 ± 0.06	7.7 ± 0.09	7.1 ± 0.1	6.3 ± 0.2	4.2 ± 0.3	−0.1 ± 0.04	PMN J0423-0120
04 23 43	02 18		1.2 ± 0.05	1.0 ± 0.07	0.7 ± 0.09	0.5 ± 0.2	. . .	−0.7 ± 0.4	GB6 J0424+0226
04 24 53	00 35	109	1.3 ± 0.07	1.5 ± 0.1	1.5 ± 0.1	1.2 ± 0.2	1.4 ± 0.4	0.1 ± 0.3	GB6 J0424+0036
04 24 59	−37 57	140	1.4 ± 0.04	1.1 ± 0.09	1.3 ± 0.1	1.3 ± 0.1	0.5 ± 0.3	−0.2 ± 0.2	PMN J0424-3756
04 28 24	−37 57		1.5 ± 0.04	1.5 ± 0.07	1.5 ± 0.06	1.6 ± 0.1	1.3 ± 0.2	−0.0 ± 0.1	PMN J0428-3756[a]
04 33 12	05 21	108	2.8 ± 0.06	2.7 ± 0.1	2.5 ± 0.1	2.5 ± 0.2	2.1 ± 0.4	−0.1 ± 0.1	GB6 J0433+0521
04 38 31	−12 49		0.6 ± 0.05	0.9 ± 0.1	0.8 ± 0.09	0.7 ± 0.1	0.8 ± 0.3	0.2 ± 0.3	PMN J0438-1251
04 40 14	−43 33	147	2.3 ± 0.05	2.0 ± 0.08	1.8 ± 0.07	1.3 ± 0.1	. . .	−0.4 ± 0.1	PMN J0440-4332
04 42 51	−00 18		1.0 ± 0.05	0.9 ± 0.08	1.2 ± 0.1	1.0 ± 0.3	1.2 ± 0.3	0.1 ± 0.3	PMN J0442-0017
04 49 06	−81 00	175	1.6 ± 0.04	1.8 ± 0.07	1.5 ± 0.07	1.4 ± 0.1	1.1 ± 0.2	−0.1 ± 0.1	PMN J0450-8100
04 53 21	−28 07	131	1.7 ± 0.05	1.7 ± 0.07	1.5 ± 0.07	1.5 ± 0.2	1.1 ± 0.2	−0.2 ± 0.2	PMN J0453-2807
04 55 54	−46 17	151	4.3 ± 0.05	4.2 ± 0.08	4.0 ± 0.08	3.5 ± 0.2	2.9 ± 0.3	−0.1 ± 0.07	PMN J0455-4616
04 56 57	−23 21	128	2.6 ± 0.04	2.6 ± 0.06	2.4 ± 0.09	2.1 ± 0.1	. . .	−0.2 ± 0.1	PMN J0457-2324
05 01 19	−01 59		1.0 ± 0.07	1.1 ± 0.1	1.0 ± 0.1	1.0 ± 0.2	. . .	0.0 ± 0.3	PMN J0501-0159
05 06 11	−06 27		1.1 ± 0.04	1.0 ± 0.07	0.8 ± 0.09	. . .	. . .	−0.5 ± 0.4	. . .
05 06 54	−61 08	154	2.2 ± 0.04	2.0 ± 0.06	1.7 ± 0.06	1.1 ± 0.1	0.7 ± 0.2	−0.5 ± 0.1	PMN J0506-6109[a]
05 13 48	−20 16		0.8 ± 0.04	0.8 ± 0.06	0.7 ± 0.07	0.5 ± 0.2	. . .	−0.3 ± 0.3	PMN J0513-2016
05 13 53	−21 54	127	1.2 ± 0.03	1.2 ± 0.05	1.0 ± 0.08	0.7 ± 0.2	0.8 ± 0.2	−0.3 ± 0.2	PMN J0513-2159
05 15 06	−45 58		. . .	0.4 ± 0.08	0.9 ± 0.1	1.0 ± 0.1	. . .	1.0 ± 0.8	PMN J0515-4556[a]
05 17 21	−62 23		0.7 ± 0.03	0.6 ± 0.06	0.7 ± 0.06	0.6 ± 0.2	. . .	−0.1 ± 0.3	PMN J0515-6220
05 19 19	−05 40	116	2.5 ± 0.06	1.7 ± 0.07	1.3 ± 0.08	0.5 ± 0.2	1.0 ± 0.2	−1.0 ± 0.2	. . .[c]
05 19 43	−45 46	150	7.2 ± 0.04	5.7 ± 0.07	4.7 ± 0.09	3.6 ± 0.1	2.1 ± 0.3	−0.7 ± 0.05	PMN J0519-4546[a]
05 23 02	−36 27	139	4.5 ± 0.04	4.2 ± 0.07	3.9 ± 0.08	3.7 ± 0.2	2.8 ± 0.2	−0.3 ± 0.06	PMN J0522-3628
05 25 05	−23 37		0.8 ± 0.04	0.9 ± 0.06	0.7 ± 0.06	0.9 ± 0.1	0.8 ± 0.2	0.0 ± 0.2	PMN J0525-2338[a]
05 25 44	−48 26		1.0 ± 0.05	1.4 ± 0.07	1.3 ± 0.08	1.1 ± 0.09	0.8 ± 0.2	0.2 ± 0.2	PMN J0526-4830[a]
05 27 05	19 18		0.5 ± 0.05	. . .	. . .	. . .	0.7 ± 0.3	0.3 ± 0.8	. . .
05 27 37	−12 41	122	1.5 ± 0.05	1.6 ± 0.08	1.4 ± 0.1	1.1 ± 0.1	. . .	−0.2 ± 0.2	PMN J0527-1241
05 32 22	18 50		0.2 ± 0.05	0.6 ± 0.06	0.6 ± 0.07	. . .	. . .	1.3 ± 0.9	GB6 J0532+1857
05 33 24	48 24		0.9 ± 0.06	1.1 ± 0.1	0.9 ± 0.1	0.7 ± 0.2	0.7 ± 0.3	−0.1 ± 0.4	GB6 J0533+4822
05 34 26	−61 06		0.6 ± 0.03	0.6 ± 0.04	0.6 ± 0.05	0.6 ± 0.07	0.5 ± 0.1	−0.1 ± 0.2	PMN J0534-6106
05 35 53	19 58		. . .	0.3 ± 0.1	. . .	. . .	0.9 ± 0.4	1.2 ± 1	GB6 J0535+1951
05 37 02	−66 18		0.4 ± 0.03	0.6 ± 0.05	0.5 ± 0.04	0.5 ± 0.07	0.8 ± 0.1	0.3 ± 0.2	PMN J0537-6620
05 38 51	−44 05	148	5.8 ± 0.04	6.2 ± 0.07	6.2 ± 0.08	5.8 ± 0.1	4.8 ± 0.3	0.0 ± 0.04	PMN J0538-4405
05 39 49	−28 44		0.6 ± 0.07	0.6 ± 0.08	0.7 ± 0.09	0.8 ± 0.1	. . .	0.2 ± 0.4	PMN J0539-2839
05 40 43	−54 14	152	1.3 ± 0.04	1.3 ± 0.06	1.2 ± 0.08	1.0 ± 0.08	0.7 ± 0.1	−0.2 ± 0.2	PMN J0540-5418
05 42 29	49 51	095	1.8 ± 0.06	1.4 ± 0.09	1.3 ± 0.1	0.7 ± 0.2	. . .	−0.7 ± 0.3	GB6 J0542+4951
05 43 18	−73 30		0.5 ± 0.05	0.6 ± 0.05	0.6 ± 0.06	0.3 ± 0.1	. . .	0.2 ± 0.5	PMN J0541-7332
05 46 50	−67 22		. . .	0.3 ± 0.04	0.6 ± 0.05	0.3 ± 0.07	0.7 ± 0.1	0.4 ± 0.4	PMN J0547-6728
05 50 40	−57 31	153	1.3 ± 0.03	1.1 ± 0.04	1.1 ± 0.07	0.9 ± 0.09	. . .	−0.4 ± 0.2	PMN J0550-5732
05 51 54	37 42		1.2 ± 0.05	1.2 ± 0.07	1.0 ± 0.08	. . .	1.0 ± 0.3	−0.2 ± 0.3	GB6 J0551+3751[a]
05 52 15	−66 38		. . .	0.4 ± 0.03	0.3 ± 0.05	0.4 ± 0.09	. . .	−0.0 ± 0.9	. . .
05 55 49	39 45	100	3.1 ± 0.05	2.2 ± 0.08	1.7 ± 0.08	1.4 ± 0.2	. . .	−0.9 ± 0.2	GB6 J0555+3948
06 06 59	67 23	091	1.2 ± 0.03	0.9 ± 0.05	0.7 ± 0.07	0.6 ± 0.2	. . .	−0.9 ± 0.3	GB6 J0607+6720[a]
06 08 49	−22 20		1.1 ± 0.04	1.1 ± 0.05	0.9 ± 0.06	0.8 ± 0.1	0.6 ± 0.2	−0.4 ± 0.2	PMN J0608-2220
06 09 14	−60 49		0.3 ± 0.03	0.2 ± 0.05	0.5 ± 0.06	0.6 ± 0.07	. . .	0.6 ± 0.4	PMN J0609-6042[a]
06 09 37	−15 41	126	3.5 ± 0.05	3.1 ± 0.08	2.8 ± 0.1	2.0 ± 0.2	1.5 ± 0.4	−0.4 ± 0.1	PMN J0609-1542
06 21 01	−25 15		0.5 ± 0.06	0.4 ± 0.1	0.3 ± 0.1	. . .	. . .	−0.8 ± 1	PMN J0620-2515
06 23 07	−64 36		1.0 ± 0.03	0.8 ± 0.04	0.8 ± 0.04	0.8 ± 0.06	0.8 ± 0.1	−0.2 ± 0.1	PMN J0623-6436
06 26 38	−35 21		0.6 ± 0.05	0.3 ± 0.1	. . .	. . .	. . .	−2.1 ± 3	PMN J0627-3529
06 29 29	−19 58	130	1.5 ± 0.04	1.4 ± 0.06	1.4 ± 0.09	1.2 ± 0.3	. . .	−0.1 ± 0.2	PMN J0629-1959
06 32 40	−69 27		0.4 ± 0.03	0.5 ± 0.04	0.4 ± 0.04	0.6 ± 0.1	0.7 ± 0.1	0.4 ± 0.2	. . .
06 33 50	−22 17	135	0.5 ± 0.05	0.6 ± 0.06	0.7 ± 0.07	0.9 ± 0.1	. . .	0.7 ± 0.4	PMN J0633-2223
06 34 38	−23 36		0.7 ± 0.04	0.6 ± 0.07	0.6 ± 0.06	0.6 ± 0.2	0.4 ± 0.2	−0.3 ± 0.3	PMN J0634-2335

Table 5
(Continued)

R.A. (hms)	Decl. (dm)	ID	K (Jy)	Ka (Jy)	Q (Jy)	V (Jy)	W (Jy)	α	5 GHz ID
06 35 50	−75 17	167	4.4 ± 0.04	3.9 ± 0.05	3.6 ± 0.06	2.8 ± 0.1	2.2 ± 0.3	−0.4 ± 0.05	PMN J0635-7516
06 36 33	−20 31	134	1.2 ± 0.04	1.2 ± 0.05	1.0 ± 0.07	0.7 ± 0.1	. . .	−0.3 ± 0.2	PMN J0636-2041[a]
06 39 41	73 27	087	0.7 ± 0.05	0.6 ± 0.08	0.7 ± 0.08	0.7 ± 0.1	. . .	0.0 ± 0.3	GB6 J0639+7324
06 46 30	44 49	099	2.9 ± 0.06	2.4 ± 0.09	2.1 ± 0.1	1.6 ± 0.2	1.5 ± 0.3	−0.6 ± 0.1	GB6 J0646+4451
06 48 29	−17 44		0.4 ± 0.1	0.9 ± 0.09	0.8 ± 0.09	1.2 ± 0.2	1.1 ± 0.3	0.5 ± 0.5	PMN J0648-1744
06 51 57	−64 51		0.2 ± 0.04	0.4 ± 0.06	0.5 ± 0.06	0.5 ± 0.08	. . .	0.9 ± 0.5	. . .
06 52 23	−27 39		0.3 ± 0.04	0.6 ± 0.06	0.2 ± 0.05	. . .	1.2 ± 0.3	0.9 ± 0.4	. . .
06 59 54	17 06		1.2 ± 0.05	1.2 ± 0.08	1.0 ± 0.09	0.7 ± 0.2	. . .	−0.2 ± 0.3	GB6 J0700+1709[a]
07 20 38	04 03		0.9 ± 0.05	0.7 ± 0.07	0.6 ± 0.08	. . .	. . .	−0.6 ± 0.5	GB6 J0720+0404
07 21 50	71 22		1.6 ± 0.04	1.7 ± 0.06	1.8 ± 0.07	1.7 ± 0.1	1.6 ± 0.2	0.1 ± 0.1	GB6 J0721+7120
07 25 54	−00 51		1.0 ± 0.09	1.3 ± 0.1	1.2 ± 0.09	1.2 ± 0.2	1.3 ± 0.6	0.2 ± 0.3	PMN J0725-0054
07 27 01	67 45		0.6 ± 0.04	0.5 ± 0.06	0.6 ± 0.09	0.4 ± 0.1	0.6 ± 0.2	−0.2 ± 0.4	GB6 J0728+6748
07 30 19	−11 42		4.6 ± 0.05	4.3 ± 0.08	3.9 ± 0.09	3.1 ± 0.2	2.2 ± 0.4	−0.3 ± 0.07	PMN J0730-1141
07 34 19	50 21		1.1 ± 0.05	1.1 ± 0.08	1.1 ± 0.08	1.0 ± 0.2	1.0 ± 0.2	0.0 ± 0.2	GB6 J0733+5022[a]
07 38 11	17 43	113	1.2 ± 0.05	1.2 ± 0.09	0.9 ± 0.1	1.1 ± 0.2	. . .	−0.2 ± 0.3	GB6 J0738+1742
07 39 16	01 36	124	1.7 ± 0.05	1.8 ± 0.09	2.0 ± 0.1	2.0 ± 0.2	. . .	0.2 ± 0.2	GB6 J0739+0136
07 41 18	31 11	107	1.2 ± 0.05	1.1 ± 0.08	0.8 ± 0.1	0.9 ± 0.2	. . .	−0.5 ± 0.3	GB6 J0741+3112
07 43 44	−67 27	161	1.2 ± 0.04	0.9 ± 0.06	0.7 ± 0.07	0.7 ± 0.2	0.8 ± 0.2	−0.6 ± 0.2	PMN J0743-6726
07 45 31	10 15	118	1.1 ± 0.05	1.0 ± 0.08	0.7 ± 0.09	0.4 ± 0.1	. . .	−0.6 ± 0.4	GB6 J0745+1011
07 46 04	−00 45		1.1 ± 0.06	1.0 ± 0.1	0.8 ± 0.09	0.8 ± 0.1	0.6 ± 0.2	−0.3 ± 0.3	PMN J0745-0044
07 48 11	−16 50		1.0 ± 0.03	1.3 ± 0.05	1.0 ± 0.05	0.6 ± 0.1	. . .	0.1 ± 0.2	PMN J0748-1639[a]
07 50 53	12 30	117	3.2 ± 0.05	3.1 ± 0.08	2.9 ± 0.1	2.4 ± 0.2	1.9 ± 0.3	−0.2 ± 0.1	GB6 J0750+1231
07 53 35	53 53		1.1 ± 0.05	1.1 ± 0.06	0.8 ± 0.09	0.9 ± 0.1	0.7 ± 0.3	−0.3 ± 0.3	GB6 J0753+5353[a]
07 56 22	−80 52		1.1 ± 0.03	0.7 ± 0.05	0.3 ± 0.07	0.3 ± 0.1	. . .	−1.5 ± 0.4	PMN J0759-8059
07 57 03	09 57	120	1.3 ± 0.07	1.4 ± 0.1	1.5 ± 0.1	1.3 ± 0.2	. . .	0.1 ± 0.3	GB6 J0757+0956
08 05 38	61 28		0.7 ± 0.04	0.5 ± 0.06	0.6 ± 0.1	. . .	. . .	−0.4 ± 0.6	. . .
08 08 20	−07 50	133	1.3 ± 0.04	1.3 ± 0.07	1.2 ± 0.09	1.3 ± 0.1	0.8 ± 0.2	−0.1 ± 0.2	PMN J0808-0751
08 08 42	49 51		0.7 ± 0.06	1.1 ± 0.1	0.9 ± 0.1	. . .	. . .	0.5 ± 0.5	GB6 J0808+4950[a]
08 13 23	48 18		1.0 ± 0.06	1.0 ± 0.07	0.8 ± 0.08	. . .	. . .	−0.3 ± 0.4	GB6 J0813+4813
08 16 20	−24 25	145	0.8 ± 0.04	1.0 ± 0.05	0.9 ± 0.07	0.8 ± 0.1	. . .	0.2 ± 0.3	PMN J0816-2421
08 18 31	42 24		1.0 ± 0.06	1.1 ± 0.06	0.9 ± 0.09	0.9 ± 0.2	0.8 ± 0.3	−0.1 ± 0.3	GB6 J0818+4222
08 23 23	22 24		1.2 ± 0.06	1.2 ± 0.08	1.1 ± 0.1	0.7 ± 0.2	0.9 ± 0.3	−0.2 ± 0.3	GB6 J0823+2223
08 24 57	39 14		1.2 ± 0.06	1.1 ± 0.09	1.1 ± 0.1	0.9 ± 0.2	. . .	−0.2 ± 0.3	GB6 J0824+3916[a]
08 25 48	03 11	125	1.8 ± 0.05	1.9 ± 0.08	1.8 ± 0.1	1.7 ± 0.2	. . .	0.0 ± 0.2	GB6 J0825+0309
08 26 09	−22 32		0.8 ± 0.04	0.8 ± 0.08	0.7 ± 0.08	1.1 ± 0.2	. . .	0.1 ± 0.3	PMN J0826-2230
08 30 59	24 11	112	1.3 ± 0.07	1.4 ± 0.1	1.5 ± 0.1	1.5 ± 0.2	1.2 ± 0.3	0.1 ± 0.2	GB6 J0830+2410
08 31 24	04 28		0.7 ± 0.07	0.6 ± 0.2	. . .	. . .	0.8 ± 0.3	0.1 ± 0.5	GB6 J0831+0429
08 34 36	55 34		1.0 ± 0.05	0.8 ± 0.06	0.7 ± 0.08	0.6 ± 0.2	0.8 ± 0.3	−0.5 ± 0.3	GB6 J0834+5534
08 36 47	−20 14	144	2.7 ± 0.05	2.3 ± 0.07	2.1 ± 0.09	1.5 ± 0.2	0.7 ± 0.3	−0.5 ± 0.1	PMN J0836-2017
08 38 08	58 23		1.2 ± 0.04	1.2 ± 0.06	1.0 ± 0.07	0.8 ± 0.1	. . .	−0.3 ± 0.2	GB6 J0837+5825[a]
08 40 42	13 12	121	1.8 ± 0.06	1.8 ± 0.09	1.6 ± 0.1	1.0 ± 0.2	. . .	−0.2 ± 0.2	GB6 J0840+1312
08 41 27	70 54	089	1.8 ± 0.04	1.8 ± 0.07	1.7 ± 0.08	1.7 ± 0.1	0.5 ± 0.2	−0.1 ± 0.1	GB6 J0841+7053
08 47 45	−07 04		0.9 ± 0.05	1.0 ± 0.08	1.0 ± 0.1	1.2 ± 0.2	. . .	0.2 ± 0.3	PMN J0847-0703
08 54 46	20 05	115	3.7 ± 0.06	4.2 ± 0.1	3.9 ± 0.1	3.9 ± 0.2	3.2 ± 0.4	0.0 ± 0.09	GB6 J0854+2006
09 02 19	−14 13		1.3 ± 0.05	1.3 ± 0.07	1.2 ± 0.07	1.0 ± 0.1	1.2 ± 0.2	−0.1 ± 0.2	PMN J0902-1415
09 03 34	46 48		1.0 ± 0.06	0.9 ± 0.09	0.7 ± 0.09	0.5 ± 0.1	. . .	−0.7 ± 0.4	GB6 J0903+4650
09 04 24	−57 33		0.9 ± 0.05	1.0 ± 0.07	0.9 ± 0.07	1.1 ± 0.1	0.6 ± 0.2	0.0 ± 0.2	PMN J0904-5735
09 07 55	−20 19		1.1 ± 0.04	1.0 ± 0.09	0.6 ± 0.09	. . .	. . .	−0.7 ± 0.5	PMN J0907-2026
09 09 17	01 19	132	2.0 ± 0.06	1.8 ± 0.1	1.7 ± 0.1	1.7 ± 0.3	. . .	−0.2 ± 0.2	GB6 J0909+0121
09 09 49	42 53		1.0 ± 0.07	1.1 ± 0.1	1.1 ± 0.1	0.8 ± 0.1	. . .	−0.0 ± 0.4	GB6 J0909+4253
09 14 40	02 49		1.5 ± 0.05	1.6 ± 0.08	1.4 ± 0.08	1.0 ± 0.1	1.4 ± 0.2	−0.1 ± 0.2	GB6 J0914+0245
09 18 11	−12 03	143	2.1 ± 0.06	1.1 ± 0.1	0.9 ± 0.2	0.9 ± 0.3	. . .	−1.4 ± 0.4	PMN J0918-1205
09 20 41	44 41		1.5 ± 0.06	1.6 ± 0.1	1.6 ± 0.09	1.5 ± 0.2	. . .	0.0 ± 0.2	GB6 J0920+4441
09 21 05	62 15		1.0 ± 0.04	0.8 ± 0.06	0.9 ± 0.1	0.6 ± 0.2	. . .	−0.3 ± 0.3	GB6 J0921+6215
09 21 39	−26 19		1.5 ± 0.05	1.4 ± 0.08	1.2 ± 0.09	1.1 ± 0.2	. . .	−0.3 ± 0.2	PMN J0921-2618
09 23 13	−40 04		1.1 ± 0.04	1.1 ± 0.07	0.9 ± 0.06	1.2 ± 0.2	0.6 ± 0.2	−0.2 ± 0.2	PMN J0922-3959[a]
09 27 05	39 01	105	7.5 ± 0.06	6.5 ± 0.1	5.8 ± 0.09	4.6 ± 0.2	3.1 ± 0.3	−0.5 ± 0.05	GB6 J0927+3902
09 48 55	40 38	104	1.4 ± 0.06	1.6 ± 0.09	1.5 ± 0.09	1.3 ± 0.2	1.0 ± 0.2	−0.1 ± 0.2	GB6 J0948+4039
09 55 49	69 35	088	1.4 ± 0.05	1.2 ± 0.06	1.0 ± 0.06	0.9 ± 0.1	1.0 ± 0.2	−0.4 ± 0.2	GB6 J0955+6940
09 56 38	25 13		0.9 ± 0.05	1.1 ± 0.1	0.9 ± 0.1	0.6 ± 0.2	0.9 ± 0.3	−0.0 ± 0.3	GB6 J0956+2515
09 57 24	55 26		1.0 ± 0.05	0.9 ± 0.09	1.0 ± 0.1	0.6 ± 0.2	. . .	−0.2 ± 0.3	GB6 J0957+5522[a]
09 58 08	47 21	098	1.5 ± 0.05	1.4 ± 0.08	1.4 ± 0.07	0.9 ± 0.1	. . .	−0.3 ± 0.2	GB6 J0958+4725
09 59 10	65 30		1.0 ± 0.04	0.9 ± 0.06	0.8 ± 0.07	0.8 ± 0.1	. . .	−0.3 ± 0.3	GB6 J0958+6534
10 05 46	34 57		0.7 ± 0.06	0.6 ± 0.07	0.4 ± 0.1	. . .	. . .	−0.7 ± 0.7	GB6 J1006+3453[a]
10 14 03	23 05	119	1.1 ± 0.05	0.9 ± 0.1	0.7 ± 0.07	0.4 ± 0.1	. . .	−0.7 ± 0.4	GB6 J1014+2301
10 15 19	−45 10		1.2 ± 0.03	0.8 ± 0.05	0.6 ± 0.06	. . .	. . .	−1.0 ± 0.3	PMN J1014-4508

Table 5
(Continued)

R.A. (hms)	Decl. (dm)	ID	K (Jy)	Ka (Jy)	Q (Jy)	V (Jy)	W (Jy)	α	5 GHz ID
10 17 37	35 52		0.8 ± 0.05	0.9 ± 0.08	0.7 ± 0.1	0.6 ± 0.1	0.5 ± 0.2	−0.3 ± 0.3	GB6 J1018+3550
10 18 49	−31 28		1.0 ± 0.04	0.9 ± 0.06	0.8 ± 0.06	0.8 ± 0.1	0.8 ± 0.4	−0.2 ± 0.3	PMN J1018-3123
10 21 51	40 02		0.9 ± 0.04	1.0 ± 0.06	0.8 ± 0.07	0.4 ± 0.1	0.6 ± 0.2	−0.3 ± 0.3	GB6 J1022+4004
10 32 40	41 18	103	1.0 ± 0.05	0.9 ± 0.09	0.8 ± 0.1	0.8 ± 0.2	0.6 ± 0.2	−0.3 ± 0.3	GB6 J1033+4115
10 33 44	60 50		0.8 ± 0.03	0.9 ± 0.05	0.6 ± 0.05	0.8 ± 0.1	0.6 ± 0.2	−0.1 ± 0.2	GB6 J1033+6051[a]
10 36 39	−37 37		0.8 ± 0.04	0.7 ± 0.05	0.5 ± 0.1	0.3 ± 0.09	. . .	−0.6 ± 0.4	PMN J1036-3744
10 37 19	−29 34		1.8 ± 0.05	1.8 ± 0.08	1.7 ± 0.1	1.9 ± 0.2	1.4 ± 0.3	−0.1 ± 0.2	PMN J1037-2934
10 38 35	05 10	142	1.4 ± 0.05	1.4 ± 0.1	1.1 ± 0.1	1.2 ± 0.2	. . .	−0.2 ± 0.3	GB6 J1038+0512
10 41 23	06 11		1.2 ± 0.06	1.3 ± 0.1	1.2 ± 0.1	1.2 ± 0.2	. . .	0.1 ± 0.3	GB6 J1041+0610
10 41 40	−47 38	163	1.2 ± 0.05	0.9 ± 0.07	0.6 ± 0.06	. . .	1.1 ± 0.2	−0.5 ± 0.2	PMN J1041-4740
10 42 59	24 05		0.9 ± 0.06	0.8 ± 0.1	0.9 ± 0.1	1.1 ± 0.1	0.9 ± 0.3	0.1 ± 0.3	GB6 J1043+2408
10 47 30	71 43	083	1.2 ± 0.05	1.1 ± 0.1	1.1 ± 0.09	. . .	. . .	−0.2 ± 0.3	GB6 J1048+7143
10 47 57	−19 10		1.3 ± 0.05	1.0 ± 0.08	1.0 ± 0.1	1.0 ± 0.2	. . .	−0.4 ± 0.3	PMN J1048-1909
10 54 20	81 10		1.0 ± 0.04	0.8 ± 0.06	0.7 ± 0.06	. . .	. . .	−0.6 ± 0.3	. . .
10 58 27	01 34	149	5.0 ± 0.05	4.8 ± 0.08	4.7 ± 0.1	4.4 ± 0.2	3.0 ± 0.3	−0.2 ± 0.06	GB6 J1058+0133
10 59 11	−80 03	176	2.4 ± 0.04	2.6 ± 0.07	2.5 ± 0.07	2.6 ± 0.1	1.4 ± 0.2	−0.0 ± 0.09	PMN J1058-8003
11 02 12	−44 03		0.7 ± 0.03	0.9 ± 0.05	0.8 ± 0.09	0.7 ± 0.1	. . .	0.2 ± 0.3	PMN J1102-4404
11 02 48	72 28		0.9 ± 0.04	0.9 ± 0.07	0.8 ± 0.05	0.6 ± 0.2	. . .	−0.3 ± 0.3	GB6 J1101+7225[a]
11 07 12	−44 46	166	1.6 ± 0.03	1.5 ± 0.05	1.1 ± 0.06	1.3 ± 0.2	0.7 ± 0.2	−0.3 ± 0.2	PMN J1107-4449
11 17 57	−46 33		1.1 ± 0.03	0.8 ± 0.06	0.7 ± 0.07	0.5 ± 0.1	. . .	−0.7 ± 0.3	PMN J1118-4634
11 18 34	−12 32		1.1 ± 0.05	1.0 ± 0.07	0.8 ± 0.08	0.6 ± 0.2	. . .	−0.5 ± 0.3	PMN J1118-1232[a]
11 18 50	12 38		1.1 ± 0.06	0.9 ± 0.1	1.0 ± 0.1	0.8 ± 0.2	. . .	−0.3 ± 0.3	GB6 J1118+1234
11 27 06	−18 57	159	1.6 ± 0.06	1.6 ± 0.1	1.4 ± 0.09	1.3 ± 0.2	1.2 ± 0.2	−0.2 ± 0.2	PMN J1127-1857
11 30 13	−14 51	157	2.0 ± 0.06	1.7 ± 0.1	1.9 ± 0.1	1.3 ± 0.2	. . .	−0.3 ± 0.2	PMN J1130-1449
11 30 47	38 15	101	1.2 ± 0.05	1.0 ± 0.07	1.0 ± 0.1	0.7 ± 0.1	1.5 ± 0.7	−0.4 ± 0.3	GB6 J1130+3815[a]
11 36 58	−74 16		0.8 ± 0.04	0.7 ± 0.07	0.5 ± 0.08	0.4 ± 0.1	. . .	−0.7 ± 0.4	PMN J1136-7415
11 44 59	−69 58		0.8 ± 0.05	0.7 ± 0.07	0.7 ± 0.06	0.8 ± 0.1	. . .	−0.1 ± 0.3	PMN J1145-6953
11 46 14	−48 41		0.7 ± 0.04	0.7 ± 0.05	0.5 ± 0.06	0.9 ± 0.1	0.6 ± 0.2	0.0 ± 0.2	PMN J1145-4836[a]
11 46 50	40 00		1.1 ± 0.05	1.2 ± 0.06	1.2 ± 0.07	0.6 ± 0.2	1.7 ± 0.7	0.1 ± 0.3	GB6 J1146+3958[a]
11 47 07	−38 11	169	2.2 ± 0.05	2.3 ± 0.08	2.1 ± 0.08	1.9 ± 0.2	1.0 ± 0.3	−0.1 ± 0.1	PMN J1147-3812
11 50 19	−79 26		1.3 ± 0.04	0.8 ± 0.05	0.6 ± 0.06	0.7 ± 0.1	. . .	−1.1 ± 0.3	PMN J1150-7918
11 50 53	−00 24		0.8 ± 0.07	0.7 ± 0.1	0.7 ± 0.1	. . .	0.6 ± 0.3	−0.2 ± 0.5	PMN J1150-0024
11 53 14	49 32	090	2.2 ± 0.04	2.1 ± 0.06	2.0 ± 0.07	1.7 ± 0.1	1.0 ± 0.2	−0.2 ± 0.1	GB6 J1153+4931[a]
11 54 09	−35 16		0.9 ± 0.05	0.9 ± 0.09	0.7 ± 0.08	0.6 ± 0.1	. . .	−0.4 ± 0.3	PMN J1153-3522
11 54 41	81 04	078	1.2 ± 0.05	1.0 ± 0.08	0.9 ± 0.09	0.9 ± 0.1	. . .	−0.4 ± 0.2	1Jy 1150+81
11 57 48	16 37		0.9 ± 0.05	1.1 ± 0.07	0.9 ± 0.07	0.9 ± 0.1	. . .	0.1 ± 0.3	GB6 J1157+1639
11 59 36	29 15	111	2.0 ± 0.05	2.0 ± 0.08	1.9 ± 0.09	1.7 ± 0.2	1.9 ± 0.5	−0.1 ± 0.1	GB6 J1159+2914
12 03 28	48 08		0.8 ± 0.03	0.7 ± 0.05	0.6 ± 0.08	0.5 ± 0.2	. . .	−0.4 ± 0.4	GB6 J1203+4803[a]
12 05 48	−26 39		0.9 ± 0.05	0.8 ± 0.07	0.8 ± 0.08	0.5 ± 0.1	1.3 ± 0.6	−0.1 ± 0.3	PMN J1205-2634
12 07 43	−52 18		0.5 ± 0.04	1.0 ± 0.05	0.7 ± 0.06	0.7 ± 0.1	. . .	0.4 ± 0.3	. . .
12 08 35	−24 01	172	1.2 ± 0.05	0.9 ± 0.07	0.7 ± 0.1	0.6 ± 0.2	. . .	−0.8 ± 0.4	PMN J1209-2406
12 09 26	−52 27		0.8 ± 0.09	1.1 ± 0.05	. . .	. . .	. . .	1.0 ± 0.7	. . .
12 11 26	−52 35		3.8 ± 0.03	2.2 ± 0.04	1.6 ± 0.06	0.8 ± 0.1	. . .	−1.5 ± 0.1	PMN J1212-5235
12 15 57	−17 29	173	1.5 ± 0.05	1.3 ± 0.09	1.2 ± 0.08	0.7 ± 0.2	. . .	−0.5 ± 0.2	PMN J1215-1731
12 18 53	48 30		0.8 ± 0.03	0.8 ± 0.04	0.8 ± 0.07	0.8 ± 0.1	0.6 ± 0.2	0.0 ± 0.2	GB6 J1219+4830
12 19 21	05 49	164	2.8 ± 0.05	2.2 ± 0.08	2.0 ± 0.1	1.4 ± 0.2	1.5 ± 0.3	−0.6 ± 0.1	GB6 J1219+0549A[a]
12 22 11	04 14		0.8 ± 0.07	0.8 ± 0.1	0.9 ± 0.1	0.7 ± 0.2	. . .	0.1 ± 0.5	GB6 J1222+0413
12 22 59	−83 06	178	0.9 ± 0.04	1.1 ± 0.05	0.9 ± 0.05	0.7 ± 0.1	0.5 ± 0.2	0.0 ± 0.2	PMN J1224-8312
12 24 19	13 03		0.5 ± 0.1	0.5 ± 0.06	. . .	0.4 ± 0.2	. . .	−0.1 ± 1	GB6 J1224+1310
12 26 55	−44 35		0.5 ± 0.07	0.7 ± 0.08	0.9 ± 0.09	0.9 ± 0.1	. . .	0.6 ± 0.4	PMN J1227-4436
12 29 06	02 03	170	22.7 ± 0.05	20.6 ± 0.09	18.8 ± 0.1	16.2 ± 0.2	11.4 ± 0.3	−0.3 ± 0.02	GB6 J1229+0202
12 30 51	12 23	165	20.8 ± 0.05	16.1 ± 0.08	13.5 ± 0.1	9.7 ± 0.2	6.5 ± 0.4	−0.7 ± 0.02	GB6 J1230+1223
12 39 25	07 28		1.2 ± 0.05	1.0 ± 0.08	0.8 ± 0.08	1.0 ± 0.1	. . .	−0.4 ± 0.3	GB6 J1239+0730
12 46 54	−25 46	177	1.3 ± 0.05	1.3 ± 0.1	1.5 ± 0.09	1.7 ± 0.2	1.0 ± 0.4	0.3 ± 0.2	PMN J1246-2547
12 48 51	−45 58		0.9 ± 0.06	0.9 ± 0.08	0.9 ± 0.09	0.7 ± 0.1	. . .	−0.0 ± 0.4	PMN J1248-4559
12 56 12	−05 47	181	18.0 ± 0.06	18.6 ± 0.09	18.4 ± 0.1	17.1 ± 0.2	13.7 ± 0.4	−0.0 ± 0.02	PMN J1256-0547
12 58 08	−32 00	180	1.3 ± 0.04	1.1 ± 0.07	1.0 ± 0.08	0.6 ± 0.1	. . .	−0.5 ± 0.3	PMN J1257-3154
12 58 22	32 28		0.7 ± 0.05	0.6 ± 0.07	0.8 ± 0.1	0.3 ± 0.1	. . .	−0.1 ± 0.5	GB6 J1257+3229[a]
12 59 23	51 42		0.6 ± 0.05	0.7 ± 0.08	0.6 ± 0.08	1.0 ± 0.2	0.8 ± 0.2	0.4 ± 0.3	GB6 J1259+5141[a]
13 02 15	57 48		0.8 ± 0.04	0.7 ± 0.07	0.5 ± 0.09	0.6 ± 0.1	0.5 ± 0.2	−0.5 ± 0.4	GB6 J1302+5748[a]
13 05 55	−49 30		1.1 ± 0.04	1.0 ± 0.07	0.8 ± 0.08	1.0 ± 0.2	0.5 ± 0.2	−0.2 ± 0.3	PMN J1305-4928
13 10 40	32 22	052	2.4 ± 0.05	2.4 ± 0.08	2.1 ± 0.08	1.5 ± 0.2	1.2 ± 0.3	−0.3 ± 0.1	GB6 J1310+3220
13 16 07	−33 37	182	1.8 ± 0.05	1.8 ± 0.08	1.9 ± 0.09	2.0 ± 0.1	1.3 ± 0.2	0.1 ± 0.1	PMN J1316-3339
13 18 37	−42 14		. . .	. . .	0.4 ± 0.08	0.3 ± 0.1	. . .	−0.9 ± 3	. . .
13 24 30	−10 48		0.8 ± 0.07	0.7 ± 0.1	0.9 ± 0.1	1.0 ± 0.2	1.7 ± 0.5	0.4 ± 0.3	PMN J1324-1049
13 27 25	22 10		1.1 ± 0.06	1.1 ± 0.08	0.9 ± 0.08	0.9 ± 0.2	. . .	−0.2 ± 0.3	GB6 J1327+2210[a]

Table 5
(Continued)

R.A. (hms)	Decl. (dm)	ID	K (Jy)	Ka (Jy)	Q (Jy)	V (Jy)	W (Jy)	α	5 GHz ID
13 29 26	32 01	040	1.1 ± 0.03	0.7 ± 0.06	0.6 ± 0.07	0.6 ± 0.2	. . .	−0.9 ± 0.3	GB6 J1329+3154
13 30 55	25 02		1.2 ± 0.05	1.1 ± 0.06	0.9 ± 0.07	0.7 ± 0.1	0.6 ± 0.2	−0.5 ± 0.2	GB6 J1330+2509[a]
13 31 17	30 31	026	2.3 ± 0.05	1.8 ± 0.08	1.5 ± 0.1	1.2 ± 0.2	. . .	−0.7 ± 0.2	GB6 J1331+3030
13 32 52	01 59		1.4 ± 0.05	1.5 ± 0.07	1.4 ± 0.1	0.8 ± 0.2	1.3 ± 0.6	−0.1 ± 0.2	GB6 J1332+0200
13 33 24	27 23		0.9 ± 0.05	0.9 ± 0.07	0.7 ± 0.08	0.7 ± 0.1	. . .	−0.2 ± 0.3	GB6 J1333+2725[a]
13 36 51	−33 58	185	2.0 ± 0.05	1.5 ± 0.07	1.2 ± 0.08	0.9 ± 0.2	0.8 ± 0.2	−0.8 ± 0.2	PMN J1336-3358
13 37 40	−12 57	188	6.2 ± 0.06	6.4 ± 0.09	6.5 ± 0.1	6.0 ± 0.2	4.6 ± 0.4	0.0 ± 0.05	PMN J1337-1257
13 43 56	66 01		0.7 ± 0.05	0.3 ± 0.08	0.4 ± 0.1	. . .	. . .	−1.1 ± 0.9	GB6 J1344+6606[a]
13 47 47	12 18		1.1 ± 0.06	1.2 ± 0.08	0.9 ± 0.08	0.9 ± 0.1	. . .	−0.1 ± 0.3	GB6 J1347+1217
13 52 29	31 25		0.7 ± 0.04	0.6 ± 0.09	0.7 ± 0.08	0.5 ± 0.1	. . .	−0.2 ± 0.4	GB6 J1352+3126
13 54 49	−10 42	197	1.4 ± 0.05	1.0 ± 0.09	0.9 ± 0.2	0.8 ± 0.3	. . .	−0.7 ± 0.4	PMN J1354-1041
13 56 41	76 45		0.9 ± 0.05	0.9 ± 0.1	0.9 ± 0.09	1.0 ± 0.1	0.6 ± 0.3	0.0 ± 0.3	. . .[d]
13 56 57	19 19	004	1.7 ± 0.05	1.8 ± 0.08	1.6 ± 0.09	1.5 ± 0.2	1.2 ± 0.3	−0.1 ± 0.2	GB6 J1357+1919
13 56 59	−15 24		0.7 ± 0.08	. . .	0.6 ± 0.2	0.6 ± 0.2	0.9 ± 0.2	0.1 ± 0.4	PMN J1357-1527
14 08 54	−07 49	203	1.0 ± 0.07	1.0 ± 0.1	0.9 ± 0.1	. . .	. . .	−0.2 ± 0.5	1Jy 1406-076
14 11 12	52 15		1.0 ± 0.04	0.6 ± 0.1	0.5 ± 0.08	. . .	. . .	−1.1 ± 0.5	GB6 J1411+5212
14 15 52	13 24		1.0 ± 0.05	1.1 ± 0.08	0.9 ± 0.08	0.9 ± 0.1	1.0 ± 0.3	−0.1 ± 0.3	GB6 J1415+1320
14 19 36	54 26		0.9 ± 0.05	0.9 ± 0.08	0.8 ± 0.08	1.3 ± 0.2	1.1 ± 0.4	0.2 ± 0.3	GB6 J1419+5423[a]
14 19 39	38 22	042	1.0 ± 0.04	1.1 ± 0.06	1.1 ± 0.05	1.1 ± 0.1	1.1 ± 0.4	0.1 ± 0.2	GB6 J1419+3822
14 20 14	27 04		1.0 ± 0.04	1.1 ± 0.06	1.0 ± 0.06	0.7 ± 0.1	0.7 ± 0.2	−0.1 ± 0.2	GB6 J1419+2706[a]
14 27 27	−33 02	193	1.0 ± 0.05	1.4 ± 0.08	1.5 ± 0.1	1.3 ± 0.1	. . .	0.4 ± 0.2	PMN J1427-3306
14 27 53	−42 05	191	3.0 ± 0.05	2.7 ± 0.07	2.5 ± 0.09	2.3 ± 0.2	1.5 ± 0.3	−0.3 ± 0.1	PMN J1427-4206
14 37 16	63 35		0.7 ± 0.05	0.5 ± 0.1	. . .	0.6 ± 0.1	. . .	−0.1 ± 0.5	GB6 J1436+6336[a]
14 42 55	51 56		0.8 ± 0.04	1.0 ± 0.06	0.9 ± 0.06	0.9 ± 0.1	. . .	0.1 ± 0.3	GB6 J1443+5201
14 46 50	−16 21		1.0 ± 0.05	1.0 ± 0.07	0.8 ± 0.07	0.7 ± 0.1	0.6 ± 0.2	−0.3 ± 0.3	. . .
14 54 21	−37 49		1.3 ± 0.06	1.0 ± 0.07	1.1 ± 0.1	0.9 ± 0.2	1.4 ± 0.3	−0.3 ± 0.3	PMN J1454-3747
14 57 21	−35 36		0.8 ± 0.08	1.0 ± 0.1	1.0 ± 0.09	0.8 ± 0.2	1.2 ± 0.3	0.2 ± 0.3	PMN J1457-3538
14 58 31	71 40	071	1.3 ± 0.06	1.2 ± 0.1	0.8 ± 0.08	0.8 ± 0.1	. . .	−0.6 ± 0.3	GB6 J1459+7140
15 03 02	−41 57		2.5 ± 0.05	2.0 ± 0.07	1.7 ± 0.08	1.0 ± 0.1	1.1 ± 0.2	−0.7 ± 0.1	PMN J1503-4154
15 04 30	10 30	006	1.8 ± 0.05	1.6 ± 0.08	1.4 ± 0.08	1.0 ± 0.1	1.1 ± 0.3	−0.4 ± 0.2	GB6 J1504+1029
15 06 56	−16 43		1.3 ± 0.07	0.4 ± 0.1	0.8 ± 0.2	0.8 ± 0.2	0.9 ± 0.3	−0.5 ± 0.3	PMN J1507-1652[a]
15 10 34	−05 47		1.2 ± 0.06	1.1 ± 0.08	1.1 ± 0.09	0.9 ± 0.2	. . .	−0.2 ± 0.3	PMN J1510-0543
15 12 46	−09 05	207	1.9 ± 0.06	1.8 ± 0.09	2.0 ± 0.1	1.9 ± 0.2	1.8 ± 0.3	−0.0 ± 0.2	1Jy 1510-08
15 13 49	−09 58		1.5 ± 0.06	1.0 ± 0.1	0.8 ± 0.1	1.2 ± 0.2	0.9 ± 0.4	−0.5 ± 0.3	. . .
15 16 42	00 14	002	1.6 ± 0.05	1.8 ± 0.07	1.6 ± 0.08	1.6 ± 0.2	0.8 ± 0.3	−0.0 ± 0.2	GB6 J1516+0015
15 17 45	−24 21	205	2.2 ± 0.05	2.2 ± 0.09	2.1 ± 0.1	2.1 ± 0.2	1.1 ± 0.4	−0.1 ± 0.1	PMN J1517-2422
15 29 15	30 57		0.5 ± 0.03	0.6 ± 0.04	0.4 ± 0.05	0.7 ± 0.09	0.6 ± 0.1	0.1 ± 0.2	. . .
15 34 55	01 27		0.8 ± 0.06	0.8 ± 0.09	0.9 ± 0.1	1.1 ± 0.2	. . .	0.1 ± 0.4	GB6 J1534+0131
15 40 58	14 47		1.1 ± 0.05	0.9 ± 0.07	0.8 ± 0.09	0.8 ± 0.2	. . .	−0.5 ± 0.3	GB6 J1540+1447
15 49 25	50 36		0.8 ± 0.05	0.6 ± 0.08	0.8 ± 0.1	0.5 ± 0.2	. . .	−0.2 ± 0.4	GB6 J1549+5038
15 49 32	02 36	005	2.8 ± 0.06	2.9 ± 0.09	2.4 ± 0.09	2.1 ± 0.2	2.0 ± 0.4	−0.2 ± 0.1	GB6 J1549+0237
15 50 38	05 26	007	2.7 ± 0.05	2.4 ± 0.08	2.0 ± 0.09	2.0 ± 0.2	1.4 ± 0.3	−0.4 ± 0.1	GB6 J1550+0527
16 02 07	33 31		0.9 ± 0.03	0.8 ± 0.06	0.8 ± 0.05	0.5 ± 0.1	. . .	−0.3 ± 0.2	GB6 J1602+3326
16 04 29	57 18		0.8 ± 0.04	0.8 ± 0.06	0.8 ± 0.05	0.6 ± 0.09	. . .	−0.1 ± 0.2	GB6 J1604+5714[a]
16 08 52	10 28	009	1.9 ± 0.05	1.9 ± 0.08	1.8 ± 0.08	1.4 ± 0.1	1.1 ± 0.3	−0.2 ± 0.1	GB6 J1608+1029
16 13 41	34 12	023	3.9 ± 0.04	3.5 ± 0.07	3.1 ± 0.07	2.5 ± 0.1	1.8 ± 0.3	−0.4 ± 0.07	GB6 J1613+3412
16 18 01	−77 16	183	2.3 ± 0.04	2.1 ± 0.07	1.8 ± 0.07	1.6 ± 0.1	0.8 ± 0.2	−0.4 ± 0.1	PMN J1617-7717
16 23 21	−68 18		0.7 ± 0.03	0.6 ± 0.04	0.6 ± 0.06	. . .	. . .	−0.4 ± 0.4	PMN J1624-6809
16 26 15	41 28		1.0 ± 0.04	0.8 ± 0.07	0.8 ± 0.07	0.7 ± 0.1	. . .	−0.4 ± 0.3	GB6 J1625+4134
16 33 17	82 27	076	1.4 ± 0.04	1.5 ± 0.06	1.5 ± 0.08	1.2 ± 0.09	0.8 ± 0.2	−0.1 ± 0.1	. . .[e]
16 35 16	38 07	033	3.7 ± 0.04	4.1 ± 0.07	3.9 ± 0.07	3.5 ± 0.1	3.2 ± 0.4	0.0 ± 0.06	GB6 J1635+3808
16 37 31	47 13		1.1 ± 0.04	1.1 ± 0.08	1.2 ± 0.08	0.9 ± 0.08	0.6 ± 0.2	−0.2 ± 0.2	GB6 J1637+4717
16 38 16	57 22	056	1.7 ± 0.04	1.7 ± 0.07	1.6 ± 0.07	1.7 ± 0.1	1.1 ± 0.2	−0.1 ± 0.1	GB6 J1638+5720
16 42 27	68 55	069	1.8 ± 0.04	1.9 ± 0.06	1.8 ± 0.07	2.0 ± 0.2	1.4 ± 0.2	−0.0 ± 0.1	GB6 J1642+6856
16 42 51	−77 13		0.8 ± 0.06	0.9 ± 0.08	0.8 ± 0.09	0.8 ± 0.1	. . .	−0.0 ± 0.3	PMN J1644-7715
16 42 52	39 48	035	6.6 ± 0.04	6.0 ± 0.07	5.4 ± 0.07	4.9 ± 0.1	3.7 ± 0.3	−0.3 ± 0.04	GB6 J1642+3948
16 48 35	41 10		0.7 ± 0.04	0.8 ± 0.08	0.8 ± 0.07	0.7 ± 0.09	0.8 ± 0.2	0.1 ± 0.2	GB6 J1648+4104[a]
16 51 06	04 57	010	1.7 ± 0.06	1.1 ± 0.1	0.9 ± 0.1	0.7 ± 0.2	. . .	−1.0 ± 0.4	GB6 J1651+0459
16 54 10	39 39	036	1.2 ± 0.04	1.2 ± 0.07	0.8 ± 0.06	0.6 ± 0.1	. . .	−0.6 ± 0.2	GB6 J1653+3945[a]
16 57 10	57 07		0.4 ± 0.05	. . .	0.6 ± 0.08	0.7 ± 0.1	0.7 ± 0.2	0.5 ± 0.3	GB6 J1657+5705
16 58 04	07 42	013	1.7 ± 0.05	1.7 ± 0.06	1.5 ± 0.08	1.4 ± 0.1	1.1 ± 0.2	−0.2 ± 0.2	GB6 J1658+0741
16 58 15	47 47		1.2 ± 0.03	1.2 ± 0.05	0.7 ± 0.06	. . .	. . .	−0.4 ± 0.3	GB6 J1658+4737
16 58 47	05 19		0.9 ± 0.05	0.7 ± 0.07	0.6 ± 0.1	0.6 ± 0.1	. . .	−0.4 ± 0.4	GB6 J1658+0515
17 00 01	68 27		0.3 ± 0.06	0.5 ± 0.07	0.6 ± 0.06	0.6 ± 0.08	0.6 ± 0.1	0.4 ± 0.4	GB6 J1700+6830
17 02 01	40 00		0.6 ± 0.04	0.8 ± 0.07	0.8 ± 0.06	0.9 ± 0.1	0.8 ± 0.2	0.4 ± 0.3	GB6 J1701+3954
17 03 35	−62 14	198	1.6 ± 0.04	1.7 ± 0.06	1.6 ± 0.07	1.4 ± 0.1	. . .	−0.0 ± 0.1	PMN J1703-6212

Table 5
(Continued)

R.A. (hms)	Decl. (dm)	ID	K (Jy)	Ka (Jy)	Q (Jy)	V (Jy)	W (Jy)	α	5 GHz ID
17 07 40	01 48		0.8 ± 0.05	0.8 ± 0.1	0.8 ± 0.07	0.7 ± 0.2	...	0.0 ± 0.4	GB6 J1707+0148
17 15 55	68 39		0.6 ± 0.03	0.5 ± 0.05	0.6 ± 0.05	0.5 ± 0.09	0.7 ± 0.2	−0.0 ± 0.2	GB6 J1716+6836
17 19 25	17 42		0.6 ± 0.05	0.4 ± 0.09	0.5 ± 0.1	0.5 ± 0.2	...	−0.4 ± 0.6	GB6 J1719+1745
17 24 02	−65 00	196	2.4 ± 0.04	2.0 ± 0.07	1.7 ± 0.08	1.2 ± 0.1	1.1 ± 0.3	−0.6 ± 0.1	PMN J1723-6500
17 27 17	45 30	043	0.9 ± 0.04	0.9 ± 0.07	0.8 ± 0.06	1.2 ± 0.2	...	0.1 ± 0.3	GB6 J1727+4530
17 28 22	04 28		0.4 ± 0.08	...	0.8 ± 0.2	1.0 ± 0.2	...	0.9 ± 0.6	GB6 J1728+0426
17 34 17	38 57	038	1.2 ± 0.04	1.3 ± 0.07	1.2 ± 0.08	1.2 ± 0.1	...	0.0 ± 0.2	GB6 J1734+3857
17 35 42	36 16		0.7 ± 0.04	0.7 ± 0.07	0.6 ± 0.06	0.2 ± 0.1	...	−0.3 ± 0.4	GB6 J1735+3616
17 36 00	−79 34	186	1.1 ± 0.04	1.3 ± 0.06	1.3 ± 0.05	0.9 ± 0.1	...	0.1 ± 0.2	PMN J1733-7935
17 36 59	06 25		0.9 ± 0.06	1.0 ± 0.06	0.8 ± 0.08	0.8 ± 0.2	...	−0.2 ± 0.4	GB6 J1737+0620[a]
17 37 48	−56 50		1.0 ± 0.04	0.9 ± 0.06	0.8 ± 0.07	...	...	−0.3 ± 0.3	...
17 38 29	50 14		0.7 ± 0.04	0.5 ± 0.06	0.5 ± 0.08	0.5 ± 0.2	...	−0.7 ± 0.5	...
17 40 13	47 40		0.9 ± 0.04	0.8 ± 0.06	0.8 ± 0.07	0.9 ± 0.1	1.0 ± 0.2	0.0 ± 0.2	GB6 J1739+4738
17 40 35	52 12	048	1.2 ± 0.04	1.2 ± 0.06	1.2 ± 0.07	1.1 ± 0.1	...	−0.1 ± 0.2	GB6 J1740+5211
17 49 13	70 06	068	0.5 ± 0.03	0.6 ± 0.04	0.7 ± 0.05	0.8 ± 0.07	0.7 ± 0.1	0.4 ± 0.2	GB6 J1748+7005
17 51 36	09 37		4.4 ± 0.05	4.6 ± 0.08	4.5 ± 0.09	4.3 ± 0.2	3.3 ± 0.3	−0.0 ± 0.06	GB6 J1751+0938
17 53 31	28 48	022	2.1 ± 0.04	2.0 ± 0.06	1.9 ± 0.07	2.0 ± 0.2	1.4 ± 0.2	−0.1 ± 0.1	GB6 J1753+2847
17 53 32	44 03		0.6 ± 0.05	0.6 ± 0.09	0.7 ± 0.07	0.7 ± 0.1	...	0.1 ± 0.3	GB6 J1753+4410[a]
17 58 58	66 32	064	0.7 ± 0.01	0.6 ± 0.02	0.6 ± 0.05	0.4 ± 0.08	...	−0.2 ± 0.2	GB6 J1758+6638[a]
17 59 51	38 53		0.9 ± 0.04	0.7 ± 0.07	0.6 ± 0.1	...	...	−0.6 ± 0.5	GB6 J1800+3848[a]
18 00 33	78 27	072	2.0 ± 0.04	1.9 ± 0.06	1.7 ± 0.07	1.7 ± 0.1	1.1 ± 0.3	−0.3 ± 0.1	1Jy 1803+78
18 01 34	44 04		1.4 ± 0.04	1.5 ± 0.06	1.6 ± 0.08	1.5 ± 0.1	0.9 ± 0.2	0.1 ± 0.1	GB6 J1801+4404
18 03 04	−65 07	199	1.1 ± 0.04	1.1 ± 0.07	1.2 ± 0.08	0.9 ± 0.2	0.9 ± 0.3	−0.0 ± 0.2	PMN J1803-6507
18 06 44	69 48	067	1.4 ± 0.03	1.4 ± 0.05	1.2 ± 0.06	1.2 ± 0.1	1.3 ± 0.3	−0.2 ± 0.1	GB6 J1806+6949
18 08 36	56 59		0.6 ± 0.04	0.6 ± 0.06	0.8 ± 0.05	0.7 ± 0.08	...	0.4 ± 0.3	GB6 J1808+5709[a]
18 11 53	06 48		0.9 ± 0.05	0.9 ± 0.1	0.7 ± 0.09	0.6 ± 0.2	0.7 ± 0.3	−0.4 ± 0.4	GB6 J1812+0651
18 12 36	55 53		0.2 ± 0.03	0.3 ± 0.09	0.5 ± 0.07	...	0.5 ± 0.2	0.9 ± 0.6	GB6 J1812+5603
18 19 59	−55 20		0.8 ± 0.07	...	0.6 ± 0.1	...	...	−0.5 ± 0.8	PMN J1819-5521
18 20 03	−63 42	200	1.7 ± 0.05	1.6 ± 0.08	1.4 ± 0.08	1.2 ± 0.1	1.3 ± 0.2	−0.3 ± 0.2	PMN J1819-6345
18 24 08	56 50	053	1.5 ± 0.04	1.2 ± 0.06	1.2 ± 0.07	1.2 ± 0.1	0.7 ± 0.2	−0.4 ± 0.2	GB6 J1824+5650
18 25 35	67 38		...	...	0.3 ± 0.09	0.6 ± 0.09	0.6 ± 0.1	0.7 ± 0.9	...
18 29 42	48 45	046	2.9 ± 0.04	2.8 ± 0.06	2.5 ± 0.07	1.8 ± 0.1	1.2 ± 0.2	−0.3 ± 0.09	GB6 J1829+4844
18 32 51	68 44		...	...	0.4 ± 0.04	0.6 ± 0.06	0.6 ± 0.1	0.6 ± 0.5	GB6 J1832+6848
18 34 23	−58 54		1.1 ± 0.04	1.0 ± 0.06	1.1 ± 0.07	0.7 ± 0.1	0.6 ± 0.3	−0.1 ± 0.2	PMN J1834-5856
18 35 06	32 47		0.8 ± 0.04	0.8 ± 0.07	0.7 ± 0.07	0.5 ± 0.1	...	−0.3 ± 0.4	GB6 J1835+3241
18 37 23	−71 05	192	1.9 ± 0.04	1.8 ± 0.05	1.5 ± 0.06	1.2 ± 0.09	...	−0.4 ± 0.1	PMN J1837-7108
18 39 36	67 18		...	...	0.7 ± 0.04	0.5 ± 0.07	0.6 ± 0.1	−0.4 ± 0.5	GB6 J1841+6718[a]
18 40 49	79 46	073	1.4 ± 0.04	1.0 ± 0.06	0.8 ± 0.09	...	...	−1.0 ± 0.3	1Jy 1845+79
18 42 49	68 08	066	1.3 ± 0.03	1.4 ± 0.04	1.4 ± 0.04	1.1 ± 0.07	0.8 ± 0.1	−0.1 ± 0.1	GB6 J1842+6809[a]
18 48 35	32 22		0.7 ± 0.05	0.6 ± 0.1	0.6 ± 0.1	...	0.6 ± 0.2	−0.2 ± 0.5	GB6 J1848+3219
18 49 33	67 05	065	1.6 ± 0.03	1.8 ± 0.05	1.8 ± 0.04	1.6 ± 0.08	...	0.1 ± 0.1	GB6 J1849+6705[a]
18 50 44	28 23	028	1.5 ± 0.04	1.1 ± 0.06	0.9 ± 0.05	0.6 ± 0.09	...	−0.8 ± 0.2	GB6 J1850+2825
19 01 48	−36 59		1.4 ± 0.04	1.2 ± 0.05	0.9 ± 0.07	1.4 ± 0.1	3.4 ± 0.3	0.3 ± 0.1	...
19 02 51	31 53	034	1.4 ± 0.04	1.1 ± 0.05	0.8 ± 0.06	...	...	−0.7 ± 0.2	GB6 J1902+3159
19 11 08	−20 06		2.3 ± 0.06	2.6 ± 0.1	2.6 ± 0.1	2.2 ± 0.2	2.6 ± 0.4	0.1 ± 0.1	PMN J1911-2006
19 15 16	−80 03		0.8 ± 0.04	0.5 ± 0.06	0.4 ± 0.06	...	...	−1.3 ± 0.6	PMN J1912-8010
19 23 29	−21 05	008	2.4 ± 0.06	2.4 ± 0.09	2.4 ± 0.1	2.3 ± 0.2	1.7 ± 0.3	−0.0 ± 0.1	PMN J1923-2104
19 24 52	−29 14		12.6 ± 0.06	12.0 ± 0.09	11.1 ± 0.1	10.4 ± 0.2	7.2 ± 0.3	−0.2 ± 0.03	PMN J1924-2914
19 27 35	61 19	059	1.0 ± 0.04	0.9 ± 0.06	0.9 ± 0.08	0.8 ± 0.1	0.4 ± 0.2	−0.2 ± 0.2	GB6 J1927+6117
19 27 42	73 57	070	3.6 ± 0.04	3.3 ± 0.05	2.8 ± 0.06	2.6 ± 0.1	1.6 ± 0.2	−0.3 ± 0.06	GB6 J1927+7357
19 37 04	−39 58		1.2 ± 0.06	1.4 ± 0.1	1.3 ± 0.1	1.1 ± 0.1	...	0.1 ± 0.3	PMN J1937-3957
19 38 25	−63 43		1.0 ± 0.04	0.8 ± 0.07	0.7 ± 0.06	0.3 ± 0.1	...	−0.6 ± 0.3	PMN J1939-6342[a]
19 39 23	−15 25		1.2 ± 0.05	1.1 ± 0.08	1.2 ± 0.08	0.7 ± 0.2	...	−0.1 ± 0.3	PMN J1939-1525
19 45 35	−55 18		0.6 ± 0.09	0.5 ± 0.08	0.4 ± 0.06	...	1.0 ± 0.3	0.1 ± 0.5	PMN J1945-5520
19 52 19	02 34		0.9 ± 0.06	0.6 ± 0.07	0.5 ± 0.09	0.7 ± 0.2	...	−0.5 ± 0.4	GB6 J1952+0230
19 55 41	51 37	051	1.0 ± 0.04	1.1 ± 0.08	0.9 ± 0.09	0.8 ± 0.1	0.6 ± 0.2	−0.1 ± 0.2	GB6 J1955+5131[a]
19 57 37	−55 19		0.9 ± 0.04	0.8 ± 0.06	0.8 ± 0.07	0.4 ± 0.1	...	−0.2 ± 0.3	...
19 58 02	−38 45	003	3.3 ± 0.05	3.4 ± 0.08	3.1 ± 0.09	2.4 ± 0.2	2.0 ± 0.3	−0.2 ± 0.1	PMN J1957-3845
20 00 58	−17 49	011	2.1 ± 0.06	2.1 ± 0.09	2.0 ± 0.1	1.9 ± 0.1	1.4 ± 0.3	−0.1 ± 0.1	PMN J2000-1748
20 05 50	77 54		0.9 ± 0.05	0.9 ± 0.08	0.8 ± 0.09	1.1 ± 0.1	0.8 ± 0.2	0.1 ± 0.2	1Jy 2007+77
20 08 16	66 14		0.8 ± 0.03	0.6 ± 0.06	0.5 ± 0.05	0.5 ± 0.1	0.6 ± 0.2	−0.6 ± 0.3	GB6 J2007+6607
20 09 53	72 32		0.6 ± 0.04	0.8 ± 0.07	0.9 ± 0.07	0.8 ± 0.1	0.7 ± 0.2	0.4 ± 0.3	GB6 J2009+7229
20 11 18	−15 47	014	1.9 ± 0.05	1.6 ± 0.1	1.5 ± 0.1	1.4 ± 0.2	2.8 ± 0.9	−0.3 ± 0.2	PMN J2011-1546
20 15 52	65 58		0.8 ± 0.03	0.8 ± 0.05	0.7 ± 0.06	0.8 ± 0.1	...	−0.0 ± 0.3	GB6 J2015+6554[a]
20 22 26	61 36	063	1.7 ± 0.05	1.5 ± 0.07	1.2 ± 0.06	1.0 ± 0.2	...	−0.5 ± 0.2	GB6 J2022+6137
20 23 42	54 26		0.7 ± 0.06	0.8 ± 0.07	0.9 ± 0.06	0.8 ± 0.1	...	0.2 ± 0.3	GB6 J2023+5427

Table 5
(Continued)

R.A. (hms)	Decl. (dm)	ID	K (Jy)	Ka (Jy)	Q (Jy)	V (Jy)	W (Jy)	α	5 GHz ID
20 24 27	17 12	031	1.0 ± 0.04	1.0 ± 0.06	0.9 ± 0.07	0.7 ± 0.1	. . .	−0.1 ± 0.3	GB6 J2024+1718[a]
20 34 48	−68 45	194	0.7 ± 0.05	0.8 ± 0.07	0.8 ± 0.06	0.8 ± 0.08	0.5 ± 0.1	0.0 ± 0.2	PMN J2035-6846
20 35 10	10 57		0.7 ± 0.06	1.1 ± 0.1	0.8 ± 0.07	0.9 ± 0.2	0.8 ± 0.2	0.2 ± 0.3	GB6 J2035+1055
20 56 11	−47 16	208	2.6 ± 0.04	2.8 ± 0.07	2.5 ± 0.08	2.3 ± 0.1	1.8 ± 0.3	−0.1 ± 0.1	PMN J2056-4714
21 01 30	03 45		1.2 ± 0.04	1.0 ± 0.07	0.8 ± 0.09	1.0 ± 0.2	. . .	−0.4 ± 0.3	GB6 J2101+0341
21 02 49	−78 31		0.6 ± 0.06	0.5 ± 0.1	0.5 ± 0.06	. . .	0.7 ± 0.3	−0.1 ± 0.5	PMN J2105-7825[a]
21 07 33	−25 21		1.0 ± 0.06	0.8 ± 0.1	0.6 ± 0.09	. . .	. . .	−0.7 ± 0.6	PMN J2107-2526[a]
21 09 32	−41 11	001	1.6 ± 0.05	1.6 ± 0.08	1.2 ± 0.1	1.2 ± 0.2	0.9 ± 0.2	−0.3 ± 0.2	PMN J2109-4110
21 09 37	35 36	049	0.9 ± 0.05	0.7 ± 0.08	0.7 ± 0.08	0.8 ± 0.1	. . .	−0.3 ± 0.3	GB6 J2109+3532[a]
21 23 41	05 36	027	2.0 ± 0.06	1.6 ± 0.08	1.4 ± 0.1	1.1 ± 0.2	0.9 ± 0.4	−0.6 ± 0.2	GB6 J2123+0535
21 24 24	25 09		0.8 ± 0.05	0.5 ± 0.07	0.4 ± 0.07	. . .	. . .	−1.2 ± 0.6	GB6 J2123+2504
21 30 01	−09 27		0.9 ± 0.06	0.8 ± 0.1	0.9 ± 0.1	0.7 ± 0.2	1.0 ± 0.3	0.0 ± 0.3	PMN J2130-0927
21 31 32	−12 06	017	2.7 ± 0.06	2.5 ± 0.09	2.4 ± 0.09	1.7 ± 0.1	1.2 ± 0.4	−0.3 ± 0.1	PMN J2131-1207
21 34 09	−01 53	020	2.0 ± 0.05	1.9 ± 0.08	1.7 ± 0.1	1.8 ± 0.2	1.5 ± 0.3	−0.2 ± 0.2	PMN J2134-0153
21 36 37	00 41	025	4.7 ± 0.06	3.7 ± 0.1	3.1 ± 0.1	1.8 ± 0.2	1.3 ± 0.3	−0.7 ± 0.1	GB6 J2136+0041
21 39 16	14 25	041	2.3 ± 0.05	2.1 ± 0.07	1.8 ± 0.08	1.3 ± 0.2	1.0 ± 0.2	−0.4 ± 0.1	GB6 J2139+1423
21 42 30	−04 36		0.5 ± 0.05	0.4 ± 0.1	0.8 ± 0.1	0.7 ± 0.1	1.0 ± 0.3	0.5 ± 0.4	PMN J2142-0437
21 43 22	17 42	044	1.2 ± 0.04	1.3 ± 0.06	0.9 ± 0.09	0.7 ± 0.1	. . .	−0.1 ± 0.3	GB6 J2143+1743[a]
21 48 03	−77 59	184	1.7 ± 0.04	1.5 ± 0.06	1.2 ± 0.06	0.7 ± 0.1	. . .	−0.6 ± 0.2	PMN J2146-7755
21 48 05	06 57	037	7.7 ± 0.05	7.3 ± 0.08	7.0 ± 0.1	6.2 ± 0.2	5.0 ± 0.4	−0.2 ± 0.04	GB6 J2148+0657
21 51 49	−30 27		1.4 ± 0.06	1.4 ± 0.09	1.4 ± 0.1	1.6 ± 0.2	1.9 ± 0.7	0.1 ± 0.2	PMN J2151-3028
21 57 06	−69 42	190	3.8 ± 0.04	3.0 ± 0.07	2.6 ± 0.06	2.0 ± 0.1	. . .	−0.6 ± 0.08	PMN J2157-6941
21 58 06	−15 02	018	2.1 ± 0.06	1.8 ± 0.08	1.7 ± 0.09	1.5 ± 0.2	. . .	−0.3 ± 0.2	PMN J2158-1501
22 02 50	42 17	058	3.6 ± 0.04	3.6 ± 0.06	3.6 ± 0.06	3.2 ± 0.1	. . .	−0.0 ± 0.06	GB6 J2202+4216
22 03 19	31 46	054	2.7 ± 0.04	2.5 ± 0.07	2.1 ± 0.09	1.7 ± 0.2	1.4 ± 0.3	−0.4 ± 0.1	GB6 J2203+3145
22 03 22	17 23	045	1.5 ± 0.05	1.6 ± 0.08	1.6 ± 0.09	1.4 ± 0.1	. . .	0.0 ± 0.2	GB6 J2203+1725
22 06 13	−18 38	016	1.9 ± 0.05	1.6 ± 0.08	1.2 ± 0.08	1.1 ± 0.2	. . .	−0.6 ± 0.2	PMN J2206-1835
22 07 17	−53 47		1.0 ± 0.05	0.9 ± 0.07	0.8 ± 0.08	0.6 ± 0.2	. . .	−0.5 ± 0.4	PMN J2207-5346
22 11 32	23 52	050	1.3 ± 0.06	1.5 ± 0.08	1.4 ± 0.07	1.1 ± 0.1	. . .	−0.0 ± 0.2	GB6 J2212+2355
22 12 48	−25 24		0.9 ± 0.06	0.7 ± 0.09	0.6 ± 0.1	0.7 ± 0.1	. . .	−0.3 ± 0.4	PMN J2213-2529[a]
22 18 51	−03 35	030	2.1 ± 0.05	1.7 ± 0.1	1.7 ± 0.1	1.4 ± 0.2	0.8 ± 0.3	−0.5 ± 0.2	PMN J2218-0335
22 21 12	−04 16		. . .	. . .	0.7 ± 0.07	0.4 ± 0.1	. . .	−1.4 ± 2	. . .
22 25 38	21 19		1.0 ± 0.06	1.1 ± 0.08	1.1 ± 0.08	1.0 ± 0.1	. . .	0.1 ± 0.3	GB6 J2225+2118
22 25 46	−04 56	029	5.8 ± 0.05	5.5 ± 0.09	4.9 ± 0.1	4.4 ± 0.2	3.6 ± 0.4	−0.3 ± 0.06	PMN J2225-0457
22 29 42	−08 33	024	2.3 ± 0.06	2.7 ± 0.1	2.6 ± 0.1	3.1 ± 0.2	2.3 ± 0.4	0.2 ± 0.1	PMN J2229-0832
22 29 45	−20 50		0.9 ± 0.06	0.8 ± 0.1	0.9 ± 0.1	1.1 ± 0.3	1.0 ± 0.2	0.1 ± 0.3	PMN J2229-2049
22 32 37	11 44	047	3.6 ± 0.06	4.1 ± 0.09	4.1 ± 0.1	4.2 ± 0.2	3.9 ± 0.3	0.2 ± 0.07	GB6 J2232+1143
22 35 10	−48 34	206	2.0 ± 0.04	2.1 ± 0.07	2.0 ± 0.09	1.7 ± 0.1	1.6 ± 0.3	−0.1 ± 0.1	PMN J2235-4835
22 36 26	28 24	057	1.2 ± 0.05	1.3 ± 0.08	1.3 ± 0.08	1.0 ± 0.1	. . .	−0.0 ± 0.2	GB6 J2236+2828
22 39 35	−57 01	201	1.3 ± 0.04	1.4 ± 0.05	1.2 ± 0.06	0.9 ± 0.09	1.3 ± 0.3	−0.1 ± 0.2	PMN J2239-5701
22 46 15	−12 07	021	2.1 ± 0.05	1.9 ± 0.1	1.8 ± 0.1	1.6 ± 0.3	. . .	−0.2 ± 0.2	PMN J2246-1206
22 47 27	−37 00		0.7 ± 0.08	0.6 ± 0.1	0.6 ± 0.1	0.4 ± 0.1	. . .	−0.3 ± 0.6	PMN J2247-3657
22 53 59	16 08	055	8.0 ± 0.05	8.5 ± 0.09	8.7 ± 0.09	9.0 ± 0.2	8.6 ± 0.3	0.1 ± 0.03	GB6 J2253+1608
22 55 47	42 01		0.9 ± 0.03	0.7 ± 0.06	0.6 ± 0.07	. . .	. . .	−0.7 ± 0.4	GB6 J2255+4202
22 56 31	−20 13	019	0.9 ± 0.05	0.8 ± 0.07	0.8 ± 0.07	0.5 ± 0.2	. . .	−0.4 ± 0.4	PMN J2256-2011
22 58 06	−27 56	012	4.8 ± 0.05	4.7 ± 0.08	4.4 ± 0.09	3.9 ± 0.2	3.2 ± 0.4	−0.2 ± 0.07	PMN J2258-2758
23 02 39	−68 06		0.7 ± 0.06	0.3 ± 0.1	0.5 ± 0.1	. . .	. . .	−1.0 ± 1	PMN J2303-6807[a]
23 11 35	34 29		0.6 ± 0.04	0.6 ± 0.07	0.7 ± 0.1	. . .	. . .	0.2 ± 0.6	GB6 J2311+3425
23 15 07	−31 36		1.0 ± 0.04	0.9 ± 0.07	0.9 ± 0.08	0.8 ± 0.2	. . .	−0.1 ± 0.3	PMN J2314-3138
23 15 53	−50 19	204	1.1 ± 0.03	1.1 ± 0.05	0.9 ± 0.06	1.2 ± 0.3	. . .	−0.2 ± 0.2	PMN J2315-5018
23 21 33	27 32		0.8 ± 0.06	0.6 ± 0.1	0.4 ± 0.1	0.8 ± 0.2	. . .	−0.2 ± 0.5	GB6 J2322+2732
23 22 23	44 46		0.8 ± 0.03	0.9 ± 0.04	0.8 ± 0.06	0.7 ± 0.1	0.8 ± 0.2	−0.0 ± 0.2	GB6 J2322+4445[a]
23 22 46	51 05		0.9 ± 0.04	0.8 ± 0.09	0.7 ± 0.06	0.6 ± 0.07	. . .	−0.5 ± 0.3	GB6 J2322+5057[a]
23 23 33	−03 14		0.7 ± 0.08	0.7 ± 0.1	0.5 ± 0.1	0.4 ± 0.2	. . .	−0.5 ± 0.7	PMN J2323-0317
23 27 37	09 38		1.1 ± 0.06	1.2 ± 0.1	1.1 ± 0.1	1.1 ± 0.2	0.9 ± 0.3	0.0 ± 0.3	GB6 J2327+0940[a]
23 29 06	−47 32		1.3 ± 0.04	1.1 ± 0.07	1.2 ± 0.1	0.9 ± 0.1	0.8 ± 0.2	−0.3 ± 0.2	PMN J2329-4730
23 30 19	33 48		0.8 ± 0.05	0.7 ± 0.06	0.7 ± 0.08	0.7 ± 0.1	. . .	−0.1 ± 0.4	GB6 J2330+3348[a]
23 30 42	10 57		1.0 ± 0.05	1.1 ± 0.08	0.9 ± 0.08	0.9 ± 0.2	. . .	−0.1 ± 0.3	GB6 J2330+1100
23 31 20	−15 59	032	1.0 ± 0.06	0.8 ± 0.1	0.7 ± 0.1	0.7 ± 0.1	0.8 ± 0.4	−0.4 ± 0.3	PMN J2331-1556
23 33 47	−23 40		1.0 ± 0.05	0.9 ± 0.07	1.0 ± 0.1	1.2 ± 0.2	0.8 ± 0.3	0.1 ± 0.3	PMN J2333-2343[a]
23 34 10	07 35		1.1 ± 0.06	1.0 ± 0.07	1.1 ± 0.08	1.3 ± 0.2	0.8 ± 0.2	0.0 ± 0.2	GB6 J2334+0736
23 34 50	−01 28		0.6 ± 0.05	1.0 ± 0.1	0.9 ± 0.1	0.7 ± 0.1	. . .	0.4 ± 0.4	PMN J2335-0131
23 35 29	−52 44	195	1.3 ± 0.03	0.8 ± 0.05	0.7 ± 0.08	0.4 ± 0.1	. . .	−1.2 ± 0.3	PMN J2336-5236[a]
23 45 14	−15 56		1.3 ± 0.05	1.0 ± 0.06	1.1 ± 0.07	1.2 ± 0.1	. . .	−0.2 ± 0.2	PMN J2345-1555
23 46 47	09 29		1.2 ± 0.05	1.2 ± 0.08	0.8 ± 0.09	0.6 ± 0.1	. . .	−0.5 ± 0.3	GB6 J2346+0930[a]
23 48 00	−49 32		0.7 ± 0.05	0.9 ± 0.05	0.7 ± 0.06	. . .	. . .	0.1 ± 0.4	. . .

Table 5
(Continued)

R.A. (hms)	Decl. (dm)	ID	K (Jy)	Ka (Jy)	Q (Jy)	V (Jy)	W (Jy)	α	5 GHz ID
23 48 14	−16 30	039	1.9 ± 0.05	1.9 ± 0.08	1.8 ± 0.08	1.6 ± 0.1	1.3 ± 0.3	−0.1 ± 0.1	PMN J2348-1631
23 49 28	38 44		0.8 ± 0.05	0.7 ± 0.1	0.4 ± 0.09	0.6 ± 0.2	0.9 ± 0.2	−0.1 ± 0.3	GB6 J2349+3849[a]
23 54 22	45 50	074	1.5 ± 0.05	1.2 ± 0.07	1.2 ± 0.09	1.0 ± 0.2	0.8 ± 0.2	−0.5 ± 0.2	GB6 J2354+4553
23 55 11	81 53		0.9 ± 0.04	0.8 ± 0.07	0.8 ± 0.06	1.2 ± 0.2	. . .	0.1 ± 0.2	NVSS J2356+8152
23 56 14	49 52	075	0.9 ± 0.03	0.8 ± 0.04	0.6 ± 0.06	0.4 ± 0.1	. . .	−0.4 ± 0.3	GB6 J2355+4950
23 57 51	−53 14	189	1.5 ± 0.04	1.3 ± 0.07	1.4 ± 0.08	1.2 ± 0.1	1.2 ± 0.2	−0.2 ± 0.1	PMN J2357-5311
23 58 04	−10 15		1.2 ± 0.05	1.4 ± 0.06	1.3 ± 0.08	1.1 ± 0.2	. . .	0.2 ± 0.2	PMN J2358-1020
23 58 52	−60 50	187	2.0 ± 0.04	1.5 ± 0.06	1.2 ± 0.06	0.9 ± 0.1	. . .	−0.8 ± 0.2	PMN J2358-6054

Notes.
[a] Indicates the source has multiple possible identifications.
[b] Source J0322-3711 (Fornax A) is extended, and the fluxes listed were obtained by aperture photometry.
[c] Source J0519-0540 is a blend of the Lynds Bright Nebulae LBN 207.65-23.11 and LBN 207.29-22.66.
[d] Source J1356+7645 is outside of the declination range of the GB6 and PMN catalogs. Identified as QSO NVSSJ135755+764320 by S. A. Trushkin (2006, private communication).
[e] Source J1633+8227 is outside of the declination range of the GB6 and PMN catalogs. It was identified as NGC 6251 by Trushkin (2003).

Table 6
WMAP CMB-free QVW Point Source Catalog

R.A. (dms)	Decl. (dms)	WMAP/QVW5 ID	Type	Q (Jy)	V (Jy)	W (Jy)	5 GHz ID	Dist. (arcmin)	Note
00 06 11.5	−06 24 57.6	J0006-0623	G	2.2 ± 0.2	1.9 ± 0.2	1.2 ± 0.4	PMN J0006-0623	1.4	
00 10 30.2	10 58 22.8	J0010+1101	G	0.9 ± 0.2	1.1 ± 0.2	1.1 ± 0.4	GB6 J0010+1058	0.4	
00 12 57.6	−39 53 49.2	J0012-3952	RadioS	0.8 ± 0.2	0.8 ± 0.2	1.0 ± 0.3	PMN J0013-3954	0.8	
00 13 44.2	40 54 21.6	QVW J0013+4051	G	0.6 ± 0.2	0.6 ± 0.2	0.5 ± 0.4	GB6 J0013+4051	3.8	
00 19 40.1	25 59 31.2	J0019+2603	QSO	0.9 ± 0.2	0.3 ± 0.2	0.5 ± 0.4	GB6 J0019+2602	3.3	
00 26 04.6	−35 12 39.6	J0026-3510	RadioS	1.4 ± 0.2	1.0 ± 0.2	0.6 ± 0.4	PMN J0026-3512	1.6	
00 29 49.7	05 53 38.4	J0029+0554	QSO	0.9 ± 0.2	0.6 ± 0.2	0.8 ± 0.4	GB6 J0029+0554B	1.4	a
00 38 10.6	−02 04 01.2	QVW J0037-0207	G	0.7 ± 0.2	0.5 ± 0.2	0.7 ± 0.4	PMN J0038-0207	4.3	
00 38 22.1	−25 01 51.6	J0038-2459	QSO	0.8 ± 0.2	1.1 ± 0.2	1.0 ± 0.4	PMN J0038-2459	3.3	
00 47 21.8	−25 14 45.6	J0047-2514	G	1.1 ± 0.2	0.9 ± 0.2	1.1 ± 0.4	PMN J0047-2517	3.5	
00 48 06.0	−73 13 08.4	. . .	SNR	1.2 ± 0.2	1.2 ± 0.2	1.4 ± 0.3	PMN J0047-7308	5.4	
00 50 01.2	−57 36 00.0	J0049-5739	QSO	1.2 ± 0.2	1.3 ± 0.2	0.7 ± 0.3	PMN J0050-5738	2.4	
00 50 57.4	−09 34 33.6	J0051-0927	QSO	0.8 ± 0.2	0.8 ± 0.2	0.5 ± 0.4	PMN J0050-0928	6.8	
00 51 13.2	−06 47 16.8	J0050-0649	QSO	1.0 ± 0.2	1.2 ± 0.2	1.0 ± 0.4	PMN J0051-0650	3.1	
00 57 48.2	30 27 28.8	QVW J0057+3026	G	1.0 ± 0.2	0.8 ± 0.2	0.2 ± 0.4	GB6 J0057+3021	6.2	
00 59 09.6	−56 56 06.0	J0100-5654	QSO	0.8 ± 0.2	0.6 ± 0.2	0.4 ± 0.3	PMN J0058-5659	4.4	b
01 00 21.1	−72 10 44.4	. . .	SNR	1.1 ± 0.2	0.9 ± 0.2	0.6 ± 0.3	PMN J0059-7210	5.3	
01 06 46.8	−40 32 42.0	J0106-4035	QSO	2.4 ± 0.1	2.1 ± 0.2	1.4 ± 0.3	PMN J0106-4034	1.6	
01 08 31.4	13 21 43.2	J0108+1319	GPair	0.8 ± 0.2	0.4 ± 0.2	−0.2 ± 0.4	GB6 J0108+1319	5.7	
01 08 33.8	01 36 18.0	J0108+0135	QSO	1.4 ± 0.2	1.4 ± 0.2	0.4 ± 0.4	GB6 J0108+0135	1.5	
01 12 17.0	35 20 31.2	. . .	QSO	0.9 ± 0.2	0.8 ± 0.2	0.1 ± 0.4	GB6 J0112+3522	2.0	
01 13 01.7	49 47 42.0	QVW J0112+4946	QSO	0.6 ± 0.2	0.6 ± 0.2	−0.0 ± 0.4	GB6 J0113+4948	4.2	
01 16 20.6	−11 36 28.8	J0116-1137	QSO	1.1 ± 0.2	1.2 ± 0.2	0.6 ± 0.4	PMN J0116-1136	2.2	
01 18 49.4	−21 36 03.6	. . .	QSO	0.8 ± 0.2	0.6 ± 0.2	0.2 ± 0.4	PMN J0118-2141	5.9	
01 21 48.5	11 51 43.2	J0121+1150	QSO	1.3 ± 0.2	0.7 ± 0.2	0.3 ± 0.4	GB6 J0121+1149	2.8	
01 25 31.7	−00 11 56.4	J0125-0010	QSO	0.9 ± 0.2	0.9 ± 0.2	0.3 ± 0.4	PMN J0125-0005	6.0	
01 32 42.7	−16 57 43.2	J0132-1653	QSO	1.3 ± 0.2	1.3 ± 0.2	1.4 ± 0.4	PMN J0132-1654	3.0	
01 36 59.5	47 53 06.0	J0137+4753	QSO	3.1 ± 0.2	3.2 ± 0.2	2.3 ± 0.4	GB6 J0136+4751	1.6	
01 37 28.1	33 10 37.2	QVW J0137+3312	QSO	0.8 ± 0.2	0.4 ± 0.2	0.3 ± 0.4	GB6 J1037+3309	2.7	
01 37 33.6	−24 30 00.0	J0137-2428	QSO	1.6 ± 0.2	1.3 ± 0.2	1.4 ± 0.3	PMN J0137-2430	1.6	
01 52 11.8	22 08 06.0	J0152+2208	QSO	1.1 ± 0.2	1.2 ± 0.2	0.6 ± 0.4	GB6 J0152+2206	1.8	
02 04 56.6	15 13 51.6	J0204+1513	QSO	1.1 ± 0.2	1.1 ± 0.2	0.4 ± 0.4	GB6 J0204+1514	1.4	
02 04 58.3	−17 03 54.0	J0205-1704	QSO	1.0 ± 0.2	0.8 ± 0.2	0.0 ± 0.4	PMN J0204-1701	2.6	
02 05 13.0	32 11 13.2	J0205+3213	QSO	1.5 ± 0.2	1.0 ± 0.2	0.7 ± 0.4	GB6 J0205+3212	2.3	
02 10 43.0	−51 01 30.0	J0210-5100	QSO	2.7 ± 0.1	2.5 ± 0.2	2.1 ± 0.3	PMN J0210-5101	0.7	
02 17 55.7	01 37 15.6	J0218+0138	QSO	0.5 ± 0.2	0.5 ± 0.2	0.2 ± 0.4	GB6 J0217+0144	7.8	b
02 21 08.4	35 54 10.8	J0220+3558	G	0.9 ± 0.2	0.9 ± 0.2	0.7 ± 0.4	GB6 J0221+3556	2.1	
02 22 44.2	43 02 09.6	J0223+4303	QSO	1.4 ± 0.2	1.0 ± 0.2	0.9 ± 0.4	GB6 J0223+4259	6.2	a
02 22 57.4	−34 40 04.8	J0222-3441	QSO	0.6 ± 0.2	0.5 ± 0.2	0.2 ± 0.3	PMN J0222-3441	1.4	
02 29 45.1	−78 45 03.6	QVW J0229-7843	QSO	0.7 ± 0.1	0.1 ± 0.2	0.2 ± 0.3	PMN J0229-7847	2.8	
02 31 41.0	13 21 32.4	J0231+1320	QSO	1.0 ± 0.2	0.9 ± 0.2	0.3 ± 0.4	GB6 J0231+1323	2.0	
02 37 49.0	28 48 18.0	J0237+2848	QSO	2.9 ± 0.2	2.7 ± 0.2	2.4 ± 0.4	GB6 J0237+2848	0.7	
02 38 40.3	16 35 45.6	J0238+1637	QSO	1.5 ± 0.2	1.6 ± 0.2	1.3 ± 0.4	GB6 J0238+1637	1.4	

Table 6
(Continued)

R.A. (dms)	Decl. (dms)	*WMAP*/QVW5 ID	Type	Q (Jy)	V (Jy)	W (Jy)	5 GHz ID	Dist. (arcmin)	Note
02 41 05.5	−08 16 48.0	J0241-0821	G	0.7 ± 0.2	0.3 ± 0.2	0.0 ± 0.4	PMN J0241-0815	1.3	
02 42 31.2	11 05 38.4	QVW J0242+1107	QSO	0.9 ± 0.2	0.7 ± 0.3	1.2 ± 0.4	GB6 J0242+1101	4.5	
02 53 21.1	−54 41 38.4	J0253-5442	QSO	2.0 ± 0.1	2.0 ± 0.2	1.9 ± 0.3	PMN J0253-5441	1.4	
02 59 26.2	−00 16 51.6	J0259-0015	QSO	0.8 ± 0.2	0.5 ± 0.2	0.3 ± 0.4	PMN J0259-0020	3.2	
03 03 33.6	47 17 45.6	. . .	QSO	0.9 ± 0.2	0.7 ± 0.2	0.9 ± 0.4	GB6 J0303+4716	1.5	
03 03 46.3	−62 10 26.4	J0303-6212	QSO	1.4 ± 0.2	1.5 ± 0.2	1.1 ± 0.3	PMN J0303-6211	1.1	
03 04 54.5	33 49 55.2	QVW J0304+3350	G	0.7 ± 0.2	0.3 ± 0.2	0.2 ± 0.4	GB6 J0304+3348	2.9	
03 08 26.4	04 10 40.8	J0308+0405	G	1.1 ± 0.2	0.7 ± 0.2	0.7 ± 0.4	GB6 J0308+0406	4.0	
03 09 23.5	10 24 25.2	J0309+1028	QSO	1.1 ± 0.2	1.2 ± 0.2	0.6 ± 0.4	GB6 J0309+1029	7.0	
03 09 53.3	−60 56 45.6	J0309-6102	QSO	0.8 ± 0.2	0.6 ± 0.2	0.4 ± 0.4	PMN J0309-6058	1.8	
03 11 38.4	−76 53 31.2	J0312-7645	QSO	1.0 ± 0.2	0.8 ± 0.2	1.1 ± 0.3	PMN J0311-7651	2.0	
03 12 36.0	41 21 50.4	. . .	G	0.7 ± 0.6	0.5 ± 0.4	0.0 ± 0.5	GB6 J0313+4120	5.1	
03 19 49.0	41 31 22.8	J0319+4131	G	7.7 ± 0.2	6.0 ± 0.2	4.5 ± 0.4	GB6 J0319+4130	0.8	
03 22 16.1	−37 11 20.4	J0322-3711	G	2.4 ± 0.1	1.3 ± 0.2	0.5 ± 0.3	1Jy 0320-37	5.1	
03 25 30.0	22 23 16.8	J0325+2225	QSO	1.1 ± 0.2	0.7 ± 0.2	0.3 ± 0.5	GB6 J0325+2223	1.7	
03 29 51.6	−23 55 19.2	J0329-2354	QSO	1.0 ± 0.1	0.9 ± 0.2	0.7 ± 0.3	PMN J0329-2357	1.9	
03 34 12.5	−40 06 21.6	J0334-4007	QSO	1.4 ± 0.2	1.2 ± 0.2	1.2 ± 0.4	PMN J0334-4008	2.2	
03 36 49.4	−13 04 44.4	J0336-1257	QSO	0.6 ± 0.2	0.3 ± 0.2	0.1 ± 0.4	PMN J0336-1302	4.4	
03 39 30.5	−01 47 49.2	J0339-0143	QSO	1.9 ± 0.2	1.7 ± 0.2	2.1 ± 0.4	PMN J0339-0146	1.2	
03 40 25.9	−21 22 40.8	J0340-2119	QSO	0.9 ± 0.2	1.2 ± 0.2	0.5 ± 0.3	PMN J0340-2119	3.9	
03 48 30.2	−16 10 37.2	QVW J0348-1609	QSO	0.8 ± 0.2	0.7 ± 0.2	0.9 ± 0.4	PMN J0348-1610	2.2	
03 48 49.7	−27 50 31.2	J0348-2747	QSO	0.8 ± 0.2	1.2 ± 0.2	1.0 ± 0.3	PMN J0348-2749	2.4	
03 51 15.1	−11 56 06.0	. . .	QSO	0.6 ± 0.2	0.2 ± 0.2	0.5 ± 0.4	PMN J0351-1153	2.6	
03 59 01.2	10 24 03.6	J0358+1029	G	0.6 ± 0.2	0.4 ± 0.2	0.4 ± 0.5	GB6 J0358+1026	2.7	
04 02 56.9	26 04 01.2	QVW J0402+2602	QSO	0.5 ± 0.2	0.6 ± 0.2	−0.2 ± 0.4	GB6 J0403+2600	4.4	
04 03 53.3	−36 04 55.2	J0403-3604	QSO	2.9 ± 0.2	2.7 ± 0.2	2.8 ± 0.3	PMN J0403-3605	0.3	
04 05 30.5	−13 06 32.4	J0405-1304	QSO	1.5 ± 0.2	1.4 ± 0.2	1.2 ± 0.4	PMN J0405-1308	1.8	
04 06 52.8	−38 24 54.0	J0407-3825	QSO	0.9 ± 0.2	0.7 ± 0.2	0.5 ± 0.3	PMN J0406-3826	1.9	
04 07 54.2	−12 16 08.4	QVW J0407-1216	QSO	0.8 ± 0.2	0.8 ± 0.3	0.3 ± 0.4	PMN J0407-1211	4.9	
04 11 37.4	76 55 51.6	J0411+7654	G	0.7 ± 0.2	0.7 ± 0.2	0.5 ± 0.3	1Jy 0403+76	3.1	
04 23 04.1	02 22 58.8	J0423+0218	QSO	0.4 ± 0.2	0.4 ± 0.2	0.0 ± 0.4	GB6 J0422+0219	4.6	a
04 23 14.9	−01 20 20.4	J0423-0120	QSO	6.7 ± 0.2	6.2 ± 0.2	5.2 ± 0.4	PMN J0423-0120	0.4	
04 24 41.3	00 36 50.4	J0424+0035	QSO	1.6 ± 0.6	1.1 ± 0.5	1.2 ± 0.5	GB6 J0424+0036	1.5	
04 24 50.2	−37 57 50.4	J0424-3757	QSO	1.3 ± 0.1	1.3 ± 0.2	0.8 ± 0.3	PMN J0424-3756	2.1	
04 28 41.5	−37 56 09.6	J0428-3757	QSO	1.3 ± 0.1	1.5 ± 0.2	1.5 ± 0.3	PMN J0428-3756	0.3	
04 33 15.6	05 22 19.2	J0433+0521	G	2.4 ± 0.2	2.3 ± 0.2	2.3 ± 0.4	GB6 J0433+0521	1.6	
04 40 29.5	−43 32 27.6	J0440-4332	QSO	1.5 ± 0.2	1.2 ± 0.2	0.9 ± 0.4	PMN J0440-4332	2.2	
04 42 37.0	−00 13 15.6	J0442-0017	QSO	1.1 ± 0.2	0.8 ± 0.2	0.6 ± 0.4	PMN J0442-0017	4.5	
04 50 46.8	−81 03 03.6	J0449-8100	QSO	1.4 ± 0.1	1.3 ± 0.2	1.3 ± 0.3	PMN J0450-8100	2.6	
04 53 12.2	−28 09 10.8	J0453-2806	QSO	1.2 ± 0.1	1.4 ± 0.2	1.3 ± 0.3	PMN J0453-2807	1.7	
04 55 49.2	−46 16 19.2	J0455-4617	QSO	3.9 ± 0.2	3.5 ± 0.2	3.2 ± 0.4	PMN J0455-4616	0.4	
04 57 06.0	−23 24 21.6	J0456-2322	QSO	2.5 ± 0.2	2.1 ± 0.2	2.1 ± 0.4	PMN J0457-2324	1.0	
04 57 21.1	06 42 14.4	QVW J0457+0641	G	1.0 ± 0.2	0.7 ± 0.2	0.6 ± 0.4	GB6 J0457+0645	4.6	
05 01 18.2	−02 02 20.4	J0501-0159	QSO	1.0 ± 0.2	0.9 ± 0.2	0.6 ± 0.4	PMN J0501-0159	3.3	
05 06 43.9	−61 07 37.2	J0506-6108	QSO	1.6 ± 0.1	1.1 ± 0.2	0.7 ± 0.3	PMN J0506-6109	2.1	
05 09 58.3	10 18 18.0	QVW J0509+1019	QSO	0.3 ± 0.2	0.0 ± 0.2	−0.1 ± 0.4	GB6 J0509+1012	9.8	
05 10 48.7	−31 41 02.4	. . .	RadioS	0.4 ± 0.2	0.2 ± 0.2	0.3 ± 0.3	PMN J0510-3142	1.7	c
05 16 34.1	−62 09 10.8	QVW J0516-6210	QSO	0.8 ± 0.2	0.4 ± 0.2	0.2 ± 0.3	PMN J0516-6207	2.4	
05 17 43.4	45 32 52.8	. . .	RadioS	0.5 ± 0.2	0.5 ± 0.2	−0.3 ± 0.4	GB6 J0517+4536	4.8	
05 19 40.3	−45 46 37.2	J0519-4546	G	4.3 ± 0.2	3.5 ± 0.2	2.5 ± 0.4	PMN J0519-4546A	0.7	a
05 23 02.2	−36 28 08.4	J0523-3627	G	3.6 ± 0.2	3.6 ± 0.2	3.8 ± 0.4	PMN J0522-3628	0.5	
05 27 17.5	−12 39 07.2	J0527-1241	PN	1.4 ± 0.2	1.1 ± 0.2	1.2 ± 0.4	PMN J0527-1241	3.7	
05 33 30.0	48 22 51.6	. . .	QSO	0.9 ± 0.2	0.9 ± 0.2	0.9 ± 0.4	GB6 J0533+4822	2.4	
05 35 41.0	−66 10 33.6	. . .	SNR	0.4 ± 0.5	0.0 ± 0.3	0.3 ± 0.4	PMN J0535-6601	8.6	
05 36 16.8	−33 58 58.8	QVW J0536-3358	G	0.3 ± 0.1	0.5 ± 0.2	−0.2 ± 0.4	PMN J0536-3401	3.4	
05 38 49.9	−44 05 09.6	J0538-4405	QSO	6.0 ± 0.2	5.8 ± 0.2	5.4 ± 0.4	PMN J0538-4405	0.3	
05 39 52.8	−28 40 19.2	J0539-2844	QSO	0.8 ± 0.1	0.7 ± 0.2	0.5 ± 0.3	PMN J0539-2839	0.6	
05 40 45.4	−54 17 49.2	J0540-5415	RadioS	1.1 ± 0.2	1.0 ± 0.2	0.8 ± 0.3	PMN J0540-5418	0.6	
05 42 14.4	49 50 13.2	J0542+4951	QSO	1.3 ± 0.2	0.7 ± 0.2	0.4 ± 0.4	GB6 J0542+4951	3.6	
05 42 21.8	47 36 50.4	QVW J0542+4738	RadioS	0.5 ± 0.2	0.3 ± 0.2	0.6 ± 0.4	GB6 J0541+4729	9.2	
05 50 11.3	−57 34 19.2	J0550-5731	QSO	1.0 ± 0.2	0.9 ± 0.2	0.7 ± 0.4	PMN J0550-5732	1.8	
05 52 06.0	37 50 31.2	. . .	QSO	0.7 ± 0.2	0.5 ± 0.2	0.4 ± 0.4	GB6 J0552+3754	4.6	a
05 55 34.1	39 46 44.4	J0555+3942	QSO	1.7 ± 0.2	1.1 ± 0.2	1.1 ± 0.4	GB6 J0555+3948	2.2	
06 06 03.6	40 31 55.2	J0607+6723	RadioS	0.7 ± 0.2	0.4 ± 0.2	0.3 ± 0.4	GB6 J0605+4030	3.0	
06 07 25.2	67 18 32.4	J0607+6723	QSO	0.6 ± 0.1	0.6 ± 0.2	−0.1 ± 0.4	GB6 J0607+6720	3.6	

Table 6
(Continued)

R.A. (dms)	Decl. (dms)	*WMAP*/QVW5 ID	Type	Q (Jy)	V (Jy)	W (Jy)	5 GHz ID	Dist. (arcmin)	Note
06 08 55.0	−22 18 14.4	J0608-2220	QSO	0.7 ± 0.2	0.6 ± 0.2	0.9 ± 0.3	PMN J0608-2220	2.3	
06 09 38.4	−15 43 58.8	J0609-1541	QSO	2.7 ± 0.2	2.0 ± 0.2	1.2 ± 0.4	PMN J0609-1542	1.4	
06 20 25.2	−25 15 18.0	J0621-2516	QSO	0.6 ± 0.1	0.3 ± 0.2	0.2 ± 0.3	PMN J0620-2515	1.7	
06 22 59.0	−64 36 14.4	J0623-6436	G	0.7 ± 0.1	0.8 ± 0.2	1.0 ± 0.3	PMN J0623-6436	1.4	
06 26 34.3	81 58 58.8	. . .	QSO	0.4 ± 0.2	−0.1 ± 0.2	−0.1 ± 0.3	1Jy 0615+82	3.6	
06 27 21.1	−35 30 57.6	J0626-3523	G	0.4 ± 0.2	−0.2 ± 0.2	−0.5 ± 0.3	PMN J0627-3529	3.5	
06 29 36.5	−20 00 43.2	J0629-1958	RadioS	1.3 ± 0.2	0.7 ± 0.2	1.0 ± 0.4	PMN J0629-1959	3.4	
06 35 36.7	−75 15 46.8	J0635-7517	QSO	3.3 ± 0.1	2.7 ± 0.2	2.1 ± 0.3	PMN J0635-7516	0.6	
06 36 41.3	−20 38 52.8	J0636-2031	RadioS	0.6 ± 0.2	0.5 ± 0.2	0.3 ± 0.4	PMN J0636-2041	3.6	a
06 39 23.3	73 25 19.2	J0639+7327	QSO	0.8 ± 0.1	0.5 ± 0.2	0.8 ± 0.3	GB6 J0639+7324	0.5	
06 44 31.0	−23 00 32.4	. . .	. . .	0.5 ± 0.2	0.1 ± 0.2	0.2 ± 0.3	. . .	. . .	d
06 44 40.3	−24 38 45.6	. . .	. . .	0.2 ± 0.2	−0.0 ± 0.2	−0.1 ± 0.3	. . .	. . .	d
06 46 33.1	44 49 22.8	J0646+4449	QSO	2.1 ± 0.2	1.5 ± 0.2	1.4 ± 0.4	GB6 J0646+4451	2.0	
06 47 10.3	−20 33 28.8	. . .	. . .	0.4 ± 0.2	0.1 ± 0.2	−0.1 ± 0.4	. . .	. . .	d
06 48 07.2	−30 41 13.2	QVW J0648-3042	QSO	0.5 ± 0.1	0.4 ± 0.2	0.1 ± 0.4	PMN J0648-3044	3.7	
06 48 19.9	−17 46 22.8	. . .	QSO	0.8 ± 0.2	0.7 ± 0.2	0.9 ± 0.4	PMN J0648-1744	3.1	
06 54 18.0	37 11 45.6	. . .	QSO	0.6 ± 0.2	0.4 ± 0.2	0.3 ± 0.4	GB6 J0653+3705	7.3	
07 00 04.1	17 13 12.0	QVW J0700+1713	RadioS	1.0 ± 0.2	0.5 ± 0.2	0.4 ± 0.4	GB6 J0700+1709	4.0	
07 10 41.8	47 31 37.2	QVW J0710+4731	QSO	0.7 ± 0.2	0.7 ± 0.2	−0.5 ± 0.4	GB6 J0710+4732	0.8	
07 19 45.4	33 13 26.4	. . .	QSO	0.5 ± 0.2	−0.2 ± 0.2	0.1 ± 0.4	GB6 J0719+3307	8.2	
07 21 14.9	04 08 24.0	J0720+0403	RadioS	0.6 ± 0.2	0.4 ± 0.2	0.4 ± 0.4	GB6 J0721+0406	2.7	
07 21 51.8	71 20 16.8	J0721+7122	QSO	1.7 ± 0.2	1.6 ± 0.2	1.7 ± 0.3	GB6 J0721+7120	0.3	b
07 25 27.4	14 22 30.0	. . .	QSO	0.7 ± 0.2	0.6 ± 0.2	0.5 ± 0.4	GB6 J0725+1425	3.7	
07 25 51.8	−00 54 36.0	J0725-0050	G	1.2 ± 0.2	1.3 ± 0.2	1.5 ± 0.4	PMN J0725-0054	0.4	
07 28 01.9	67 51 21.6	J0727+6749	QSO	0.6 ± 0.2	0.3 ± 0.2	0.2 ± 0.4	GB6 J0728+6748	2.8	
07 30 19.9	−11 41 24.0	. . .	QSO	3.7 ± 0.2	3.0 ± 0.2	2.1 ± 0.4	PMN J0730-1141	0.2	
07 34 06.5	50 21 25.2	J0734+5021	QSO	0.8 ± 0.2	1.0 ± 0.3	1.1 ± 0.4	GB6 J0733+5022	2.3	e
07 38 22.8	17 43 44.4	J0738+1743	QSO	0.9 ± 0.2	1.0 ± 0.2	0.5 ± 0.4	GB6 J0738+1742	3.9	
07 39 21.6	01 38 49.2	J0739+0136	QSO	2.0 ± 0.2	1.9 ± 0.2	1.5 ± 0.4	GB6 J0739+0136	2.1	
07 41 42.7	31 12 14.4	J0741+3111	QSO	0.8 ± 0.2	0.3 ± 0.2	0.1 ± 0.4	GB6 J0741+3112	7.0	
07 42 59.0	−67 31 33.6	J0743-6727	QSO	0.5 ± 0.2	0.3 ± 0.2	0.3 ± 0.3	PMN J0743-6726	6.0	
07 45 32.2	10 04 26.4	J0745+1016	G	0.7 ± 0.2	0.2 ± 0.2	−0.4 ± 0.4	GB6 J0745+1011	6.8	
07 45 55.0	−00 45 10.8	J0746-0045	QSO	0.7 ± 0.2	0.7 ± 0.2	0.2 ± 0.4	PMN J0745-0044	1.1	
07 48 42.7	−16 42 39.6	. . .	RadioS	0.4 ± 0.2	0.2 ± 0.2	−0.1 ± 0.4	PMN J0748-1639	9.7	a
07 48 43.4	24 01 12.0	QVW J0748+2400	QSO	0.8 ± 0.2	0.5 ± 0.2	0.6 ± 0.5	GB6 J0748+2400	1.9	
07 50 51.1	12 31 12.0	J0750+1230	QSO	2.6 ± 0.2	2.3 ± 0.2	2.5 ± 0.4	GB6 J0750+1231	0.1	
07 53 18.0	53 42 18.0	J0753+5354	QSO	0.5 ± 0.2	0.1 ± 0.2	−0.2 ± 0.4	GB6 J0753+5353	11.0	
07 56 58.1	09 55 51.6	J0757+0957	QSO	1.5 ± 0.2	1.2 ± 0.2	1.3 ± 0.4	GB6 J0757+0956	2.1	
08 05 38.9	61 44 09.6	J0805+6133	QSO	0.6 ± 0.2	0.5 ± 0.2	0.0 ± 0.4	GB6 J0805+6144	2.5	b
08 08 06.7	49 47 31.2	QVW J0808+4947	QSO	0.8 ± 0.2	0.1 ± 0.2	0.2 ± 0.4	GB6 J0808+4950	6.2	
08 08 25.2	−07 50 56.4	J0808-0750	QSO	1.1 ± 0.2	1.3 ± 0.2	1.1 ± 0.4	PMN J0808-0751	2.4	
08 11 22.3	01 45 43.2	QVW J0811+0145	QSO	0.7 ± 0.2	0.5 ± 0.2	0.5 ± 0.5	GB6 J0811+0146	1.6	
08 16 45.6	−24 21 43.2	J0816-2425	RadioS	0.6 ± 0.2	0.6 ± 0.2	0.3 ± 0.4	PMN J0816-2421	1.4	
08 23 41.0	22 29 27.6	J0823+2225	QSO	0.8 ± 0.2	0.3 ± 0.3	0.3 ± 0.5	GB6 J0823+2223	7.3	
08 24 55.2	55 47 16.8	QVW J0825+5546	QSO	0.5 ± 0.2	0.4 ± 0.2	−0.0 ± 0.4	GB6 J0824+5552	5.4	
08 25 09.8	39 13 19.2	J0824+3914	QSO	1.0 ± 0.2	0.8 ± 0.2	0.5 ± 0.5	GB6 J0824+3916	4.4	
08 25 49.2	03 09 21.6	J0825+0311	QSO	1.6 ± 0.2	1.6 ± 0.2	1.0 ± 0.4	GB6 J0825+0309	0.2	
08 26 01.2	−22 28 51.6	. . .	QSO	0.6 ± 0.2	0.9 ± 0.2	−0.1 ± 0.4	PMN J0826-2230	1.9	
08 30 47.8	24 11 13.2	J0831+2411	QSO	1.4 ± 0.2	1.5 ± 0.3	1.7 ± 0.5	GB6 J0830+2410	1.1	
08 31 48.0	04 34 04.8	. . .	QSO	0.9 ± 0.2	0.4 ± 0.2	1.0 ± 0.4	GB6 J0831+0429	4.2	
08 36 34.1	−20 17 09.6	J0836-2015	QSO	2.0 ± 0.2	1.6 ± 0.2	0.7 ± 0.4	PMN J0836-2015	1.2	
08 37 46.1	58 23 56.4	J0838+5822	QSO	0.5 ± 0.2	0.7 ± 0.2	0.3 ± 0.4	GB6 J0837+5825	3.5	
08 39 22.1	01 02 38.4	QVW J0839+0102	QSO	0.6 ± 0.2	0.3 ± 0.2	−0.9 ± 0.4	GB6 J0839+0104	7.1	
08 40 41.8	13 12 43.2	J0840+1312	QSO	1.4 ± 0.2	1.0 ± 0.2	0.5 ± 0.5	GB6 J0840+1312	1.6	
08 41 16.8	70 53 20.4	J0841+7053	QSO	1.7 ± 0.1	1.7 ± 0.2	0.6 ± 0.3	GB6 J0841+7053	0.7	
08 47 43.4	−07 06 18.0	J0847-0704	G	0.8 ± 0.2	1.1 ± 0.2	0.2 ± 0.4	PMN J0847-0703	4.4	
08 54 51.1	20 07 08.4	J0854+2006	QSO	3.4 ± 0.2	3.8 ± 0.3	3.7 ± 0.5	GB6 J0854+2006	0.7	
09 05 26.2	−57 40 01.2	. . .	QSO	0.9 ± 0.2	1.0 ± 0.2	0.6 ± 0.4	PMN J0904-5735	6.6	
09 07 10.8	−20 21 07.2	J0907-2020	RadioS	0.7 ± 0.2	0.4 ± 0.2	−0.3 ± 0.4	PMN J0906-2019	5.1	a
09 09 11.5	01 24 25.2	J0909+0119	QSO	1.7 ± 0.2	1.6 ± 0.2	0.7 ± 0.4	GB6 J0909+0121	2.8	
09 09 27.6	42 53 34.8	J0909+4253	QSO	1.1 ± 0.2	0.7 ± 0.3	0.8 ± 0.4	GB6 J0909+4253	1.2	
09 14 34.8	02 48 14.4	J0914+0248	G	1.1 ± 0.2	0.6 ± 0.3	1.7 ± 0.4	GB6 J0914+0245	2.5	
09 18 07.7	−12 04 12.0	J0918-1203	G	1.1 ± 0.2	0.7 ± 0.2	0.4 ± 0.4	PMN J0918-1205	1.6	
09 20 57.4	44 41 34.8	J0920+4441	QSO	1.6 ± 0.2	1.4 ± 0.2	0.6 ± 0.4	GB6 J0920+4441	0.3	
09 21 27.4	−26 20 13.2	J0921-2619	QSO	1.1 ± 0.2	1.0 ± 0.2	0.3 ± 0.4	PMN J0921-2618	1.6	

Table 6
(Continued)

R.A. (dms)	Decl. (dms)	WMAP/QVW5 ID	Type	Q (Jy)	V (Jy)	W (Jy)	5 GHz ID	Dist. (arcmin)	Note
09 21 41.5	62 18 32.4	J0921+6215	QSO	1.0 ± 0.2	0.5 ± 0.2	0.2 ± 0.3	GB6 J0921+6215	2.8	
09 22 52.1	−40 01 22.8	. . .	QSO	0.9 ± 0.2	0.7 ± 0.2	0.7 ± 0.4	PMN J0922-3959	2.4	
09 27 03.4	39 01 48.0	J0927+3901	QSO	5.7 ± 0.2	4.7 ± 0.2	3.5 ± 0.4	GB6 J0927+3902	0.5	
09 28 29.3	−20 34 55.2	. . .	QSO	0.5 ± 0.2	0.3 ± 0.2	0.5 ± 0.4	PMN J0927-2034	8.9	
09 49 01.4	40 39 07.2	J0948+4038	QSO	1.3 ± 0.2	1.2 ± 0.2	1.4 ± 0.4	GB6 J0948+4039	1.4	
09 55 40.6	69 41 20.4	J0955+6935	G	0.9 ± 0.1	1.0 ± 0.2	0.9 ± 0.3	GB6 J0955+6940	1.1	
09 56 48.5	25 16 48.0	QVW J0956+2519	QSO	0.7 ± 0.2	0.7 ± 0.2	0.7 ± 0.4	GB6 J0956+2515	1.7	
09 57 40.8	55 24 50.4	J0957+5527	QSO	0.9 ± 0.2	0.7 ± 0.2	0.6 ± 0.4	GB6 J0957+5522	1.9	
09 58 26.9	65 31 26.4	J0959+6530	QSO	0.8 ± 0.1	0.8 ± 0.2	0.5 ± 0.3	GB6 J0958+6534	3.4	
09 58 32.6	47 25 04.8	J0958+4722	QSO	1.1 ± 0.2	0.7 ± 0.2	0.4 ± 0.4	GB6 J0958+4725	2.1	
10 14 44.9	22 58 26.4	J1014+2306	QSO	0.8 ± 0.2	0.6 ± 0.2	0.4 ± 0.4	GB6 J1014+2301	2.6	b
10 14 53.0	−45 04 26.4	. . .	RadioS	0.4 ± 0.1	0.1 ± 0.2	0.1 ± 0.3	PMN J1014-4508	4.2	
10 33 00.2	41 19 33.6	J1032+4118	QSO	0.7 ± 0.2	0.7 ± 0.2	0.6 ± 0.3	GB6 J1033+4115	3.6	
10 35 08.6	−20 15 03.6	QVW J1035-2016	QSO	0.7 ± 0.2	0.3 ± 0.2	−0.1 ± 0.4	PMN J1035-2011	3.9	
10 37 15.8	−29 36 54.0	J1037-2934	QSO	1.6 ± 0.2	1.6 ± 0.2	1.9 ± 0.4	PMN J1037-2934	2.6	
10 38 49.9	05 15 21.6	J1038+0510	RadioS	1.1 ± 0.2	1.0 ± 0.2	0.5 ± 0.4	GB6 J1038+0512	3.0	
10 41 22.6	06 11 52.8	J1041+0611	QSO	1.3 ± 0.2	1.0 ± 0.2	0.4 ± 0.4	GB6 J1041+0610	1.9	
10 41 25.9	−47 42 07.2	J1041-4738	RadioS	0.5 ± 0.1	0.2 ± 0.2	0.0 ± 0.3	PMN J1041-4738	3.7	
10 43 17.5	24 07 51.6	J1043+2407	QSO	1.0 ± 0.2	0.4 ± 0.2	0.8 ± 0.4	GB6 J1043+2408	2.0	
10 48 02.9	−19 08 27.6	J1047-1909	QSO	1.1 ± 0.2	0.9 ± 0.2	−0.1 ± 0.4	PMN J1048-1909	1.5	
10 48 19.7	71 43 55.2	J1047+7143	QSO	1.1 ± 0.1	0.9 ± 0.2	1.0 ± 0.3	GB6 J1048+7143	0.7	
10 57 38.9	81 10 58.8	QVW J1058+8120	G	0.5 ± 0.2	0.5 ± 0.2	1.0 ± 0.4	S5 1053+81	3.8	
10 58 29.8	01 34 55.2	J1058+0134	QSO	4.5 ± 0.2	4.3 ± 0.2	3.4 ± 0.4	GB6 J1058+0133	1.3	
10 58 59.0	−80 04 12.0	J1059-8003	QSO	2.3 ± 0.2	2.6 ± 0.2	1.6 ± 0.4	PMN J1058-8003	0.9	
11 03 12.5	72 27 46.8	. . .	QSO	0.4 ± 0.2	0.3 ± 0.2	0.1 ± 0.3	GB6 J1101+7225	6.7	
11 07 07.7	−44 51 18.0	J1107-4446	QSO	1.0 ± 0.2	1.0 ± 0.2	0.9 ± 0.4	PMN J1107-4449	2.2	
11 18 04.3	−12 32 20.4	J1118-1233	QSO	0.7 ± 0.2	0.4 ± 0.2	0.5 ± 0.4	PMN J1118-1232	3.4	
11 18 26.2	−46 34 30.0	J1118-4633	QSO	0.7 ± 0.2	0.4 ± 0.2	0.4 ± 0.4	PMN J1118-4634	0.2	
11 18 53.8	12 34 48.0	J1118+1240	QSO	0.9 ± 0.2	0.6 ± 0.2	0.6 ± 0.4	GB6 J1118+1234	1.0	
11 27 02.9	−18 54 50.4	J1127-1858	QSO	1.4 ± 0.2	1.1 ± 0.2	1.2 ± 0.4	PMN J1127-1857	2.4	
11 30 08.9	−14 49 19.2	J1130-1451	QSO	2.0 ± 0.2	1.3 ± 0.2	1.4 ± 0.4	PMN J1130-1449	0.3	
11 31 02.9	38 16 04.8	J1130+3814	QSO	1.0 ± 0.2	0.7 ± 0.2	1.2 ± 0.3	GB6 J1130+3815	1.9	
11 46 12.0	−69 53 45.6	. . .	QSO	0.8 ± 0.2	0.8 ± 0.2	0.7 ± 0.4	PMN J1145-6953	1.6	
11 47 01.2	39 58 04.8	J1146+4001	QSO	0.8 ± 0.2	0.5 ± 0.2	1.2 ± 0.3	GB6 J1146+3958	0.8	
11 47 06.5	−38 12 21.6	J1147-3811	QSO	1.8 ± 0.2	1.9 ± 0.2	1.5 ± 0.4	PMN J1147-3812	0.8	
11 50 14.2	24 18 39.6	QVW J1150+2417	QSO	0.6 ± 0.2	0.5 ± 0.2	0.2 ± 0.4	GB6 J1150+2417	1.4	
11 52 46.8	81 00 54.0	J1155+8104	QSO	0.9 ± 0.2	0.9 ± 0.2	0.3 ± 0.4	1Jy 1150+81	2.6	
11 53 22.6	49 32 13.2	J1153+4932	G	1.7 ± 0.2	1.6 ± 0.2	1.6 ± 0.3	GB6 J1153+4931	1.0	
11 59 37.0	29 14 56.4	J1159+2915	QSO	1.7 ± 0.2	1.7 ± 0.2	1.6 ± 0.3	GB6 J1159+2914	1.0	
12 03 00.0	−05 28 08.4	. . .	QSO	0.2 ± 0.2	−0.0 ± 0.2	−0.3 ± 0.4	PMN J1202-0528	6.0	
12 03 43.4	48 03 28.8	J1203+4808	G	0.5 ± 0.2	0.3 ± 0.2	0.1 ± 0.4	GB6 J1203+4803	2.4	
12 09 18.7	−24 05 24.0	J1209-2403	QSO	0.6 ± 0.2	0.4 ± 0.2	0.3 ± 0.4	PMN J1209-2406	3.6	
12 15 55.4	−17 32 20.4	J1215-1729	G	0.9 ± 0.2	0.7 ± 0.2	0.8 ± 0.4	PMN J1215-1731	2.3	
12 19 28.1	05 47 27.6	J1219+0549	G	1.9 ± 0.2	1.3 ± 0.2	1.1 ± 0.4	1Jy 1216+06	2.1	
12 22 23.0	04 13 40.8	J1222+0414	QSO	0.9 ± 0.5	0.7 ± 0.3	1.0 ± 0.4	GB6 J1222+0413	0.6	
12 25 13.9	21 20 27.6	. . .	QSO	0.7 ± 0.2	0.4 ± 0.2	−0.2 ± 0.4	GB6 J1224+2122	4.9	
12 29 06.7	02 03 10.8	J1229+0203	QSO	18.0 ± 0.2	15.9 ± 0.2	13.2 ± 0.4	GB6 J1229+0202	0.4	
12 30 49.0	12 23 27.6	J1230+1223	G	12.8 ± 0.2	9.5 ± 0.2	7.6 ± 0.4	GB6 J1230+1223	0.1	
12 47 00.2	−25 48 28.8	J1246-2547	QSO	1.4 ± 0.2	1.6 ± 0.2	0.7 ± 0.4	PMN J1246-2547	3.0	
12 48 16.6	−45 58 58.8	J1248-4600	RadioS	0.9 ± 0.2	0.8 ± 0.2	0.9 ± 0.4	PMN J1248-4559	2.1	
12 54 42.5	11 40 04.8	J1254+1142	QSO	0.5 ± 0.2	0.0 ± 0.2	0.0 ± 0.4	GB6 J1254+1141	1.4	
12 55 16.1	−71 35 24.0	. . .	QSO	0.6 ± 0.1	0.2 ± 0.2	−0.1 ± 0.4	PMN J1254-7138	3.3	
12 56 11.8	−05 47 27.6	J1256-0547	QSO	17.6 ± 0.2	17.0 ± 0.2	14.5 ± 0.4	PMN J1256-0547	0.4	
12 58 03.8	32 28 22.8	J1258+3226	RadioS	0.8 ± 0.2	0.4 ± 0.2	0.1 ± 0.3	GB6 J1257+3229	1.8	
12 58 04.1	−31 53 34.8	J1258-3158	QSO	1.0 ± 0.2	0.5 ± 0.2	0.9 ± 0.4	PMN J1257-3154	1.7	
12 59 46.6	51 43 08.4	J1259+5141	RadioS	0.7 ± 0.1	0.7 ± 0.2	0.6 ± 0.3	GB6 J1259+5141	3.2	
13 05 19.4	−49 33 43.2	J1305-4930	G	0.7 ± 0.2	0.5 ± 0.2	0.3 ± 0.4	PMN J1305-4928	5.7	
13 10 32.2	32 23 38.4	J1310+3222	QSO	1.8 ± 0.2	1.6 ± 0.2	1.0 ± 0.3	GB6 J1310+3220	2.8	
13 16 10.3	−33 37 22.8	J1316-3337	QSO	1.7 ± 0.2	1.9 ± 0.2	1.4 ± 0.4	PMN J1316-3339	2.0	
13 19 05.3	−12 26 31.2	QVW J1319-1226	RadioS	0.4 ± 0.2	0.1 ± 0.2	−0.5 ± 0.4	PMN J1319-1217	9.1	
13 26 55.7	22 07 55.2	J1327+2213	QSO	0.8 ± 0.2	0.8 ± 0.2	0.8 ± 0.4	GB6 J1327+2210	3.0	
13 29 27.6	32 00 14.4	J1329+3200	QSO	0.4 ± 0.2	0.2 ± 0.2	0.1 ± 0.3	GB6 J1329+3154	8.0	b
13 31 14.2	30 29 06.0	J1331+3030	QSO	1.5 ± 0.2	1.1 ± 0.2	0.6 ± 0.3	GB6 J1331+3030	2.0	
13 32 52.3	02 01 44.4	J1332+0200	G	1.1 ± 0.2	1.0 ± 0.2	1.2 ± 0.4	GB6 J1332+0200	1.1	
13 33 07.2	27 24 25.2	J1333+2723	RadioS	0.6 ± 0.2	0.5 ± 0.2	0.9 ± 0.3	GB6 J1333+2725	1.0	

Table 6
(Continued)

R.A. (dms)	Decl. (dms)	WMAP/QVW5 ID	Type	Q (Jy)	V (Jy)	W (Jy)	5 GHz ID	Dist. (arcmin)	Note
13 36 30.0	−34 00 18.0	J1336-3358	G	0.8 ± 0.2	0.8 ± 0.2	0.5 ± 0.4	PMN J1336-3358	2.8	
13 37 39.8	−12 57 14.4	J1337-1257	QSO	6.4 ± 0.2	6.1 ± 0.2	5.1 ± 0.4	PMN J1337-1257	0.1	
13 43 42.7	66 03 54.0	J1343+6601	QSO	0.5 ± 0.2	0.3 ± 0.2	0.4 ± 0.3	GB6 J1344+6606	3.5	a
13 52 08.9	31 23 56.4	. . .	G	0.6 ± 0.1	0.4 ± 0.2	0.5 ± 0.4	GB6 J1352+3126	3.5	
13 54 46.1	−10 43 01.2	J1354-1041	QSO	0.9 ± 0.2	0.9 ± 0.2	0.6 ± 0.4	PMN J1354-1041	2.0	
13 57 09.1	19 19 33.6	J1356+1919	QSO	1.5 ± 0.2	1.5 ± 0.2	1.3 ± 0.3	GB6 J1357+1919	1.2	
13 59 11.0	76 45 21.6	J1355+7647	QSO	0.9 ± 0.1	0.6 ± 0.2	0.3 ± 0.3	S5 1357+76	4.8	b
13 59 25.7	01 56 31.2	QVW J1359+0159	QSO	0.7 ± 0.2	0.5 ± 0.2	0.2 ± 0.4	GB6 J1359+0159	3.3	
14 08 56.6	−07 51 14.4	J1408-0749	QSO	0.9 ± 0.2	0.5 ± 0.2	0.8 ± 0.4	1Jy 1406-076	1.2	
14 09 04.6	−27 01 01.2	. . .	QSO	0.6 ± 0.2	0.0 ± 0.2	0.1 ± 0.4	PMN J1409-2657	10.8	a
14 11 19.4	52 13 55.2	J1411+5217	G	0.5 ± 0.2	0.1 ± 0.2	0.1 ± 0.3	GB6 J1411+5212	1.7	
14 15 54.5	13 13 55.2	J1415+1322	QSO	0.6 ± 0.2	0.4 ± 0.2	0.1 ± 0.4	GB6 J1415+1320	6.5	
14 19 53.3	54 26 42.0	J1419+5425	QSO	0.9 ± 0.1	1.3 ± 0.2	1.4 ± 0.3	GB6 J1419+5423	3.4	
14 19 59.8	38 22 58.8	J1419+3823	QSO	0.7 ± 0.1	1.0 ± 0.2	0.8 ± 0.3	GB6 J1419+3822	2.9	
14 27 31.2	−33 07 12.0	J1427-3302	RadioS	1.3 ± 0.2	1.2 ± 0.2	1.0 ± 0.4	PMN J1427-3306	2.0	
14 27 59.3	−42 05 06.0	J1427-4206	QSO	2.4 ± 0.2	2.2 ± 0.2	1.5 ± 0.4	PMN J1427-4206	1.3	
14 39 28.3	49 58 01.2	J1440+4958	G	0.6 ± 0.2	0.4 ± 0.2	0.1 ± 0.3	GB6 J1439+4958	3.1	e
14 46 41.5	17 22 44.4	QVW J1446+1723	QSO	0.7 ± 0.2	0.5 ± 0.2	0.6 ± 0.3	GB6 J1446+1721	2.2	
14 54 17.8	−37 47 09.6	. . .	QSO	1.1 ± 0.2	0.8 ± 0.2	1.1 ± 0.4	PMN J1454-3747	2.0	
14 58 48.5	71 41 16.8	J1458+7140	QSO	0.7 ± 0.1	0.6 ± 0.2	0.7 ± 0.3	GB6 J1459+7140	1.8	
15 03 00.7	−41 55 58.8	. . .	SNR	1.2 ± 0.2	1.0 ± 0.2	0.9 ± 0.4	PMN J1502-4206	12.4	a
15 04 36.2	10 27 39.6	J1504+1030	QSO	1.3 ± 0.2	0.9 ± 0.2	1.1 ± 0.4	GB6 J1504+1029	3.6	
15 07 10.1	−16 55 01.2	J1506-1644	QSO	1.1 ± 0.2	0.4 ± 0.2	0.6 ± 0.4	PMN J1507-1652	2.8	
15 07 12.7	42 41 16.8	QVW J1507+4241	QSO	0.6 ± 0.1	0.5 ± 0.2	0.6 ± 0.3	GB6 J1506+4239	4.3	
15 10 44.2	−05 42 46.8	J1510-0546	QSO	1.0 ± 0.2	0.7 ± 0.2	0.8 ± 0.4	PMN J1510-0543	2.2	
15 12 43.4	−09 05 60.0	J1512-0904	QSO	2.1 ± 0.2	1.8 ± 0.2	2.2 ± 0.4	1Jy 1510-08	1.8	
15 13 42.7	−10 15 00.0	J1514-1013	QSO	0.9 ± 0.2	0.8 ± 0.3	0.8 ± 0.4	PMN J1513-1012	3.0	e
15 16 44.2	00 12 39.6	J1516+0014	G	1.2 ± 0.2	1.5 ± 0.2	1.1 ± 0.4	GB6 J1516+0015	2.7	
15 17 44.2	−24 22 44.4	J1517-2421	G	2.0 ± 0.2	2.1 ± 0.2	1.6 ± 0.4	PMN J1517-2422	0.5	
15 34 52.3	01 26 34.8	QVW J1534+0125	QSO	1.0 ± 0.2	0.7 ± 0.2	0.3 ± 0.4	GB6 J1534+0131	4.5	
15 40 49.7	14 48 57.6	J1540+1447	QSO	0.9 ± 0.2	0.8 ± 0.2	0.3 ± 0.4	GB6 J1540+1447	1.3	
15 49 09.6	50 35 45.6	J1549+5036	QSO	0.9 ± 0.1	0.7 ± 0.2	0.2 ± 0.3	GB6 J1549+5038	2.7	
15 49 33.4	02 35 34.8	J1549+0236	QSO	2.2 ± 0.2	2.0 ± 0.2	2.2 ± 0.4	GB6 J1549+0237	1.8	
15 50 33.1	05 28 01.2	J1550+0526	QSO	1.8 ± 0.2	2.0 ± 0.2	1.8 ± 0.4	GB6 J1550+0527	1.1	
15 54 07.9	−79 14 56.4	J1556-7912	G	0.5 ± 0.2	−0.2 ± 0.2	−0.3 ± 0.4	PMN J1556-7914	7.9	e
16 02 15.4	33 26 56.4	J1601+3329	G	0.6 ± 0.2	0.4 ± 0.2	0.9 ± 0.3	GB6 J1602+3326	1.6	
16 04 10.3	57 17 34.8	J1604+5718	QSO	0.6 ± 0.1	0.5 ± 0.2	0.6 ± 0.3	GB6 J1604+5714	4.7	a
16 08 43.9	10 30 25.2	J1608+1027	QSO	1.5 ± 0.2	1.3 ± 0.2	1.2 ± 0.3	GB6 J1608+1029	1.5	
16 13 43.0	34 12 39.6	J1613+3412	QSO	2.9 ± 0.1	2.5 ± 0.2	1.8 ± 0.3	GB6 J1613+3412	0.5	
16 17 54.0	−77 18 10.8	J1618-7716	QSO	1.7 ± 0.2	1.5 ± 0.2	1.1 ± 0.4	PMN J1617-7717	1.0	
16 25 55.2	41 30 21.6	J1626+4127	QSO	0.5 ± 0.2	0.6 ± 0.2	0.5 ± 0.4	GB6 J1625+4134	4.2	
16 33 53.8	82 29 27.6	J1633+8226	G	1.3 ± 0.1	1.0 ± 0.2	1.1 ± 0.3	S5 1637+82	3.9	
16 35 19.9	38 08 06.0	J1635+3807	QSO	3.4 ± 0.4	3.4 ± 0.4	3.2 ± 0.4	GB6 J1635+3808	0.8	
16 37 40.1	47 13 30.0	J1637+4713	QSO	1.1 ± 0.2	0.8 ± 0.2	0.8 ± 0.4	GB6 J1637+4717	4.2	
16 38 19.7	57 18 36.0	J1638+5722	QSO	1.6 ± 0.1	1.6 ± 0.2	1.1 ± 0.3	GB6 J1638+5720	2.1	
16 41 59.5	68 57 00.0	J1642+6854	QSO	2.0 ± 0.1	1.7 ± 0.2	1.3 ± 0.3	GB6 J1642+6856	0.7	
16 42 57.1	39 48 54.0	J1642+3948	QSO	5.1 ± 0.3	4.8 ± 0.3	4.2 ± 0.4	GB6 J1642+3948	0.3	
16 45 36.7	−77 13 22.8	J1643-7712	G	0.7 ± 0.2	0.6 ± 0.2	0.4 ± 0.4	PMN J1644-7715	5.0	e
16 48 01.7	−64 34 40.8	QVW J1648-6434	RadioS	0.4 ± 0.1	0.4 ± 0.2	−0.2 ± 0.4	PMN J1647-6437	4.2	
16 48 33.8	41 04 48.0	J1648+4114	QSO	0.4 ± 0.4	0.5 ± 0.4	0.4 ± 0.4	GB6 J1648+4104	1.0	e
16 51 07.0	04 59 27.6	J1651+0458	G	1.0 ± 0.2	0.8 ± 0.2	0.1 ± 0.4	GB6 J1651+0459	0.7	
16 54 08.4	39 47 24.0	J1654+3939	G	0.7 ± 0.4	0.5 ± 0.4	0.6 ± 0.4	GB6 J1653+3945	3.4	
16 58 08.4	07 42 50.4	J1658+0742	QSO	1.3 ± 0.2	1.3 ± 0.2	1.2 ± 0.4	GB6 J1658+0741	1.5	
16 58 14.2	47 57 21.6	J1657+4754	RadioS	0.3 ± 0.2	0.1 ± 0.2	−0.0 ± 0.3	GB6 J1657+4808	12.2	b
16 59 58.1	68 32 27.6	J1659+6827	G	0.7 ± 0.2	0.6 ± 0.2	0.4 ± 0.3	GB6 J1700+6830	2.6	
17 03 21.4	−62 13 37.2	J1703-6214	RadioS	1.4 ± 0.2	1.2 ± 0.2	1.2 ± 0.4	PMN J1703-6212	2.1	
17 15 38.4	68 39 43.2	J1715+6839	QSO	0.6 ± 0.1	0.4 ± 0.2	0.3 ± 0.3	GB6 J1716+6836	4.4	
17 19 14.6	17 45 43.2	QVW J1719+1743	QSO	0.6 ± 0.2	0.3 ± 0.2	0.3 ± 0.4	GB6 J1719+1745	0.7	
17 23 48.0	−64 58 33.6	J1724-6500	G	1.5 ± 0.1	1.3 ± 0.2	1.7 ± 0.4	PMN J1723-6500	2.2	
17 27 20.9	45 28 40.8	J1727+4530	G	0.8 ± 0.2	1.0 ± 0.2	0.8 ± 0.3	GB6 J1727+4530	2.5	
17 28 22.1	04 28 30.0	QVW J1728+0429	QSO	1.1 ± 0.2	1.0 ± 0.2	0.3 ± 0.4	GB6 J1728+0426	1.7	
17 28 45.6	12 14 31.2	. . .	QSO	0.3 ± 0.2	−0.1 ± 0.2	−0.6 ± 0.4	GB6 J1728+1215	9.3	
17 34 28.3	38 56 06.0	J1734+3857	QSO	1.1 ± 0.2	1.1 ± 0.2	1.0 ± 0.4	GB6 J1734+3857	2.2	
17 34 57.8	−79 35 42.0	J1737-7934	QSO	1.0 ± 0.2	0.8 ± 0.2	0.9 ± 0.3	PMN J1733-7935	3.5	
17 37 08.6	06 19 26.4	. . .	QSO	0.8 ± 0.2	0.7 ± 0.2	0.5 ± 0.4	GB6 J1737+0620	2.0	

Table 6
(Continued)

R.A. (dms)	Decl. (dms)	WMAP/QVW5 ID	Type	Q (Jy)	V (Jy)	W (Jy)	5 GHz ID	Dist. (arcmin)	Note
17 37 16.1	−56 32 49.2	QVW J1737-5635	G	0.7 ± 0.2	−0.0 ± 0.2	0.4 ± 0.4	PMN J1737-5633	3.2	
17 39 55.2	47 40 26.4	J1740+4740	QSO	0.7 ± 0.1	0.7 ± 0.2	0.8 ± 0.3	GB6 J1739+4738	2.4	
17 40 28.8	52 11 52.8	J1740+5212	QSO	1.1 ± 0.1	1.0 ± 0.2	0.6 ± 0.3	GB6 J1740+5211	1.2	
17 48 59.0	70 05 24.0	J1748+7006	QSO	0.6 ± 0.2	0.8 ± 0.2	0.9 ± 0.3	GB6 J1748+7005	2.3	
17 51 32.9	09 38 56.4	. . .	QSO	4.4 ± 0.2	4.3 ± 0.2	3.8 ± 0.4	GB6 J1751+0938	0.1	
17 53 16.8	44 07 30.0	J1753+4408	QSO	0.7 ± 0.2	0.6 ± 0.2	0.8 ± 0.4	GB6 J1753+4410	2.8	
17 53 50.9	28 49 30.0	J1753+2848	RadioS	1.8 ± 0.1	1.8 ± 0.2	1.3 ± 0.3	GB6 J1753+2847	2.4	
17 56 43.9	15 34 04.8	QVW J1756+1534	RadioS	0.5 ± 0.2	0.2 ± 0.2	0.2 ± 0.4	GB6 J1756+1535	2.6	
18 00 25.7	38 48 28.8	J1759+3852	QSO	0.7 ± 0.1	0.3 ± 0.2	0.1 ± 0.3	GB6 J1800+3848	0.2	
18 00 34.8	78 27 28.8	J1800+7827	QSO	1.6 ± 0.2	1.5 ± 0.2	1.4 ± 0.3	1Jy 1803+78	0.8	
18 01 26.6	44 04 04.8	J1801+4404	QSO	1.5 ± 0.2	1.5 ± 0.2	1.1 ± 0.4	GB6 J1801+4404	1.0	
18 03 20.4	−65 06 43.2	J1803-6507	RadioS	1.1 ± 0.2	0.8 ± 0.2	1.1 ± 0.4	PMN J1803-6507	0.9	
18 06 44.2	69 49 19.2	J1806+6949	G	1.3 ± 0.1	1.2 ± 0.2	1.0 ± 0.3	GB6 J1806+6949	0.7	
18 12 04.1	06 49 30.0	. . .	PN	0.8 ± 0.2	0.7 ± 0.2	0.5 ± 0.4	GB6 J1812+0651	2.0	
18 19 28.8	−63 45 18.0	J1820-6343	G	1.1 ± 0.2	1.2 ± 0.2	0.9 ± 0.4	PMN J1819-6345	0.9	
18 19 56.9	−55 17 24.0	J1819-5521	QSO	0.7 ± 0.2	0.4 ± 0.2	0.2 ± 0.4	PMN J1819-5521	4.3	
18 22 49.4	15 57 07.2	QVW J1822+1556	RadioS	0.4 ± 0.2	0.1 ± 0.2	−0.1 ± 0.4	GB6 J1822+1600	9.9	
18 23 31.2	69 00 25.2	QVW J1823+6854	RadioS	0.3 ± 0.2	0.2 ± 0.2	−0.1 ± 0.3	GB6 J1823+6857	2.5	
18 23 58.1	56 50 52.8	J1824+5650	QSO	1.2 ± 0.1	1.0 ± 0.2	0.9 ± 0.3	GB6 J1824+5650	1.2	
18 29 39.4	48 44 42.0	J1829+4845	QSO	2.4 ± 0.1	1.8 ± 0.2	1.7 ± 0.3	GB6 J1829+4844	1.2	
18 34 25.0	−58 55 37.2	J1834-5854	QSO	1.0 ± 0.2	0.6 ± 0.2	0.6 ± 0.4	PMN J1834-5856	1.1	
18 35 08.6	32 37 22.8	J1835+3245	G	0.7 ± 0.1	0.3 ± 0.2	−0.3 ± 0.3	GB6 J1835+3241	4.4	
18 37 07.2	−71 08 06.0	J1837-7106	QSO	1.1 ± 0.1	1.0 ± 0.2	0.7 ± 0.3	PMN J1837-7108	1.7	
18 42 05.5	79 44 49.2	J1840+7946	G	0.8 ± 0.2	0.6 ± 0.2	0.2 ± 0.3	1Jy 1845+79	1.2	
18 42 25.7	68 09 07.2	J1842+6808	QSO	1.2 ± 0.2	1.0 ± 0.2	1.0 ± 0.3	GB6 J1842+6809	0.7	
18 48 20.6	32 19 48.0	J1848+3223	QSO	0.7 ± 0.1	0.6 ± 0.2	1.0 ± 0.3	GB6 J1848+3219	0.8	
18 49 20.6	67 04 26.4	J1849+6705	QSO	1.8 ± 0.2	1.7 ± 0.2	1.6 ± 0.3	GB6 J1849+6705	1.4	
18 50 13.0	28 20 31.2	J1850+2823	QSO	0.6 ± 0.1	0.3 ± 0.2	0.1 ± 0.3	GB6 J1850+2825	5.6	
18 55 18.2	73 52 30.0	QVW J1855+7350	QSO	0.5 ± 0.2	0.4 ± 0.2	0.1 ± 0.3	GB6 J1854+7351	2.1	
19 03 10.8	31 57 10.8	J1902+3153	QSO	0.5 ± 0.1	0.4 ± 0.2	0.3 ± 0.3	GB6 J1902+3159	3.9	
19 11 10.3	−20 07 01.2	. . .	QSO	2.5 ± 0.2	2.3 ± 0.2	2.8 ± 0.4	PMN J1911-2006	0.2	
19 12 35.3	37 45 28.8	QVW J1912+3747	QSO	0.4 ± 0.2	0.1 ± 0.2	−0.2 ± 0.4	GB6 J1912+3740	5.4	
19 13 41.3	−80 04 12.0	. . .	QSO	0.5 ± 0.2	0.4 ± 0.2	−0.0 ± 0.4	PMN J1912-8010	6.5	
19 17 21.8	55 31 55.2	QVW J1917+5533	QSO	0.3 ± 0.1	−0.2 ± 0.2	−0.4 ± 0.3	GB6 J1916+5544	13.2	a
19 23 27.8	−21 04 08.4	J1923-2105	QSO	2.3 ± 0.2	2.2 ± 0.2	2.1 ± 0.4	PMN J1923-2104	1.1	
19 24 50.9	−29 14 34.8	J1924-2914	QSO	10.7 ± 0.2	10.2 ± 0.2	8.0 ± 0.4	PMN J1924-2914	0.1	
19 27 22.3	61 17 27.6	J1927+6119	QSO	1.0 ± 0.1	0.8 ± 0.2	0.4 ± 0.3	GB6 J1927+6117	0.9	
19 27 58.8	73 57 14.4	J1927+7357	QSO	2.4 ± 0.1	2.5 ± 0.2	1.9 ± 0.3	GB6 J1927+7357	1.0	
19 28 15.4	32 33 54.0	. . .	. . .	0.3 ± 0.1	0.1 ± 0.2	−0.2 ± 0.3	GB6 J1927+3236	6.8	
19 37 12.7	−39 55 51.6	J1937-3957	QSO	1.5 ± 0.2	1.2 ± 0.2	1.6 ± 0.4	PMN J1937-3957	2.1	
19 39 37.2	−15 26 27.6	J1939-1525	QSO	0.7 ± 0.2	0.6 ± 0.2	0.5 ± 0.4	PMN J1939-1525	2.7	
19 41 00.5	46 00 32.4	. . .	. . .	−0.1 ± 0.2	−0.2 ± 0.2	−0.4 ± 0.4	GB6 J1940+4605	7.0	
19 46 01.0	−55 26 09.6	QVW J1946-5528	G	0.3 ± 0.2	−0.0 ± 0.2	−0.2 ± 0.4	PMN J1945-5520	7.4	
19 55 49.7	51 34 01.2	J1955+5139	QSO	0.9 ± 0.1	0.7 ± 0.2	0.5 ± 0.3	GB6 J1955+5131	2.4	
19 58 06.2	−38 45 32.4	J1958-3845	QSO	3.0 ± 0.2	2.4 ± 0.2	1.9 ± 0.4	PMN J1957-3845	1.3	
20 00 52.8	−17 46 55.2	J2000-1749	QSO	1.8 ± 0.2	1.8 ± 0.2	1.7 ± 0.4	PMN J2000-1748	2.4	
20 04 34.6	77 50 60.0	J2005+7755	QSO	1.0 ± 0.1	0.9 ± 0.2	1.1 ± 0.4	1Jy 2007+77	3.4	
20 09 05.8	−48 47 20.4	QVW J2009-4846	QSO	0.8 ± 0.2	0.6 ± 0.2	0.3 ± 0.4	PMN J2009-4849	4.1	
20 10 15.4	72 32 09.6	. . .	QSO	0.9 ± 0.1	0.9 ± 0.2	0.8 ± 0.3	GB6 J2009+7229	3.4	
20 11 16.3	−15 44 20.4	J2011-1547	QSO	1.6 ± 0.2	1.2 ± 0.2	1.0 ± 0.4	PMN J2011-1546	2.4	
20 22 21.6	61 37 04.8	J2022+6136	G	1.1 ± 0.1	0.8 ± 0.2	0.2 ± 0.3	GB6 J2022+6137	1.8	
20 23 37.2	54 30 54.0	J2023+5426	RadioS	0.6 ± 0.2	0.7 ± 0.2	0.6 ± 0.4	GB6 J2023+5427	4.2	
20 56 09.1	−32 05 02.4	. . .	RadioS	0.8 ± 0.2	0.5 ± 0.2	0.2 ± 0.4	PMN J2056-3207	3.8	
20 56 10.1	−47 15 07.2	J2056-4716	QSO	2.2 ± 0.2	2.1 ± 0.2	2.2 ± 0.4	PMN J2056-4714	0.9	
21 01 38.4	03 38 09.6	J2101+0344	QSO	0.8 ± 0.2	0.9 ± 0.2	0.5 ± 0.4	PMN J2101+0341	3.0	
21 04 42.5	−78 25 51.6	. . .	QSO	0.7 ± 0.2	0.7 ± 0.2	0.6 ± 0.3	PMN J2105-7825	3.1	
21 07 04.1	−25 24 43.2	QVW J2106-2521	GTrpl	0.7 ± 0.2	0.7 ± 0.2	0.1 ± 0.4	PMN J2107-2526	4.5	
21 09 19.4	35 32 31.2	J2109+3537	G	0.8 ± 0.2	0.7 ± 0.2	0.2 ± 0.3	GB6 J2109+3532	2.6	
21 09 22.3	−41 07 12.0	J2109-4113	QSO	1.2 ± 0.2	1.0 ± 0.2	0.7 ± 0.4	PMN J2109-4110	3.7	
21 20 20.9	32 25 19.2	. . .	. . .	0.2 ± 0.2	−0.0 ± 0.2	−0.2 ± 0.3	. . .	. . .	d
21 23 39.1	05 33 36.0	J2123+0536	QSO	1.5 ± 0.2	1.0 ± 0.2	0.6 ± 0.4	GB6 J2123+0535	2.3	
21 29 07.0	−15 39 03.6	QVW J2129-1535	QSO	0.7 ± 0.2	0.3 ± 0.2	0.3 ± 0.4	PMN J2129-1538	1.2	
21 31 39.1	−12 08 09.6	J2131-1207	QSO	2.1 ± 0.2	1.6 ± 0.2	1.3 ± 0.4	PMN J2131-1207	1.4	
21 33 39.8	38 02 42.0	QVW J2133+3804	RadioS	0.1 ± 0.1	0.1 ± 0.2	−0.3 ± 0.3	GB6 J2133+3812	10.0	
21 34 11.8	−01 54 39.6	J2134-0154	QSO	1.6 ± 0.2	1.6 ± 0.2	1.5 ± 0.4	PMN J2134-0153	1.3	

Table 6
(Continued)

R.A. (dms)	Decl. (dms)	*WMAP*/QVW5 ID	Type	Q (Jy)	V (Jy)	W (Jy)	5 GHz ID	Dist. (arcmin)	Note
21 36 37.4	00 41 34.8	J2136+0041	QSO	3.2 ± 0.2	1.8 ± 0.2	1.2 ± 0.4	GB6 J2136+0041	0.3	
21 39 04.8	14 25 37.2	J2139+1425	QSO	1.3 ± 0.2	1.2 ± 0.2	1.2 ± 0.4	GB6 J2139+1423	2.2	
21 43 08.9	17 43 40.8	J2143+1741	QSO	0.6 ± 0.2	0.4 ± 0.2	0.5 ± 0.4	GB6 J2143+1743	6.3	
21 46 42.7	−78 00 18.0	J2148-7758	QSO	0.9 ± 0.2	0.7 ± 0.2	0.3 ± 0.3	PMN J2146-7755	4.4	
21 48 05.0	06 57 43.2	J2148+0657	QSO	6.8 ± 0.2	6.1 ± 0.2	4.8 ± 0.4	GB6 J2148+0657	0.0	
21 51 56.9	−30 28 33.6	J2151-3027	QSO	1.4 ± 0.2	1.5 ± 0.2	1.1 ± 0.4	PMN J2151-3028	0.5	
21 57 04.3	−69 41 02.4	J2157-6942	G	2.4 ± 0.1	1.9 ± 0.2	1.3 ± 0.4	PMN J2157-6941	0.6	
21 58 11.5	−15 02 38.4	J2158-1501	QSO	1.6 ± 0.2	1.4 ± 0.2	0.8 ± 0.4	PMN J2158-1501	1.9	
22 02 46.1	42 16 22.8	J2202+4217	QSO	3.3 ± 0.1	3.2 ± 0.2	3.4 ± 0.4	GB6 J2202+4216	0.4	
22 03 16.3	31 46 22.8	J2203+3146	QSO	2.1 ± 0.2	1.7 ± 0.2	1.3 ± 0.4	GB6 J2203+3145	0.7	
22 03 22.6	17 26 31.2	J2203+1723	QSO	1.5 ± 0.2	1.4 ± 0.2	0.8 ± 0.4	GB6 J2203+1725	1.3	
22 06 01.9	−18 36 28.8	J2206-1838	QSO	0.8 ± 0.2	1.0 ± 0.2	0.6 ± 0.4	PMN J2206-1835	2.3	
22 07 46.8	−53 43 44.4	J2207-5348	QSO	0.8 ± 0.2	0.4 ± 0.2	0.3 ± 0.3	PMN J2207-5346	2.8	
22 11 53.0	23 56 02.4	J2211+2352	QSO	1.0 ± 0.2	1.1 ± 0.2	1.1 ± 0.4	GB6 J2212+2355	3.0	
22 18 56.9	−03 34 33.6	J2218-0335	QSO	1.8 ± 0.4	1.5 ± 0.4	0.8 ± 0.4	PMN J2218-0335	1.7	
22 20 14.6	43 16 12.0	...	...	0.4 ± 0.1	0.2 ± 0.2	−0.0 ± 0.3	...	...	d
22 25 24.7	21 17 31.2	J2225+2119	QSO	0.8 ± 0.2	0.9 ± 0.2	0.8 ± 0.4	GB6 J2225+2118	3.1	
22 25 48.7	−04 57 07.2	J2225-0455	QSO	4.7 ± 0.2	4.1 ± 0.2	3.8 ± 0.4	PMN J2225-0457	0.6	
22 29 35.8	−08 30 50.4	J2229-0833	QSO	2.5 ± 0.2	2.8 ± 0.2	2.4 ± 0.4	PMN J2229-0832	2.3	
22 30 37.9	38 43 15.6	...	...	0.1 ± 0.2	0.1 ± 0.2	−0.2 ± 0.4	...	...	d
22 32 36.2	11 43 04.8	J2232+1144	QSO	4.0 ± 0.2	4.1 ± 0.2	4.9 ± 0.4	GB6 J2232+1143	0.9	
22 35 18.7	−48 35 49.2	J2235-4834	QSO	1.9 ± 0.2	1.7 ± 0.2	1.9 ± 0.4	PMN J2235-4835	0.9	
22 36 17.5	28 30 46.8	J2236+2824	QSO	1.1 ± 0.2	0.7 ± 0.2	0.7 ± 0.4	GB6 J2236+2828	2.0	
22 39 20.4	−57 01 15.6	J2239-5701	RadioS	0.8 ± 0.2	0.8 ± 0.2	1.2 ± 0.3	PMN J2239-5701	1.2	
22 46 23.8	−12 07 58.8	J2246-1208	QSO	2.0 ± 0.2	1.4 ± 0.2	0.8 ± 0.4	PMN J2246-1206	1.9	
22 48 54.7	−32 31 30.0	...	QSO	0.8 ± 0.2	0.4 ± 0.2	−0.2 ± 0.4	PMN J2248-3236	6.0	
22 53 58.8	16 08 45.6	J2254+1608	QSO	8.3 ± 0.2	8.9 ± 0.2	9.2 ± 0.4	GB6 J2253+1608	0.2	
22 55 34.3	42 03 50.4	J2255+4201	QSO	0.6 ± 0.1	0.3 ± 0.2	−0.3 ± 0.3	GB6 J2255+4202	1.1	
22 56 47.8	−20 13 19.2	J2256-2014	QSO	0.8 ± 0.2	0.3 ± 0.2	0.4 ± 0.4	PMN J2256-2011	2.3	
22 58 07.2	−27 57 54.0	J2258-2757	QSO	4.1 ± 0.2	3.9 ± 0.2	3.4 ± 0.4	PMN J2258-2758	0.6	
23 03 52.8	−68 04 58.8	J2302-6808	QSO	0.8 ± 0.1	0.2 ± 0.2	−0.0 ± 0.3	PMN J2303-6807	3.0	
23 11 02.9	34 23 52.8	QVW J2311+3424	QSO	0.7 ± 0.2	0.7 ± 0.2	0.4 ± 0.4	GB6 J2311+3425	1.3	
23 13 32.4	72 45 39.6	...	RadioS	0.3 ± 0.1	0.3 ± 0.2	0.2 ± 0.4	GB6 J2312+7241	6.9	
23 14 19.4	72 53 20.4	...	RadioS	0.1 ± 0.1	−0.0 ± 0.2	−0.2 ± 0.4	GB6 J2312+7241	14.9	
23 15 46.6	−50 17 45.6	J2315-5018	RadioS	0.8 ± 0.2	0.7 ± 0.2	0.1 ± 0.3	PMN J2315-5018	1.0	
23 21 55.9	51 03 10.8	J2322+5105	QSO	0.6 ± 0.1	0.4 ± 0.2	0.2 ± 0.3	GB6 J2322+5057	7.2	
23 23 32.6	−03 20 52.8	QVW J2323-0319	QSO	0.8 ± 0.2	0.9 ± 0.2	−0.1 ± 0.4	PMN J2323-0317	3.9	
23 27 35.8	09 39 07.2	J2327+0937	QSO	1.1 ± 0.2	1.1 ± 0.2	1.1 ± 0.4	GB6 J2327+0940	1.2	
23 29 22.3	−47 27 50.4	J2329-4733	QSO	1.2 ± 0.2	0.7 ± 0.2	0.9 ± 0.4	PMN J2329-4730	2.6	
23 33 39.4	−23 40 26.4	J2333-2340	G	0.9 ± 0.2	0.7 ± 0.2	0.6 ± 0.4	PMN J2333-2343	4.8	a
23 35 44.4	−52 42 25.2	J2335-5243	QSO	0.6 ± 0.1	0.2 ± 0.2	−0.1 ± 0.3	PMN J2336-5236	7.4	a
23 48 01.2	−16 30 28.8	J2348-1630	QSO	1.7 ± 0.2	1.6 ± 0.3	1.4 ± 0.4	PMN J2348-1631	0.9	
23 54 17.3	45 53 20.4	J2354+4550	QSO	1.1 ± 0.2	0.9 ± 0.2	1.2 ± 0.4	GB6 J2354+4553	0.9	
23 56 23.5	−68 18 57.6	...	QSO	0.5 ± 0.2	0.3 ± 0.2	−0.1 ± 0.3	PMN J2356-6820	2.5	
23 56 51.6	81 56 20.4	J2354+8152	QSO	0.6 ± 0.1	0.8 ± 0.2	0.7 ± 0.3	S5 2353+81	3.6	b
23 57 51.4	−53 08 56.4	J2357-5314	QSO	1.5 ± 0.1	1.1 ± 0.2	1.0 ± 0.3	PMN J2357-5311	2.4	
23 57 59.3	−45 56 13.2	QVW J2357-4556	RadioS	0.3 ± 0.2	0.2 ± 0.2	0.3 ± 0.4	PMN J2358-4555	1.2	
23 59 01.7	−60 55 37.2	J2358-6050	G	1.1 ± 0.2	0.7 ± 0.2	0.2 ± 0.3	PMN J2358-6054	1.4	
23 59 39.1	39 18 07.2	QVW J2359+3916	QSO	0.6 ± 0.2	0.5 ± 0.2	0.0 ± 0.4	GB6 J2358+3922	8.7	

Notes.

[a] Indicates this source has multiple identifications. The source listed here is the brighter one or the one with small offset when fluxes are comparable.

[b] The source is associated with a different 5 GHz source than noted in the *WMAP* five-year point source catalog.

[c] The source position is fitted to the local maximum of a 5×5 pixel neighborhood as there are two bright pixels within one Q-band beam, both of which are the brightest in their 3×3 pixel neighborhood.

[d] Indicates no 5 GHz counterpart could be identified for the source.

[e] Indicates the source is in the three-year *WMAP* point source catalog, but not in the five-year catalog.

spectral index differences. The distribution of spectral index in the five *WMAP* bands for the sources that are only in the five-band catalog is similar to that for the sources common to both catalogs. The differences are thought to be largely caused by Eddington bias in the five-band source detections due to

CMB fluctuations and noise. At low flux levels, the five-band method tends to detect point sources located on positive CMB fluctuations and to overestimate their fluxes, and it tends to miss sources located in negative CMB fluctuations. This was shown by application of the method to simulated sky maps (Wright

et al. 2009), and its effect is also seen in the comparison by Chen & Wright (2009) of five-year fluxes from the five-band method with those from the CMB-free method in Q, V, and W bands.

7. CONCLUSIONS

Even with all the uncertainty regarding foregrounds in the Galactic plane, we find no evidence for foreground contamination outside our current KQ85y7 analysis mask. Further, the cleaning process requires only three simple power-law foregrounds and leaves no more than 15 μK of residuals in the CMB temperature power spectrum.

We find no evidence of polarized foregrounds beyond those from soft (steep-spectrum) synchrotron and thermal dust emission. In particular, we see no indication of an energetic population of synchrotron-emitting electrons near the Galactic center.

Additional years of data have allowed us to detect a combined 62 new point sources using two techniques, a 12% increase from the five-year data release. A total of 346 point sources are in common between the two techniques.

More and more evidence is indicating that within a few degrees of the Galactic plane, the behavior of low-frequency foregrounds is complicated and has not been completely understood. *WMAP* data show a rapidly steepening spectrum from 20 to 40 GHz, which may be explained as emission from spinning dust grains. The leading systematic, beam asymmetry, does not appear able to alter the spectrum enough to eliminate the need for spinning dust or a similar component. ARCADE data appear consistent with the spinning dust explanation, although some discrepancies remain as to the relative strength of the emission. More data at frequencies where spinning dust emission is expected to be strongest (10–40 GHz) would be very helpful.

REFERENCES

Bennett, C., et al. 2011, ApJS, 192, 17
Bennett, C. L., et al. 2003, ApJS, 148, 97
Chen, X., & Wright, E. L. 2008, ApJ, 681, 747
Chen, X., & Wright, E. L. 2009, ApJ, 694, 222
Culverhouse, T., et al. 2010, ApJ, 722, 1057
Dobler, G., & Finkbeiner, D. P. 2008a, ApJ, 680, 1222
Dobler, G., & Finkbeiner, D. P. 2008b, ApJ, 680, 1235
Dobler, G., Finkbeiner, D. P., Cholis, I., Slatyer, T. R., & Weiner, N. 2010, ApJ, 717, 825
Draine, B. T., & Lazarian, A. 1998a, ApJ, 494, L19
Draine, B. T., & Lazarian, A. 1998b, ApJ, 508, 157
Draine, B. T., & Lazarian, A. 1999, ApJ, 512, 740
Dunkley, J., et al. 2009a, ApJS, 180, 306
Dunkley, J., et al. 2009b, in AIP Conf. Ser. 1141, Prospects for Polarized Foreground Removal, ed. S. Dodelson et al. (New York: AIP), 222
Eriksen, H. K., et al. 2007, ApJ, 656, 641
Finkbeiner, D. P. 2003, ApJS, 146, 407
Finkbeiner, D. P. 2004, ApJ, 614, 186
Finkbeiner, D. P., Davis, M., & Schlegel, D. J. 1999, ApJ, 524, 867
Fixsen, D. J., et al. 2009, ApJ, submitted (arXiv:0901.0555)
Gold, B., et al. 2009, ApJS, 180, 265
Gorski, K. M., Hivon, E., Banday, A. J., Wandelt, B. D., Hansen, F. K., Reinecke, M., & Bartlemann, M. 2005, ApJ, 622, 759
Gregory, P. C., Scott, W. K., Douglas, K., & Condon, J. J. 1996, ApJS, 103, 427
Griffith, M. R., Wright, A. E., Burke, B. F., & Ekers, R. D. 1994, ApJS, 90, 179
Griffith, M. R., Wright, A. E., Burke, B. F., & Ekers, R. D. 1995, ApJS, 97, 347
Haslam, C. G. T., Klein, U., Salter, C. J., Stoffel, H., Wilson, W. E., Cleary, M. N., Cooke, D. J., & Thomasson, P. 1981, A&A, 100, 209
Healey, S. E., Fuhrmann, L., Taylor, G. B., Romani, R. W., & Readhead, A. C. S. 2009, AJ, 138, 1032
Hinshaw, G., et al. 2007, ApJS, 170, 288
Hooper, D., Finkbeiner, D. P., & Dobler, G. 2007, Phys. Rev. D, 76, 083012
Jarosik, N., et al. 2011, ApJS, 192, 14
Kim, J., Naselsky, P., & Christensen, P. R. 2008, Phys. Rev. D, 77, 103002
Kogut, A., et al. 2009, ApJ, submitted (arXiv:0901.0562)
Komatsu, E., et al. 2011, ApJS, 192, 18
Kühr, H., Witzel, A., Pauliny-Toth, I. I. K., & Nauber, U. 1981, A&AS, 45, 367
Kunz, M., Trotta, R., & Parkinson, D. R. 2006, Phys. Rev. D, 74, 023503
Larson, D., et al. 2011, ApJS, 192, 16
Lawson, K. D., Mayer, C. J., Osborne, J. L., & Parkinson, M. L. 1987, MNRAS, 225, 307
Lazarian, A., & Draine, B. T. 2000, ApJ, 536, L15
Lewis, A., Challinor, A., & Lasenby, A. 2000, ApJ, 538, 473
Page, L., et al. 2007, ApJS, 170, 335
Refregier, A., Spergel, D. N., & Herbig, T. 2000, ApJ, 531, 31
Scaife, T. A. C. A. M. M., et al. 2009, MNRAS, 400, 1394
Schlegel, D. J., Finkbeiner, D. P., & Davis, M. 1998, ApJ, 500, 525
Singal, J., et al. 2009, ApJ, submitted (arXiv:0901.0546)
Tegmark, M., & de Oliveira-Costa, A. 1998, ApJ, 500, L83
Tibbs, C. T., et al. 2010, MNRAS, 402, 1969
Trushkin, S. A. 2003, Bull. Spec. Astrophys. Obs. N. Caucasus, 55, 90
Veneziani, M., et al. 2010, ApJ, 713, 959
Vio, R., & Andreani, P. 2009, arXiv:0910.4294
Weiland, J., et al. 2011, ApJS, 192, 19
Wright, A. E., Griffith, M. R., Burke, B. F., & Ekers, R. D. 1994, ApJS, 91, 111
Wright, A. E., Griffith, M. R., Hunt, A. J., Troup, E., Burke, B. F., & Ekers, R. D. 1996, ApJS, 103, 145
Wright, E. L., et al. 2009, ApJS, 180, 283